5th International Workshop

Computational Experiment
in AeroAcoustics
CEAA2018

September 19-22, 2018

Svetlogorsk, Kaliningrad region
Russia

Book of abstracts

MOSCOW – 2018

Computational Experiment in Aeroacoustics. CEAA2018: 5th International Workshop, Svetlogorsk, Kaliningrad region, Russia, September 19-22, 2018: Book of abstracts. – Moscow: Keldysh Institute, 2018. – 134 p.

The Book collects the abstracts of invited lectures, keynote technical presentations, sponsor presentations and contributed talks presented at 5th International Workshop "Computational Experiment in AeroAcoustics" (CEAA2018 Workshop). The Workshop is organized by Keldysh Institute of Applied Mathematics of Russian Academy of Sciences, Moscow, with assistance from Central Aerohydrodynamical Institute (TsAGI), Zhukovsky, Immanuel Kant Baltic Federal University, Kaliningrad, and Municipal Administration of Svetlogorsk. The scientific forum is supported by the Russian Foundation of Basic Research (Project No. 18-01-20074) and Official sponsors. The Workshop is held in Svetlogorsk, Kaliningrad region, Russia, September 19-22, 2018.

ORGANIZER

Keldysh Institute of Applied Mathematics of Russian Academy of Sciences (KIAM), Moscow, Russia

with assistance from

Central Aerohydrodynamical Institute (TsAGI), Zhukovsky, Russia
Immanuel Kant Baltic Federal University, Kaliningrad, Russia
Municipal Administration of Svetlogorsk, Russia

SPONSORS

 Sukhoi Aviation Holding Company

 Central Institute of Aviation Motors

 NUMECA Russia

PROGRAMME COMMITTEE

Chairmen

Boris CHETVERUSHKIN, Prof., Full member of RAS, Keldysh Institute of Applied Mathematics of RAS, Russia

Tatiana KOZUBSKAYA, D.Sci., Keldysh Institute of Applied Mathematics of RAS, Russia

Members of Organizing Committee

Michael DUMBSER, Prof., University of Trento, Italy

Vladimir GOLUBEV, Prof., Embry-Riddle Aeronautical University, USA

Charles HIRSCH, Prof., Vrije Universiteit Brussel, Belgium

Jerome HUBER, Dr., AIRBUS OPERATIONS SAS, Toulouse, France

Marc JACOB, Prof., ISAE-SUPAERO, Toulouse Area, France

Sergey KARABASOV, D.Sci., Queen Mary University, London, UK

Viktor KOPIEV, Prof., Central Aerohydrodynamic Intstitute (TsAGI), Moscow, Russia

Alexey KUDRYAVTSEV, D.Sci., Khristianovich Institute of Theoretical and Applied Mathematics of SB RAS, Novosibirsk, Russia

Ulf MICHEL, Prof., Dr.-Ing., CFD Software E+F GmbH, Berlin, Germany

Alexey MIRONOV, Dr., Central Institute of Aviation Motors (CIAM), Moscow, Russia

Mikhail STRELETS, Prof., Peter the Great St.Petersburg Polytechnic University, Russia

Vladimir TITAREV, Dr., FRC CSC RAS, Central Aerohydrodynamic Institute (TsAGI), Moscow, Russia

Xin ZHANG, Prof., Hong Kong University of Science and Technology, HONG KONG

ORGANIZING COMMITTEE

Tatiana KOZUBSKAYA, KIAM, Chairman

Anatoly ALEXANDROV, KIAM

Vladimir BOBKOV, KIAM

Ludwig DORODNICYN, MSU

Alexey DUBEN, KIAM

Andrey GOROBETS, KIAM

Marina PRIMAK, KIAM

Larisa SOKOLOVA, KIAM,

Mikhail SURNACHEV, KIAM

Vladislav VERSHKOV, TsAGI

Natalia ZHDANOVA, KIAM

INVITED LECTURES

AEROACOUSTIC CHARACTERIZATION OF TURBO-MACHINERY

Mats Åbom

KTH-The Royal Inst. of Technology, Marcus Wallenberg Laboratory for Sound and Vibration Research, SE-100 44 Stockholm, matsabom@kth.se

Acoustic analogies such as Lighthill can be regarded as linear aero-acoustic models which imply that they can be formulated using so called "multi-ports". A multi-port model has a "passive" part describing the scattering and an "active" part describing the sound generation. Multi-port techniques are particularly useful for ducted systems where the acoustic field can be projected on a known basis of acoustic modes [1]. Assuming a time-invariant system a multi-port can in the frequency domain be described by:

$$\mathbf{p}_+ = \mathbf{S}\mathbf{p}_- + \mathbf{p}_{+s} \ , \qquad (1)$$

where $\mathbf{p}$ is a state-vector containing acoustic modal pressure amplitudes, $\mathbf{S}$ is the scattering matrix ("passive" part), $\mathbf{p}_{+s}$ is the source vector or "active" part and +/- denotes propagation out from or into the system.
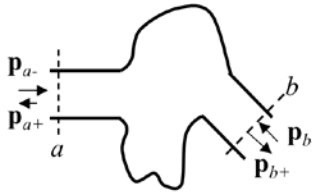

Fig. 1. A ducted multi-port with two openings *a* and *b*

The projection of the field on acoustic modes reduces the effect of turbulence in the data and further improvement is possible by combining data at different cross-sections. Note that the form of Eq. (1) implies that the source data ($\mathbf{p}_{+s}$) is reflection-free, i.e., it corresponds to an infinite system. This is very convenient both in experiments and for numerical modelling and facilitates comparison of numerical and experimental data. In principle a multi-port gives a complete acoustic characterization of a ducted component and any duct system with turbo-machines can be reduced to a network of multi-ports. At KTH experimental techniques for multi-port eduction have been developed since the 1990's [2–5]. More recently multi-port methods have with success also been applied to numerical data and here examples of these efforts will be presented.

The general procedure to determine a multi-port is based on a two-step method. First the system is tested by sending in waves ("modes") and determining the reflected and transmitted waves. If the multi-port is active filtering or correlation methods are applied to eliminate the influence of the source field on the procedure. In the second step the active part is determined by applying Eq. (1) with a known $\mathbf{S}$.

Kierkegaard et al. [6] proposed a frequency domain Linearized Navier Stokes Equations method (LNSE) to determine the scattering or "passive" part of multi-ports. The method requires that the background mean flow first is solved, e.g., by a RANS solver and then the LNSE equations can be solved using standard FEM methods. Using a frequency domain approach eliminates absolute instabilities and convective instabilities are controlled by the viscosity. In Ref. [7] Kierkegaard et al. applied the LNSE method to predict whistling for a ducted orifice by computing the complete ("passive") 2-port for the system and applying the Nyquist condition. More recently [8] it has been found that for certain cases, e.g. a T-junction, it is crucial to include eddy viscosity or turbulent dissipation of the acoustic field in the LNSE model.

Alenius et al. [9] applied Large Eddy Simulations (LES) and computed both the "active" and "passive" part of the plane wave 2-port for an orifice plate. The structure of the source part was also studied using so called Dynamic Mode Decomposition ("Koopman modes"). The scattering was computed using harmonic incident waves and turbulence was supressed by time domain averaging as well as projecting the field on a propagating plane wave mode. Using reflection-free boundaries the source part could be directly computed from $\mathbf{p}_+$, i.e., by projecting the pressure on the plane wave mode.

In the most recent KTH work multi-port methods were applied to develop new and more efficient modelling tools for complex duct systems [10]. A key aspect of the work was to apply and test multi-ports also beyond the plane wave range. One example of the results can be found in the paper by Shur et al. [11] analysing an axial fan unit for aircraft climate systems. In the paper the reflection free acoustic source data for the fan is extracted by projecting the field computed using compressible IDDES ("Improved Detached Delayed Eddy Simulation") on the acoustic modes. The results demonstrate the usefulness of the multi-port approach for an adequate comparison of numerical and experimental data. Other results from the work concerns modelling of single and tandem orifice plates, see Sack et al. [12]. The flow modelling is based on a compressible IDDES which is time averaged and used as background flow for a LNSE model of the scattering. The source or "active" part is then computed from IDDES by applying Eq. (1). Note this type of mixed approach is computationally much more efficient then using IDDES or LES to compute both the "passive" and "active" part. Of course with the risk of a larger error for cases when eddy viscosity effects are important.

References

1. H. Bodén and M. Åbom, 1995. Modelling of fluid machines as sources of sound in duct and pipe systems. *Acta Acustica* 3, Dec., pp. 1-12.
2. J. Lavrentjev, M. Åbom and H. Bodén, 1995, A measurement method for determining the source data of acoustic two-port sources. *Journal of Sound and Vibration* 183, 517-531.
3. J. Lavrentjev and M. Åbom, 1995. A measurement method to determine the source-data of acoustic N-port sources. *Journal of Sound and Vibration* 197, 1-16.
4. A. Holmberg, M. Åbom and H. Bodén, 2011. Accurate experimental two-port analysis of flow generated sound. *Journal of Sound and Vibration*, DOI: 10.1016/j.jsv.2011.07.041.
5. S. Sack, M. Åbom, G. Efraimsson, 2016. On Acoustic Multi-Port Characterisation Including Higher Order Modes. *Acta Acustica united with Acustica* Vol. 102, pp 834 – 850.
6. A. Kierkegaard, S. Boij and G. Efraimsson, 2010. A frequency domain linearized Navier-Stokes equations approach to acoustic propagation in flow ducts with sharp edges, *J. Acoustical Soc. of America* 127, 710-719.
7. A. Kierkegaard, S. Allam, G. Efraimsson and M. Åbom, 2012. Simulations of whistling and the whistling potentiality of an in-duct orifice with linear aeroacoustics. *Journal of Sound and Vibration*, Vol. 331, pp 1084-1096.
8. L. Du, A. Holmberg, M. Karlsson and M. Åbom, 2016. Sound amplification at a rectangular T-junction with merging mean flows. *Journal of Sound and Vibration*, Vol. 367, pp 69-83.
9. E. Alenius, M. Åbom and L. Fuchs, 2015. Large eddy simulations of acoustic-flow interaction at an orifice plate. *Journal of Sound and Vibration*, Vol. 345, pp 162-177.
10. https://www.idealvent.eu/
11. M. Shur, M. Strelets, A. Travin, J. Christophe, K. Kucukcoskun, C. Schram, S. Sack, M. Åbom, 2017. Experimental/Numerical Study of Ducted-Fan Noise: Effect of Duct Inlet Shape. *AIAA Journal* 56 (3), pp 979-996.
12. S. Sack, M. Shur, M. Åbom, M. Strelets, A. Travin, 2017. Numerical eduction of active multi-port data for in-duct obstructions. *Journal of Sound and Vibration* 411, pp 328-345.

JET AEROACOUSTICS: SOME INSIGHTS FROM NUMERICAL EXPERIMENTS

Sanjiva K. Lele[1]

[1]*Stanford University, Stanford, USA, lele@stanford.edu*

In this talk I plan to discuss the computational and physical modeling issues, which need to be carefully addressed in numerical simulations of turbulent subsonic and supersonic jets, to achieve accurate prediction of the laboratory measurements of the mean flow, turbulence, and near- and far-field sound radiation, see [1] for details. Next, I will discuss how the simulation data can be used to gain some insights into jet aeroacoustics, such as characterizing the dominant noise source mechanisms and their modeling for engineering purposes. I will also emphasize the use of numerical experiments to learn about sound source mechanisms, and end the talk with a discussion of some open issues.

References

1. S. K. Lele and J. W. Nichols. A Second Golden Age of Aeroacoustics ? Phil. Trans. Roy. Soc. A, 2014, **372**, 20130321.

ON THE IDENTIFICATION OF SOLID SOUND SOURCES VIA THE FFOWCS WILLIAMS-HAWKINGS INTEGRAL

P.R. Spalart

Boeing Commercial Airplanes, Seattle, USA, philippe.r.spalart@boeing.com

The Ffowcs Williams-Hawkings (FWH, [1]) formula shown here in its far-field approximation (eqn. 1) is extremely valuable in computational aeroacoustics, and is widely used to post-process unsteady simulations, in order to calculate the sound at distances beyond the accurate range of the numerical grid. The formula distinguishes the monopole and dipole contributions from the solid surfaces Σ (third and second lines) and that from the quadrupoles present in the fluid (first line). Curle showed that at low Mach numbers, the solid-surface terms dominate [2]. Furthermore, for compact sources, the unsteady force on the body dominates. Very few studies have explicitly included the quadrupoles in the volume, but many have used a permeable FWH surface Σ, which in principle surrounds the quadrupoles, giving valid results independent of Mach number. However, in spite of some serious doubts over the solid-surface approach [3], many people in the field prefer using it, partly due to simplicity and partly because of some difficulties associated with turbulence crossing the permeable surface.

$$4\pi|\mathbf{x}|(1-M_r)p'(\mathbf{x},t) = \frac{x_j x_l}{|\mathbf{x}|^2 c_0^2}\frac{\partial^2}{\partial t^2}\int_V \{T_{jl}\}_{ret}\,dV$$

$$+ \frac{x_j}{|\mathbf{x}|c_0}\frac{\partial}{\partial t}\int_\Sigma \{p'n_j + \rho u_j(u_n-U_n)\}_{ret}\,d\Sigma$$

$$+ \frac{\partial}{\partial t}\int_\Sigma \{\rho_0 u_n + \rho'(u_n-U_n)\}_{ret}\,d\Sigma$$

$$(1)$$

Our purpose is to explore these effects, using two model problems. An additional attraction of the solid-surface approach is the idea of identifying the "true" source of the sound by computing separately the integrals for different components; in a landing gear, one may ask whether the wheel, the door, the post or the cavity "makes more noise," and is therefore the better candidate for noise-reduction technology [4, 5]. We wish to determine whether this "self-evident" argument gives a rigorous and effective approach. Our focus is on air-frame noise, because the neglect of quadrupoles is much less defendable for engine noise. One key feature is the shielding of sound towards various directions; any approach that fails to reflect this shielding will be suspect.

Our first problem does not involve quadrupoles, but leads to the identification of sound sources, and shielding. As shown in Fig. 1a, a dipole is placed

under a sphere. This is a generic model for an aircraft component such as a wheel applying an unsteady force to the fluid. The "straightforward" identification approach would calculate the solid-FWH sound field, and declare that "this is the sound of this part of the airplane." Here, the sound field of the dipole is known analytically. The dipole is injected into the flow field over a small volume, and is therefore "a compact source." We only show cases with a vertical dipole (F_y), but results with a horizontal dipole led to the same conclusions.
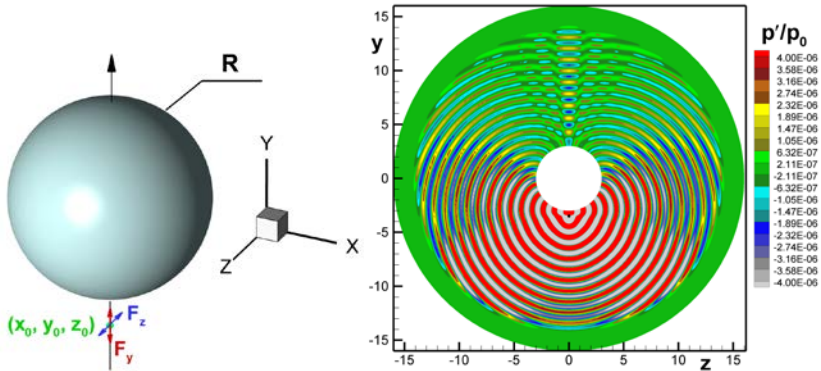
Fig. 1. Dipole placed under sphere; left, geometry; right, pressure field

There is no flow, and the walls are treated as free-slip surfaces. The parameters are as follows: the wave-length is 1/3 times the sphere radius R, and the dipole is ½ a wave-length away from the surface. This creates interference patterns with 45 degrees for the dominant direction, as seen in Fig. 1b; other cases, with different offsets for the dipole, produced different patterns. As could be expected, the shielding by the sphere in the upward direction is very definite.

We now turn to quantitative results, comparing the sound at a distance of 11 wave-lengths λ from the origin. A FWH utility, valid in the near-field, was provided by Drs. A. Dyben and T. Kozubskaya of Keldysh Institute of Applied Mathematics (Moscow) and allows comparisons with the direct output of the simulation, where the grid is still fine; the same conclusions would be reached for far-field sound, but the simulation cannot provide that, since the grid coarsens for large r (and a sponge layer was introduced). In Fig. 2a the simulation result, in magenta, confirms the interference pattern and the shielding seen in Fig. 1b. The peak level at ±45 degrees is 25dB higher than the lowest level, in the straight-up direction. This result is accurately reproduced by the permeable FWH formula, independently of the radius of the FWH sphere (blue and green curves). The sound field of the dipole itself (black), in contrast, does not reproduce shielding; the only difference between the up and down direction is due to the difference in distance (14.5 λ versus 7.5 λ). It also misses the interference

patterns. The sound field of the dipole with an opposite image dipole inside the sphere (not shown) does capture interference, to leading order, but that does not provide a very practical method.
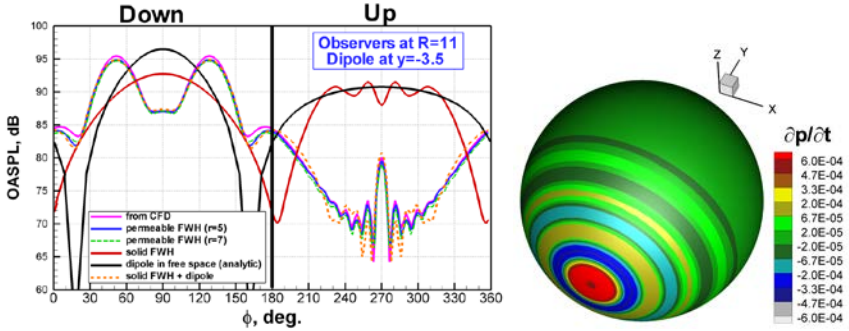

Fig. 2. Left, sound extracted from simulation, and produced by integral formulas; right, FWH surface term on the sphere

Of more interest are the results of the sphere's solid-surface contribution, in red, and its combination with the dipole, in orange. In the upwards direction, the two almost cancel. This combination gives a very accurate answer, almost as good as the permeable formula. On a theoretical basis, this may be unsurprising, since this problem has no quadrupoles. However, in practice, this shows that while the dipole is the true source of sound, the calculation of the sound field must include the sphere's contribution, which in practice would mean the airplane's fuselage and wing. Figure 2b shows the FWH integrand on the sphere, in other words the "footprint" of the dipole. Its extent appears to be a few times the distance from the dipole to the surface.

Next, a generic fuselage with a simplified landing-gear cavity is considered, as illustrated in Fig. 3. This flow having quadrupoles, the results may not be as close to perfection as in the first case, but we expect strong effects of shielding, with the approach separating various parts of the surface in the FWH integral possibly leading to paradoxes.

The flow is treated with Delayed Detached-Eddy Simulation, with most of the fuselage boundary layer in quasi-steady RANS mode, and strong clustering of the grid near the cavity. The Mach number is 0.25 and the Reynolds number based on fuselage diameter D is 10^7. The simulation produces the expected highly unsteady shear layer bounding the cavity, and weaker but fine-scale vorticity in it. Turbulence then propagates along the body. The pressure field is marked by waves with a wavelength slightly longer than D (somewhat controlled by grid spacing).
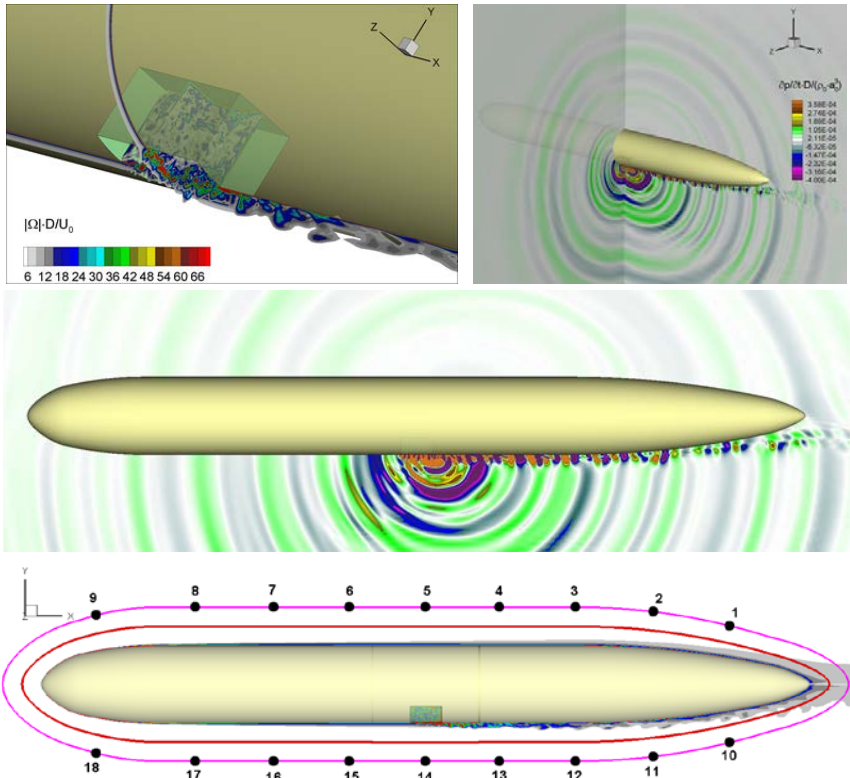
Fig. 3. Simplified landing-gear cavity. Top left, vorticity contours; top right and middle, pressure field (time derivative); bottom, permeable surfaces
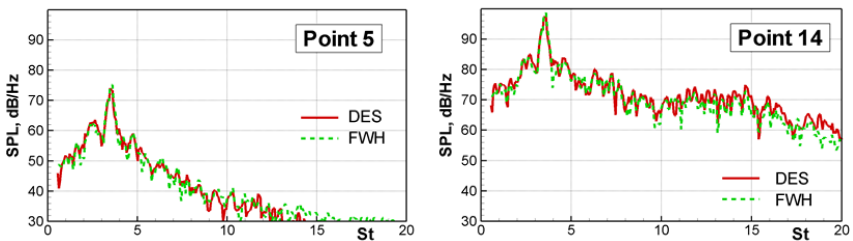

Fig. 4. Spectra from simulation and from permeable-surface integral at two points above and below fuselage (see Fig. 3)

Figure 4 shows that the permeable-surface FWH formula reproduces the sound in the simulation very accurately. This includes the strong sheltering, since the sound level at Point 5, above the body, is about 25dB lower than at

14

Point 14, below it. On the other hand, the spectrum shape for low frequencies is very similar at those two points, which we have not explained yet.
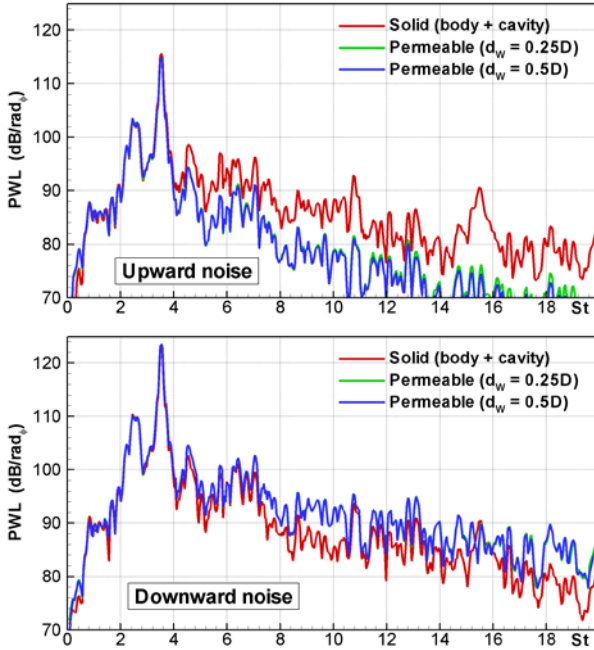

Fig. 5. Sound power levels in the vertical direction with different FWH approaches; far-field results; upper graph: upwards; lower graph: downwards

Figure 5 presents results in the upwards and downwards direction, which are not as simple as for the sphere-dipole case. The difference between directions is weaker than in Fig. 4, around 8dB, due to this applying in the far field.

The solid and permeable results in Fig. 5 are almost identical up to a Strouhal number of 4, and in particular the peak at $St \sim 3.5$ is identical. Given a Mach number of 0.25, this corresponds although loosely with the dominant wave of Fig. 3. For St larger than 4, the two results diverge, and the solid-FWH calculations essentially miss the shielding effect, even though these are results with the full surface (cavity and fuselage skin), an approach which was successful for the sphere-dipole case. This appears to reflect the quadrupole contribution, which would have constructive interference with the surface terms in one direction, and destructive interference in the other direction. The relative success of the solid formula for low frequencies (which would not be relevant in airline practice) has not been explained yet; in particular, a simple argument such as the source being compact does not seem to apply since $\lambda \sim D$.

The dominant frequency is of interest. If we assume that the large eddies in the mixing layer propagate at half the freestream velocity, $St = 3.5$ corresponds to an eddy spacing of $D/7$, which is larger than the visual spacing in the simulation. The Strouhal number based on cavity length L is 1.4, which would approximately correspond with the third Rossiter mode, using

$$St_L = (n-\gamma)/(M+1/\kappa)$$

with $\gamma=0.25$ and $\kappa=0.57$. This is not very conclusive. Finally, the cavity length and depth are 0.4 D and 0.2 D, respectively, so that conjectures based on half- or quarter-wavelength modes are not satisfied either.

Overall, our results strongly support the permeable-surface FWH formula, and indicate that the solid-surface formula can be misleading regarding the actual sources of sound, and in particular fail to capture directional effects.

Acknowledgements

References

1. J.E. Ffowcs Williams, D.L. Hawkings. Sound generation by turbulence and surfaces in arbitrary motion. *Phil. Trans. Roy. Soc. A*, 1969, 264-321.
2. N. Curle. The influence of solid boundaries upon aerodynamic sound. *Proc. Roy. Soc.* **A231**, 1955, 505-514.
3. P.R. Spalart. On the precise implications of acoustic analogies for aerodynamic noise at low Mach numbers. *J. Sound Vib.* **332**, 2013, 2808-2815.
4. J.-C. Giret. Simulations aux grandes échelles des écoulements instationnaires turbulents autour des trains d'atterrissage pour la prédiction du bruit aérodynamique. Thesis, INP Toulouse, May 2014
5. P.R.G. de Azevedo Jr, W.R. Wolf. Noise Prediction of the LAGOON Landing Gear Using Acoustic Analogy and Proper Orthogonal Decomposition. AIAA-2016-2768.

NEXT STEPS IN WIND TUNNEL AEROACOUSTICS: MEASUREMENTS AT FLIGHT-REYNOLDS NUMBERS

Thomas Ahlefeldt

German Aerospace Center (DLR), Göttingen, Germany, thomas.ahlefeldt@dlr.de

In my talk I will present the microphone array measurement technique which was advanced at the DLR Göttingen for the use in cryogenic and/or pressurized wind tunnels [1]. This extends the range for acoustic measurements on scaled aircraft models in start and landing configuration up to real-flight Reynolds numbers. This abstract describes the measurements carried out in the European Transonic Wind Tunnel (ETW) and presents the results.

In the talk I will also give additional examples for measurements performed in a cryogenic wind tunnel [2-3] and give an insight in the comparability of microphone array measurements. In the example chosen, results obtained from the same model but different wind tunnels are being compared [4].

Motivation

The use of microphone arrays to acquire acoustic data of scaled models in wind tunnels has become a standard measurement technique. However, the comparison of the results obtained in the wind tunnel to those obtained at real flight tests usually reveals differences. These differences are attributable to a lack of model fidelity, installation effects, a discrepancy in Reynolds number, and the applicability of the assumptions made in phased array processing [5]. The work presented in the following is focused on the effect of varying Reynolds number.

Measurement setup

The ETW facility is a high Reynolds number transonic wind tunnel with a 2.0 m × 2.4 m closed test section. By injection of liquid nitrogen, the wind tunnel can be operated over a temperature range from 110 K up to 310 K and the total pressure can be varied between approximately 115 kPa and 450 kPa. Thereby the ETW provides a testing environment for full-scale Reynolds numbers and independent variation of Reynolds number, Mach number, and load [6].

Figure 1 shows the measurement setup with the half-model in high lift configuration (scale 1:13.6) in the center of the test section of the ETW. The positioning of the microphones was limited to discrete dummy windows and side wall slots as can be seen on the left side of Figure 1. For the sensors, Brüel & Kjær cryogenic-type sensor of type 4944A were used. This sensor was developed

together with the DLR and the ETW. The corresponding frequency response measurements at different pressures and temperatures were performed in a cryogenic vessel at the ETW site. They exhibited a non-linear combination of the amplitude response caused by varying the static pressure or temperature separately [1,7].

Measurements were taken for several Mach numbers, Reynolds numbers and angles of attack. In order to additionally assess the influence of the different load on the model at higher pressures (deformation), several measurement points were chosen to give the following features: (1) comparisons at same deformation but different Reynolds numbers, (2) comparisons at the same Reynolds number but different deformations. Thus, the effect of the elastic deformation can be separated from the effect of the Reynolds number.
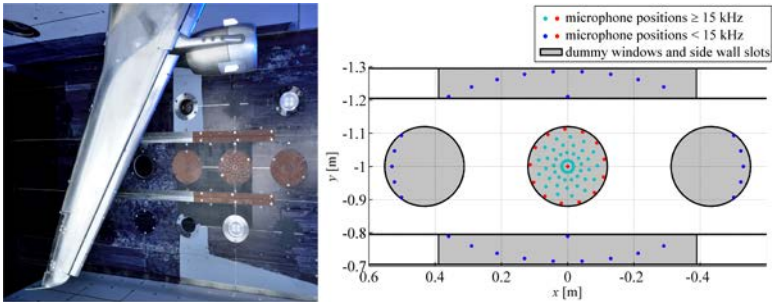

Fig. 1: Photo of the setup and arrangement of microphones.

Algorithms and Assumptions

For the reconstruction of the source auto powers on a chosen grid, the conventional beamforming approach in the frequency domain was used [8].

The limitation for the microphone positioning lead to strong side lobes in the beamforming procedure caused by insufficient spatial sampling. Here, results will be shown using the pseudo-deconvolution method CLEAN-SC [9].

For the calculation of the results, several assumptions are to be made. Independent of the cryogenic/pressurized environment, the phase shift of each reconstructed source was calculated using a point source assumption under homogeneous flow conditions.

For the comparison of results obtained at different temperatures and pressures, the influence of those quantities must be considered in terms of corrections. First, a correction is required to take into account the alteration of the radiated sound pressure caused by the different temperatures and pressures. This correction will be also dependent on the assumptions made for the nature of the source. Here, the main contributing kind of source from the half-model in the

test section is considered to be dipole sources [1]. This correction can be derived from the Ffowcs-Williams–Hawkings solution of the acoustic analogy with surface sources in the far-field. The resulting decibel correction for dipole sources with consideration of different temperatures and static pressures in the test section is given by (for details see [1]):

$$\Delta \ \mathrm{dB} = 20 \log_{10}\left(\frac{\rho a^2}{\rho_0 a_0^2}\right)$$

Here, the density is taken as $\rho_0 = 1.25$ kg$/$m^3 and the speed of sound as $a_0 = 337$ m$/$s (values for pure nitrogen at international standard atmosphere conditions). Second, as an additional normalization approach, the results are be compared at the same Strouhal number to account for the different flow velocities, where even the Mach numbers are still the same at these different temperatures and pressures.

With the application of these assumptions, differences found in a comparison can be related to source mechanisms not scaling as a compact dipole source or with the Strouhal number (i.e., Reynolds number effects, cavity or jet noise).

Experimental Results

The source maps were computed over an equidistant discrete grid with 69,165 grid points covering the region of interest in an observation plane of 1.30×1.32 m on the half-model. Exemplary results are shown in figure 2. It shows a comparison of results at Reynolds numbers of 1.43×10^6 and 20.06×10^6. In general, the source maps exhibit dominant sources at the inboard slats, slat tracks, and flap side edge, with less dominant sources at the flap and the flap track fairings. At a Strouhal number of 20 the source maps are almost equal showing the same source positions and the same level. However, for a Strouhal number of 130, the source map for the real-flight Reynolds number exhibits differences. Sources with a significantly increased noise level appear on the inner flap and on one flap fairing. The sources on the inner flap are the most dominant ones for the real flight Reynolds number case. On the other hand, the sources on the slat are significantly decreased.

For a closer observation, figure 3 shows spectra taken at an angle of attack of 3 deg. Each spectrum represents different areas on the wing, the slat and the flap area. The spectra were calculated by integrating the CLEAN-SC results over the grid points covering the slat or flap area.

For the comparison of the slat spectra one important effect of the Reynolds number can be observed: various slat tone peaks disappear for higher Reynolds numbers. These so called "slat tones" are related to different noise mechanisms occurring at the slat cove. They can be considered a model artifact due to too low Reynolds numbers and manufacturing and handling constraints [10].

The comparison of the flap sources also shows various differences for both Reynolds numbers. First, a hump is visible at a Strouhal number of 40, related to the flap side edge showing a slight shift of the Strouhal number as well as of its source strength. Of major significance are two large broadband increases appearing in the Strouhal number range of 100 to 150 and 170 to 200 at the flight Reynolds number. These humps are related to sources on the inboard flap (see figure 2) and the outboard flap showing a level increase of approximately 10 dB.

$St_{1/3oct} = 20$ ($f_{full-scale,1/3oct} = 360$ Hz), M = 0.203, α = 3 deg

$St_{1/3oct} = 130$ ($f_{full-scale,1/3oct} = 2.4$ kHz), M = 0.203, α = 3 deg
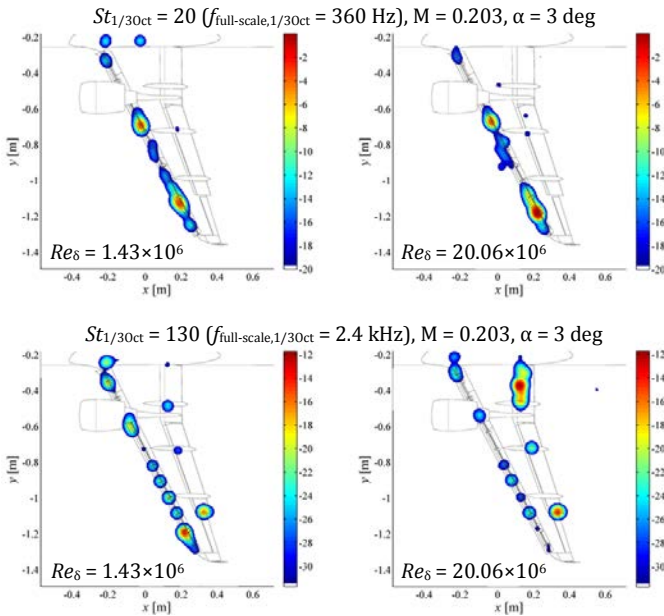
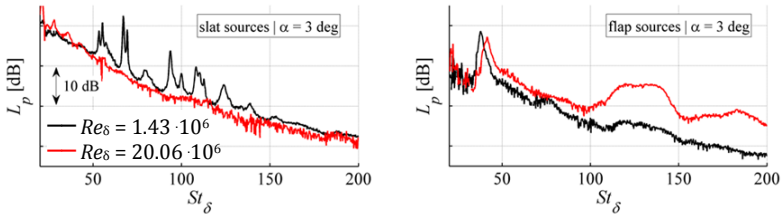Fig. 2: Comparison of source maps at different Reynolds numbers.

Fig. 3: Comparison of spectra at different Reynolds numbers (red).

In summary, several sources with a significant Reynolds number dependence were being shown. These include dominant sources on the flap at real flight Reynolds number and various peaks in the spectra with combined Strouhal and Reynolds number dependencies. The ability of measuring airframe noise at real flight Reynolds numbers now gives the possibility of separating the effect of the Reynolds number from the effects of model fidelity and Mach number on aeroacoustic behavior.

References

1. Ahlefeldt, T. "Microphone Array Measurement in European Transonic Wind Tunnel at Flight Reynolds Numbers," AIAA Journal, Vol. 55, No. 1, 2017, pp. 36–48.
2. Ahlefeldt, T., and Koop, L., "Microphone Array Measurements in a Cryogenic Wind Tunnel," AIAA Journal, Vol. 48, No. 7, 2010, pp. 1470–1479.
3. Ahlefeldt, T., "Aeroacoustic Measurements of a Scaled Half-Model at High Reynolds Numbers," AIAA Journal, Vol. 51, No. 12, 2013, pp.2783–2791.
4. Spehr C., Ahlefeldt T., "Comparison of Microphone Array Measurements in the Closed Test Section of LSWT and ETW," CEAS Aeronautical Journal, (forthcoming, accepted for publication 02-2018)
5. R.W. Stoker, R. W., Guo, Y. P., Street, G., and Burnside, N., "Airframe Noise Source Location of a 777 Aircraft in Flight and Comparisons with Past Model Scale Tests," Ninth AIAA/CEAS Aeroacoustics Conference, AIAA Paper 2003-3232, 2003.
6. Quest, J., "ETW—High Quality Test Performance in Cryogenic Environment," 21st Aerodynamic Measurement Technology and Ground Testing Conference, AIAA Paper 2000-2260, 2000
7. Ahlefeldt, T., and Quest, J., "High-Reynolds Number Aeroacoustic Testing Under Pressurised Cryogenic Conditions in PETW," 50th AIAA Aerospace Sciences Meeting Including the New Horizons Forum and Aerospace Exposition, AIAA Paper 2012-0107, 2012
8. Sitsma, P., "Experimental Techniques for Identification and Characterisation of Noise Sources," National Aerospace Lab. NLR Rept. NLRTP-2004-165, 2004
9. Sitsma, P., "CLEAN Based on Spatial Source Coherence," International Journal of Aeroacoustics, Vol. 6, No. 4, 2007, pp. 357–374
10. Dobrzynski, W., "Almost 40 Years of Airframe Noise Research: What Did We Achieve?" Journal of Aircraft, Vol. 47, No. 2, 2010, pp. 353–367

CONTRIBUTED TALKS

ON THE DEVELOPMENT OF NUMERICAL TECHNUQUE OF ROTOR AERACOUSTICS AND AERODIMAMICS CHARACTERISTICS IN FORWARD FLIGHT

I.V. Abalakin[1], **V.G. Bobkov**[1], T.K. Kozubskaya[1],
B.S. Kritsky[2], R.M. Mirgazov[2]

[1]*KIAM RAS, Moscow, Russia, bobkov@imamod.ru*
[2]*TsAGI, Zhukovsky, Russia, boris.kritsky@yandex.ru*

The results of four-blade rigid rotor with fixed blades pitch angles in forward flight CFD simulation are presented.

The numerical method used for prediction of rotor aerodynamic and acoustic characteristics implemented in in-house code NOISEtte [1] is based on a finite-volume discretization of Navier–Stokes equations using a higher-accuracy numerical scheme for unstructured hybrid meshes [2]. The numerical technique was successfully tested on a number of hovering rotor simulation problems [3, 4].

The flow in the near field around a rotor rotating at an angular velocity $\boldsymbol{\omega}$ is governed by the system of Navier–Stokes equations in a noninertial coordinate system, written in the form of conservation laws relative to the absolute velocity vector:

$$\frac{\partial \rho}{\partial t} + \operatorname{div} \rho(\mathbf{u} - \mathbf{V}) = 0$$

$$\frac{\partial \rho \mathbf{u}}{\partial t} + \operatorname{Div} \rho(\mathbf{u} - \mathbf{V}) \otimes \mathbf{u} + \nabla p = \operatorname{Div} \mathbf{S} - \rho(\boldsymbol{\omega} \times \mathbf{u}) \qquad (1)$$

$$\frac{\partial E}{\partial t} + \operatorname{div}(\mathbf{u} - \mathbf{V})E + \operatorname{div} \mathbf{u}p = \operatorname{div} \mathbf{q} + \operatorname{div} \mathbf{S}\mathbf{u}$$

where $\mathbf{V} = \boldsymbol{\omega} \times \mathbf{r}$ is the linear speed of rotation of the blade, $\mathbf{q}$ is the heat flux and $\mathbf{S}$ is the stress tensor.

For the spatial discretization of system (1) the original Edge-Based Reconstruction (EBR) scheme of higher accuracy [5] and its WENO version supporting the solutions with sharp gradients and discontinuities [6] where used. For smooth solutions these schemes provide the accuracy not less than of the second order for arbitrary unstructured meshes, and of the fifth or sixth orders for translationally symmetric meshes (i.e. uniform grid-like meshes). The higher accuracy of the EBR scheme is achieved by quasi-one-dimensional reconstructions of the variables on the extended edge-oriented stencils.

An explicit time integration scheme is restricted to unacceptably small time steps, since spatial mesh steps in boundary layer zones near solid walls are typically very small. For this reason, the time integration is performed using an implicit 2-nd order scheme with Newton linearization, which allows advancing in time with sufficiently big time steps.

The acoustic characteristics of a rotor in the far field are modeled using the integral formulation "1A" proposed by Farassat [7] on a base of the Ffowcs Williams – Hawkings (FWH) method. This "1A" formulation admits use of a control surface of an arbitrary shape but the velocity the points of the control surface is assumed to be subsonic. Otherwise, when passing over the speed of sound, the integral formula contains a singularity that makes it difficult to apply the FWH for a rotating rotor. Original solutions for this problem was proposed by authors in [8]. The key idea of this modification is the parameterization of the control surface in the absolute inertial system associated with the fuselage of the helicopter instead of the rotating coordinate system associated with the rotor. It is assumed that the control surface is a surface of revolution about the axis of the rotor. This assumption keeps the surface undeformable under the proposed parameterization. In addition, the use of a uniform grid in spherical coordinates allows simple interpolation of variables and calculation of the angular derivative at any point on the control surface. As a result, the problem reduces to calculating the surface integral with delay, with the necessary data on the surface, moving translationally with respect to the background flow. This problem is easily solved by using the "1A" formulation.

As mentioned above, the proposed approach was used for rotor aerodynamics and acoustics simulation in hovering mode. The paper represents the first author's experience of forward flight rotor simulation.
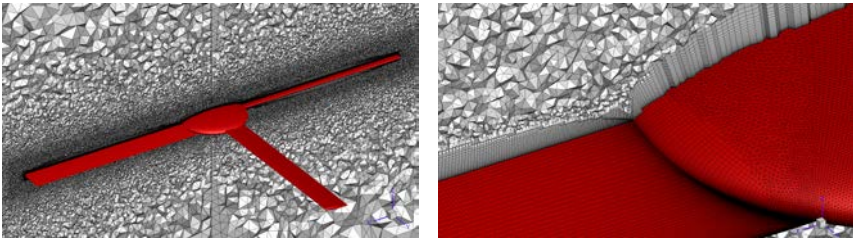

Fig. 1. Computational mesh for four-bladed rotor: overall view (left)
and boundary layers on the blade and hub (right)

The scaled rotor which is a four-blade rotor with radius 1.2 m rotating at 360 RPM in a forward flight mode with velocity 11.31 m/s. Its blades are installed at 8° pitch angle. The blade surface is formed by the NACA-23012 airfoil without twist. The Reynolds number, $Re = 0.6 \times 10^6$, is based on the chord of

the blade 0.15 m and the blade tip velocity 45.24 m/s. The rotor hub represented by ellipsoid (Fig. 1 left).

A DES approach with the SST model has been used in the simulation on a hybrid tetra-dominant mesh with 31M nodes and 136M elements with prismatic boundary layers on the blade and hub surfaces (Fig. 1 right).
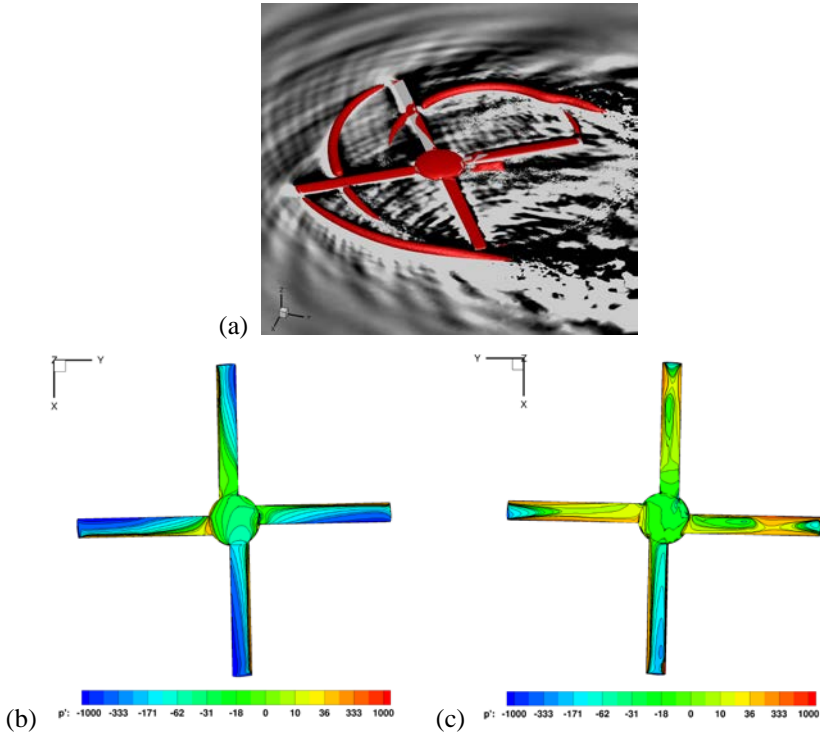

(a)

(b)

(c)

Fig. 2. Vortices structure (Q-criterion isosurfaces) and pressure pulsations time derivative in the rotor rotation plane (a) and gauge pressure distribution on the rotor top (b) and bottom (b) surfaces

The rotor aerodynamics and acoustics were evaluated. Figure 2a shows Q-criterion isosurfaces in the rotor near field. As can be seen there are blade tip vortices drifted downstream by the external flow. The pressure derivative field in the rotor rotation plane on the same figure shows several acoustic sources: point sources on the blades tips, distributed sources on the vortices surfaces and acoustic pulsations produced by interacting blade with vortical flow structures. The overall top and bottom surface pressure distribution on the rotor (Fig. 2b, c) shows thrust presence and pressure field irregularity on the blades due to blade-

vortex interaction. The acoustic and aerodynamic rotor properties are in good agreement with the theoretical and experimental data.

References

1. I.V. Abalakin, P.A. Bakhvalov, A.V. Gorobets, A.P. Duben and T.K. Kozubskaya. Parallel research code NOISEtte for large-scale CFD and CAA simulations. Vychisl. Metody Programm., 2012, v.13(3), pp. 110–125 (in Russian).
2. I.V. Abalakin, V.G. Bobkov, T.K. Kozubskaya. Multimodel approach for helicopter rotor aeroacoustic and aerodynamic characteristics modeling using numerical simulation. Keldysh Institute preprints, 2018, v.47, 32 p., DOI: 10.20948/prepr-2018-47 (in Russian).
3. I.V. Abalakin, V.A. Anikin, P.A. Bakhvalov, V.G. Bobkov, and T.K. Kozubskaya. Numerical investigation of the aerodynamic and acoustical properties of a shrouded rotor. Fluid Dynamics, 2016, v.51, pp. 419–433, DOI:10.1134/S0015462816030145
4. Abalakin Ilya, Anikin Viktor, Bakhvalov Pavel, Bobkov Vladimir, Kozubskaya Tatiana. Numerical simulation of aerodynamic and acoustic characteristics of a ducted rotor. Math. Mod. and Comp. Simul., v. 8(3), 2016, pp. 309–324, DOI:10.1134/S2070048216030030.
5. Ilya Abalakin, Pavel Bakhvalov and Tatiana Kozubskaya. Edge-based reconstruction schemes for unstructured tetrahedral meshes. Int. J. Numer. Meth. Fluids, 2016, v. 81(6), pp.331–356, DOI: 10.1002/fld.4187.
6. P. Bakhvalov and T. Kozubskaya. EBR-WENO scheme for solving gas dynamics problems with discontinuities on unstructured meshes. Comput. Fluids, 2017, v.157, pp. 312–324, DOI:10.1016/j.compfluid.2017.09.004.
7. F. Farassat. Derivation of formulations 1 and 1A of Farassat. NASA Technical Memorandum 2007-214853, NASA, Langley Research Center, Hampton, Virginia, March 2007.
8. Pavel Bakhvalov, Vladimir Bobkov, and Tatiana Kozubskaya. Technology to predict acoustic far-field disturbances in the case of calculations in a rotating reference frame. Mathematical Models and Computer Simulations, 2017, v. 9(6), pp. 717–727, DOI: 10.1134/S2070048217060035.

SYNTHETIC JETS INFLUENCE ON NOISE LEVEL AND ITS SPECTRAL PROPERTIES FOR OFF-DESIGN SUPERSONIC JET USING RANS/ILES-METHOD

L. Benderskiy, D. Lubimov, **N. Polnyakov**

Central Institute of Aviation Motors, Moscow

lyubimov@ciam.ru; leosun.ben@gmail.com; pilotnikita@gmail.com

Reducing of potential core of supersonic jets is required in various applications. This can be achieved by using two techniques: passive control (chevron jets, lobed mixers etc.) and active control (fluid injection from the micro jets to main jet). Synthetic jets (SJ) have noticeable advantages in comparison with other control techniques: they don't have working fluid and mains for its supply. However, this type of turbulent jets control is insufficiently studied due to the experimental investigation complexity or even its impossibility.

The RANS/ILES high resolution method [1] was applied to investigate SJ influence on initial section length and noise level in off-design supersonic jet from bi-conical nozzle that was studied in [2] (Fig. 1a). The temperature and pressure of ambient air is $P=100\,kPa$, $T=300\,K$. Nozzle pressure ratio is NPR=4. The total temperature at the nozzle inlet is $T^*_{in}=300\,K$. The static pressure is fixed for outlet boundary and other parameters have zero derivatives with respect to normal to the boundary. The far field asymptotic of the jet is used for outside boundary. The Re number by parameters at nozzle exit and its diameter D_e is 2.1×10^6 and adiabatic index is $\gamma = 1.4$.
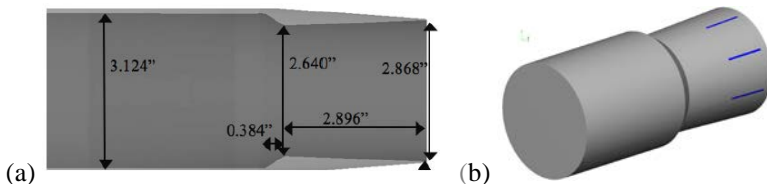

Fig. 1. (a) Nozzle geometry [2] (dimensions are in inches), (b) SJ slits location

Calculations are carried out on structured grid containing 40.3×10^6 cells that showed good agreement with available experimental data [2, 3] and calculations [2, 4].

Simulations of SJ were carried out using approximate boundary conditions [5]. SJ were injecting from eight rectangular slits inside nozzle with step of 45° in azimuthal direction as on Fig 1b. The long sides of slits were oriented along the longitudinal axis of the nozzle. Shape of slits and operating modes of SJ were chosen according to [5]. There are two parameters that determine operating mode of SJ: amplitude and frequency. The amplitude and frequency range was: $q = 50..200$ m/s, $f = 60..300$ Hz.

Simulation results analysis shows that applying of SJ with operating modes considered above reduce the length of initial section of main jet (Fig. 2). Table 1 shows operating modes of SJ and potential core length of main jet respectively. Reducing length of jets initial section and potential core can be explained by intensification of main jet`s mixing with ambient air. As a result, this process increases pulsations of pressure and velocity in shear layer.
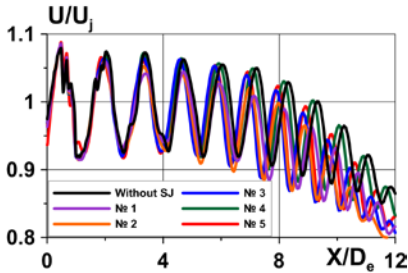

No.	q, m/s	f, Hz	L_{PC}, X/D_e
Without SJ			9.354
1	50	60	7.236
2	50	100	7.124
3	50	200	8.018
4	50	300	9.2
5	200	200	8.11

Fig. 2. Distribution of averaged longitudinal velocity along jet axis

Table 1. SJ operating modes and potential core length

It can be seen that frequency of SJ exerts the greatest influence on the initial section comparing to amplitude (No.1–4 comparing to No.3 and No.5). Reducing length of initial section by 24% was achieved on operating mode №2 with amplitude q = 50 m/s and frequency f = 100 Hz.

The noise level at near field of jet amplifies corresponding to potential core reducing and pulsation of pressure increasing. Fig. 3 shows noise level at near field. That data was obtained from line starting from 1.5D above the nozzle exit at angle of 7.4°. The good agreement can be seen between simulation data on operating mode without SJ and experimental data [2] up to X/D_e=10.
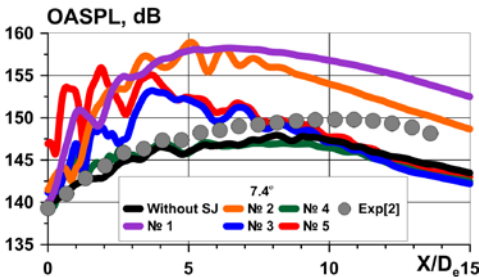

Fig. 3. SJ influence on noise level at near field

SJ frequency in operating mode №1 corresponds to Strouhal number Sh = 0.27 and is equal to frequency of screech. In Fig. 3 and Fig. 2 it can be seen that as the first natural mode of SJ oscillation approaches to the frequency of screech the overall sound pressure (OASPL) of jet at near field increases. As we can see on Figs. 4a and 4b SJ on operating mode №2 reduce power spectra density (PSD) of screech by 9 dB, but increase it on the natural mode frequency up to 137 dB. However, there is no influence on power spectra density of screech on operation mode №1.
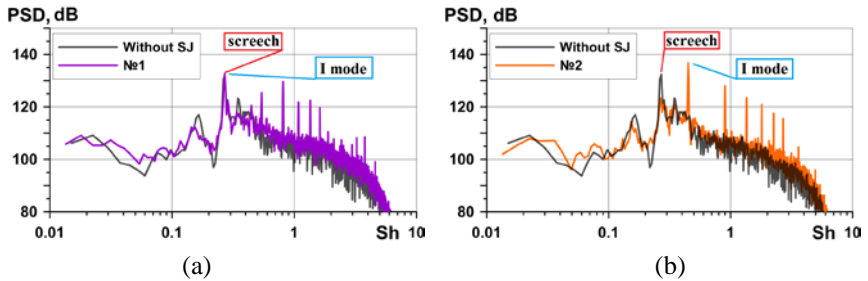
Fig. 4. SJ influence on power spectra density at near field
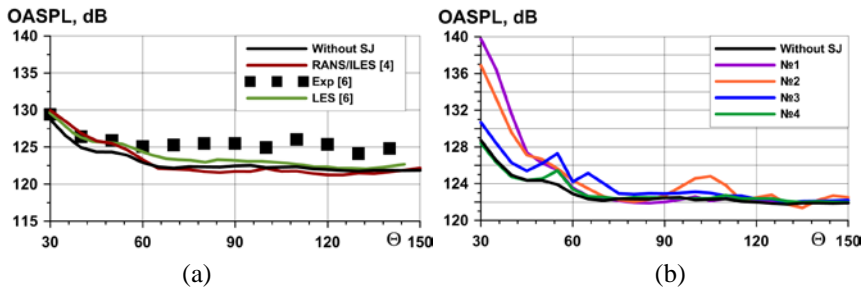

Fig. 5. Dependence of OASPL on observation angle at far field. (a) comparing with experimental data and calculations, (b) SJ influence

Fig. 5 shows noise level at far field dependence on observation angle for operating modes No.1–4. The distance between the microphones and the jet is $R/D_e=47$. The good agreement between this simulation of free jet and experimental data [6] and calculations [4, 6] can be seen in Fig. 5a. Calculation error is not more than 3%.

There are a local increases in OASPL on all operation modes of SJ and without SJ on observation angle $\theta=55°$ (Fig. 5b) and local maximum of noise on angle $\theta=110°$ on operating mode No.2. The highest influence on noise level at far field has mode No.1 and No.2.

Fig. 6 shows power spectra density for observation angles $\theta = 30°$ and $150°$ for operation modes No.1 and No.2. Noise increases on the frequency of the first and other natural modes of SJ oscillation. Screech can be observed in Fig. 6b on frequency Sh=0.27 with PSD=130 dB on operation mode without SJ. On operation mode No.2 PSD of screech decreasing by 5 dB, yet it increases by 10 dB on fundamental frequency of SJ.

Applying of SJ allowed to reduce the length of initial section by quarter. Operation mode of SJ that decreases noise level of screech on 15 dB was found. However, that operation mode increases noise level on fundamental frequency of SJ and its overtones.
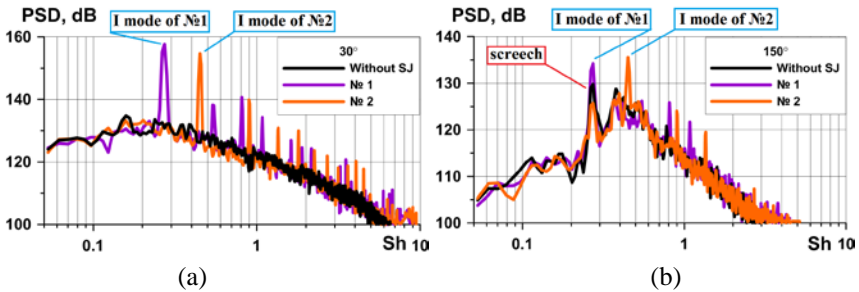
Fig. 6. Power spectra density on observation angles: (a) 30°, (b) 150°

References

1. Lyubimov, D.A. Development and application of a high-resolution technique for Jet flow computation using large eddy simulation, High Temperature, 50(3), 420-436, (2012).
2. Liu, J., Corrigan, A., Kailasanath, K., Ramammurti, R., Heeb, N., Munday, D., Gutmark, E. Impact of Deck and Jet Blast Deflector on the Flow and Acoustic Properties of Imperfectly Expanded Supersonic Jets, AIAA P., 2013-323, (2013)
3. Lau, J.C. Effects of exit Mach number and temperature on mean-flow and turbulence characteristics in round jets, J. Fluid Mech., 105, 193-218, (1981).
4. L. Benderskiy, D. Lyubimov, A. Chestnyh Effect of airport surface and jet blast deflector on supersonic jets noise using RANS/ILES-method // Proceedings of the 24rd International Congress on Sound and Vibration (ICSV24), London (United Kingdom), 23-27 July 2017, ISBN 978-1-906913-27-4.
5. Lyubimov D.A., Potekhina I.V. Application of the RANS/ILES method in analyzing the efficiency of the control of separation flows in diffusers using synthetic jets, Fluid Dynamics, 4, 144-154, (2015)
6. Liu, J., Corrigan, A.T., Kailasanath, K., Heeb, N.S., Munday, D.E., Gutmark, E.J. Computational Study of Shock-Associated Noise Characteristics Using LES, AIAA P., 2013-2199, (2013).

INFLUENCE OF THROTTLING AND SYNTHETIC JETS ON SPECTRAL PROPERTIES AND PRESSURE PULSATIONS LEVEL IN THE AIR INTAKE INTEGRATED WITH THE AIRFRAME USING RANS/ILES METHOD

L. Benderskiy, D. Lubimov, **A. Terekhova**

Central Institute of Aviation Motors, Moscow,

lyubimov@ciam.ru; leosun.ben@gmail.com; alexa.terekhova@yandex.ru

During development of an advanced aircraft, various options of integrating a power plant with an airframe of the aircraft are considered. As a rule, power plants located in the tail part of the airframe or on the wing are considered. The close arrangement of the air intake (AI) to the airframe of the aircraft leads to the fact that a thick boundary layer, which was formed on the elements of the airframe, enters the AI inlet. This, in turn, causes a great unevenness of the flow in and at the outlet of the AI itself.
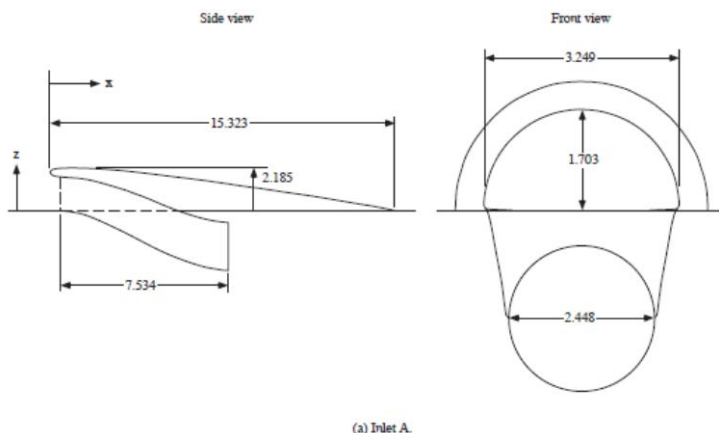

(a) Inlet A.

Fig. 1. General view of the AI geometry from the report [1]

An additional factor that increases the unevenness is the complex form of the AI (Fig. 1). It is D-shaped in the inlet and round in the outlet. In the longitudinal section, the AI diffuser is S-shaped. These factors lead to the formation of two longitudinal vortices of high intensity in the AI, which carry a low-velocity and low-energy flow from the walls of the diffuser to the core of the flow (Fig. 2).
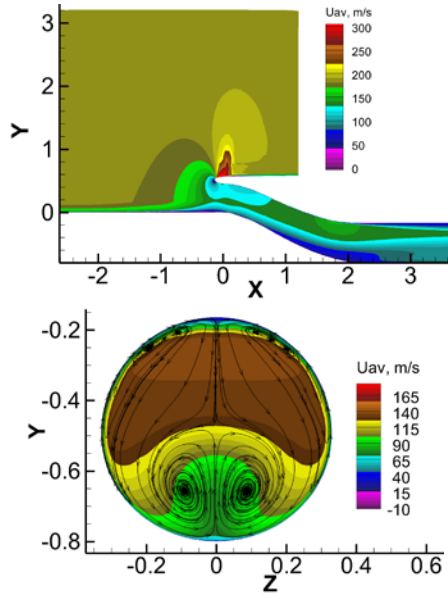
(a) section z/W=0   (b) section x/W=2.37

Fig. 2. Average longitudinal velocity fields in the AI

A large outlet AI unevenness can lead to a malfunction of the engine. In order to reduce it, various flow control methods are used: passive and active – gas-dynamic. One of the perspective methods of gas-dynamic control is synthetic jets. Their advantage lies in compactness, independence from the working fluid and the possibility of shutdown. The work of synthetic jets is reduced to alternating cycles of blowing gas into the flow from a closed cavity by changing its volume and then sucking into it a low-energy external flow. The cavity communicates only with the external flow, so the total gas flow rate is zero. In this way, synthetic jets have a noticeable advantage in comparison with other methods of gas-dynamic control: the absence of working fluid and equipment for its supply and removal. For practice, it is important to know the effect of synthetic jets not only on the unevenness of the parameters distribution in the circumferential and radial directions, but also on the spectral properties of pressure pulsations in the AI that change during the work of synthetic jets.

In this study, the flow in the AI [1], mounted on an airframe simulator plate, was researched. At the entrance to the calculation area, a boundary layer with a thickness $\delta/W=0.1544$ was set, whose profile was close to the profile of the turbulent boundary layer (W is the width of the entrance to the AI). The pronounced turbulent nature of the flow in the AI and the need to calculate turbulent pulsations, primarily of pressure pulsations, require the using of vortex-

resolving approaches. For this reason, a high-resolution RANS/ILES method [2] was used.

The calculations were carried out on a structured grid of 7×10^6 cells. The regime parameters were taken from [1]. Mach number of the external flow was 0.83, Reynolds number Re=1.3×10^6. The total parameters at the inlet to the calculation area were: P_{in}^*=220632 Pa, T_{in}^* = 144 K, static pressure at the outlet was 140431 Pa. The static pressure at the outlet from the AI channel was varied to obtain a characteristic curve. In the course of the calculations, the throttling coefficient of the AI φ was varied, several variants of the regime parameters and positions of the synthetic jets were considered.

Fig. 3 shows the distribution of pressure pulsations along the top and bottom walls, depending on the throttling degree in the AI without synthetic jets. The derivative of the longitudinal generatrix of the channel AI is torn in the output section. The curvilinear shape of the diffuser in the transverse direction turns into a circular one, and there is a slight increase of noise, which is characteristically of all the investigated φ. The pressure pulsations distribution along the top wall is qualitatively the same for the throttling degrees greater than 0.693. One can observe the peaks appearance in pressure pulsations for the throttling degrees less than 0.693. This is due to the appearance of supersonic areas, and the peaks appear precisely in the places of these supersonic areas. The peaks appear for φ more than 0.626 on the bottom wall.
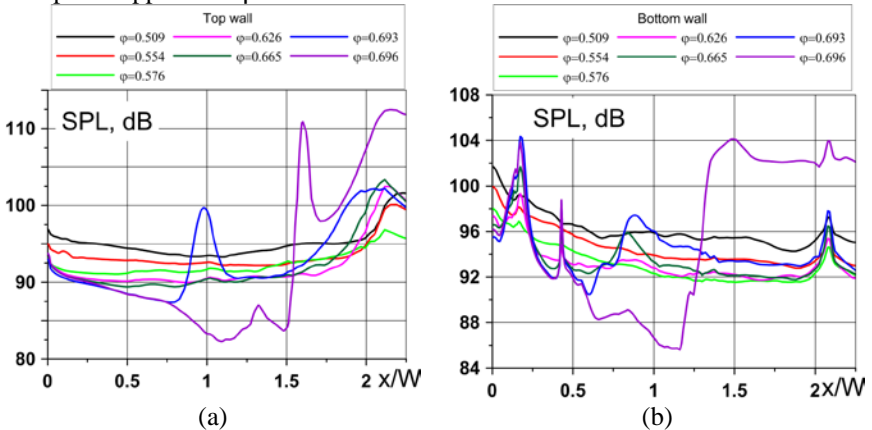

Fig. 3. Throttling influence on the integral level of pressure pulsations along the top and bottom walls of the AI

The efficiency of the synthetic jets was investigated at the operating mode (φ=0.576). Four parameters were varied: the location for blowing out synthetic jets, the amplitude q, the jets frequency f, and the angle α between the blowing-out vector of the synthetic jets and the wall. It was possible to find such options

of synthetic jets (No. 1 and No. 2) that would destroy the pair vortices formed inside the diffuser, and reduce the uneven distribution of the total pressure by 13.3% and 4.8%, respectively. Option number 1 – the pyramidal arrangement of six slits for blowing out synthetic jets on the diffuser bottom wall – the amplitude was 150 m/s, the frequency was 100 Hz. Each slit is located along the stream and the distance between them increases as it passes through the diffuser. Blowing out is carried out at an angle of 45 ° to the wall, the length of the slit was L/W≈0.28. Option number 2 – uniform arrangement of slits for blowing out synthetic jets on the diffuser bottom wall – amplitude was 150 m/s, frequency was 100 Hz. There were only six slits and each was located along the stream at equal distances from each other. Blowing out was carried out at an angle of 30° to the wall, the length of the slit was L/W≈0.29. Fig. 4 shows the influence of these synthetic jets on the total pressure pulsations level along the top and bottom walls.
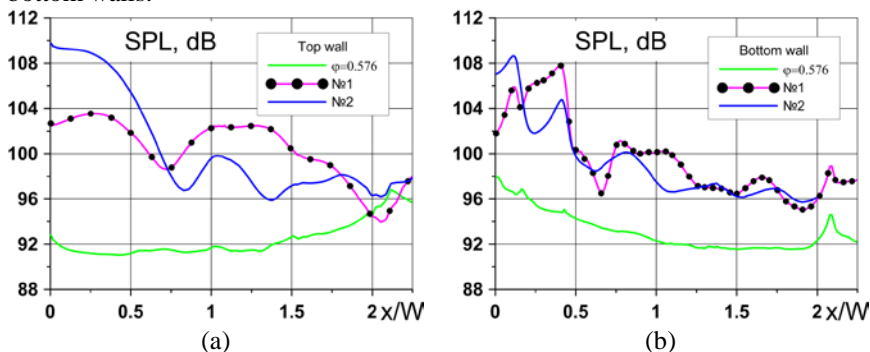

<table>
<tr><td>(a)</td><td>(b)</td></tr>
</table>

Fig. 4. Synthetic jets parameters influence on the integral noise level along the top and bottom walls

The zone of our special interest is the outlet section. It can be seen that the pressure pulsations level increases with using of synthetic jets and the curves qualitatively have a different character. Nevertheless, on the top wall in section x/W=2 the pulsations level does not change (Fig. 4a), but on the bottom wall it increases by 4 dB (Fig. 4b). Moreover, the peak area in the outlet section is retained for both options of synthetic jets, which can be seen well in Fig. 4b.

Oscillograms of the static pressure were recorded for a detailed study of the spectral properties of pressure pulsations at several points on the AI walls. Based on these data, narrow-band spectra of pressure pulsations were received for various throttling values, both for the AI without and with synthetic jets.

References

1. Berrier B.L., Carter M.B., and Allan B.G. High Reynolds Number Investigation of a Flush-Mounted, S-Duct Inlet with Large Amounts of Boundary Layer Ingestion // NASA/TP. 2005. №213766. 170P.
2. Lyubimov, D.A. Development and application of a high-resolution technique for Jet flow computation using large eddy simulation, High Temperature, 50(3), (2012).

TOWARDS AFFORDABLE CAA SIMULATIONS OF AIRLINER'S WINGS WITH DEPLOYED HIGH-LITF DEVICES

V. Bobkov, **A. Gorobets**, A. Duben, T. Kozubskaya,V. Tsvetkova
KIAM RAS, Moscow, Russia, cherepock@gmail.com

Vortex-resolving approaches allow to more accurately predict integral properties (lift, drag, moments, etc.) and, more importantly, to obtain non-stationary aerodynamic and acoustic characteristics. However, the use of such simulations in industrial applications is limited due to a high computing cost that arises from spatial and temporal resolution demands. The goal of the present work is to find the ways to reduce the cost of numerical prediction of aerodynamic and acoustic characteristics of a swept wing with high lift devices.

Modeling of a high aspect ratio wing requires large areas of high spatial resolution along the wingspan. Reducing the problem to a small section of a wing could be a solution. To that end, spanwise periodic boundary conditions can be applied for an unswept wing. For a swept wing there is no such a statistically uniform direction. In this case we propose to combine a RANS-resolution computing domain for a wing with a short in span LES-resolution zone inside it for capturing unsteady aerodynamic and acoustic properties.

In order to elaborate this methodology we begin with studying the well-known model configuration NASA MD-30P30N [1] that represents an unswept wing with deployed high-lift devices. This configuration allows to obtain a reasonable-quality numerical solution at rather low costs by apply periodic boundary conditions. The algorithm of our study consists of several stages:

1) compute the reference case 30P30N with periodic boundary conditions and compare it with the available experimental and numerical data;
2) investigate the potential of computing cost reduction: coarsening the resolution (especially in spanwise direction), using wall functions, optimizing mesh concentration and position of FW/H surface, etc., and analyze the corresponding changes in quality of results;
3) using the experience obtained at stage 2 in reducing the costs, compute the 30P30N case applying the approach with partial LES-resolution and compare results with the reference;
4) apply the proposed approach to a whole swept wing with deployed high-lift devices.

The present work covers stages 1) and 2) of this algorithm. The 30P30N configuration was computed using a mesh of 36 million nodes made by extrusion of a 2D base mesh in the spanwise direction. The spatial resolution of this mesh, denoted Mesh1, is in agreement with numerical studies of other authors [2]. The NOISEtte code based on the higher-accuracy EBR scheme [3] was used to perform the simulation. The distance from the turbulent zone of the

flow to the FW/H surface was minimized in order to reduce the high-resolution area. At the same time the surface was placed far enough from turbulent fluctuations and short-range spurious oscillations. The view of the instantaneous flow field and the FW/H surface are shown in Fig. 1.

Then, two reduced-resolution simulations have been carried out: one with the mesh derived from Mesh1 by coarsening it twice in the spanwise direction, denoted Mesh2, and another with the mesh derived from Mesh2 by reducing twice the number of nodes in the base 2D mesh, denoted Mesh3. Mesh2 and Mesh3 have 2 and 4 times less nodes than Mesh1, respectively.

The simulation technology focused on reduction of computing cost will be presented in detail. Comparison of results on the three meshes with experimental and numerical data and evaluation of quality of the obtained results is to be presented as well.
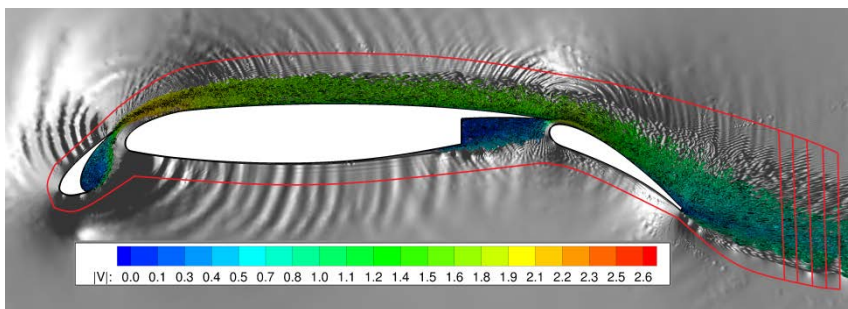
Fig. 1. Instantaneous flow field and FW/H surface contour

References

1. Kyle Pascioni, Louis N. Cattafesta, and Meelan M. Choudhari. An Experimental Investigation of the 30P30N Multi-Element High-Lift Airfoil // AIAA 2014-3062.
2. M. Choudhari and D.P. Lockard. Assessment of Slat Noise Predictions for 30P30N High-Lift Configuration from BANC-III Workshop // AIAA 2015-2844.
3. Pavel Bakhvalov, Ilya Abalakin, Tatiana Kozubskaya. Edge-based reconstruction schemes for unstructured tetrahedral meshes // Int. J. Numer. Methods Fluids. 81(6) (2016) 331–356.

A METHOD OF JET-WING INTERACTION NOISE PREDICTION AT LOW FREQUENCIES

O.P. Bychkov[1,2], **G.A. Faranosov**[1]

[1]TsAGI, Moscow Research Complex, Moscow, aeroacoustics@tsagi.ru
[2]Moscow Institute of Physics and Technology, Moscow

The importance of jet installation noise problem can be seen from a large number of recent publications [1–13]. Many papers are devoted to the development of simplified analytical models of this effect [2, 3, 5, 9, 11, 12, 13]. Analytical approaches are usually based on the considerable simplification of the initial geometry, e.g. real wing is replaced by a flat plate (all models), angle of attack is set to zero (all models except [11]), co-flow is not taken into account [2, 5, 6, 11]. Numerical high-resolution methods can be used to obtain physical assessments for realistic configurations and flow parameters [7–8], however their application is still usually restricted to selected cases due to high computational costs, and they are not convenient for parametric studied/optimization. Note that recently developed fast solvers using GPU and running on a conventional desktop computer may fill this gap [14]. However, engineering application requires reliable and fast low-order models capable to predict jet installation aeroacoustic effects with acceptable accuracy, e.g. at initial stages of aircraft design.

The present work is focused on the development of such low-order method. This work continues the previous studies of the authors related to the analytical modeling of jet-wing installation effect for model geometries of increasing complexity: 2D model [3], round jet and plate – scattering of axisymmetric mode [9], round jet and plate – scattering of spinning modes [13].

The model is tested on experimental data and the data of the numerical simulation. It is shown that the far-field spectrum of the installed configuration can be predicted on basis of near-field data of the standalone jet or installed jet for simplified and realistic configurations.

References

1. V.F. Kopiev, G.A. Faranosov, M.Yu. Zaytsev, E.V. Vlasov, R.K. Karavosov, I.V. Belyaev, N.N. Ostrikov. Intensification and suppression of jet

noise sources in the vicinity of lifting surfaces. AIAA paper 2013-2284, 2013.

2. A.V.G. Cavalieri, P. Jordan, W.R. Wolf, Y. Gervais. Scattering of wavepackets by a flat plate in the vicinity of a turbulent jet. Journal of Sound and Vibration. v. 333, 2014, pp. 6516–6531.

3. O.P. Bychkov, G.A. Faranosov. On the Possible Mechanism of the Jet Noise Intensification Near a Wing. Acoustical Physics, v. 60, No. 6, 2014, pp. 633-646.

4. J. Lawrence. Aeroacoustic Interactions of Installed Subsonic Round Jets. PhD thesis, Univ. of Southampton, 2014.

5. J. Vera, R.H. Self, M.J. Kinganz. The prediction of the radiated pressure spectrum produced by jet-wing interaction. AIAA Paper 2015-2216, 2015.

6. S. Piantanida, V. Jaunet, J. Huber, W. Wolf, P. Jordan, A.V.G. Cavalieri. Scattering of turbulent-jet wavepackets by a swept trailing edge. AIAA Paper 2015-2998, 2015.

7. F.D. da Silva, C.J. Deschamps, A.R. da Silva, L.G.C. Simoes. Assessment of Jet-Plate Interaction Noise Using the Lattice Boltzmann Method. AIAA paper, AIAA-2015-2207, 2015.

8. V.F. Kopiev, V.A. Semiletov, P.G. Yakovlev, S.A. Karabasov, G.A. Faranosov. Jet and jet–wing noise modelling based on the CABARET MILES flow solver and the Ffowcs Williams–Hawkings method. International Journal of Aeroacoustics, 2016, v. 15, No. 6-7. P.631-645.

9. O.P. Bychkov, G.A. Faranosov, S.L. Denisov, N.N. Ostrikov. Theoretical modeling of the excess noise due to jet-wing interaction. AIAA Paper 2016-2932, 2016.

10. I.V. Belyaev, M.Yu. Zaytsev, V.F. Kopiev, N.N. Ostrikov, G.A. Faranosov. Studying the effect of flap angle on the noise of interaction of a high-bypass jet with a swept wing in a co-flow. Acoustical Physics, v. 63, No. 6, 2017, pp. 14-25.

11. P.A.S. Nogueira, A.V.G. Cavalieri, P. Jordan. A model problem for sound radiation by an installed jet. Journal of Sound and Vibration, v. 391, 2017, pp. 95–115.

12. B. Lyu, A.P. Dowling, I. Naqavi. Prediction of installed jet noise. Journal of Fluid Mechanics, v. 811, 2017, pp. 234-268.

13. G.A. Faranosov, V.F. Kopiev, I.V. Belyaev, O.P. Bychkov, S.A. Chernyshev. On the Azimuthal Structure of Installed Jet Noise. AIAA paper AIAA 2017-3527, 2017.

14. A.P. Markesteijn, V.A. Semiletov, S.A. Karabasov. CABARET GPU Solver for Fast-Turn-Around Flow and Noise Calculations. AIAA-2015-2223, 2015.

NOISE RADIATED BY AN OPEN CAVITY AT LOW MACH NUMBER

J. Cante[1], A. Duben[2], A. Gorobets[2], O. Lehmkuhl[3], **R. Martin**[4], M. Soria[5]

[1] Universitat Politècnica de Catalunya, Terrassa, Spain, juan.cante@upc.edu

[2] Keldysh Institute of Applied Mathematics of RAS, Moscow, Russia

[3] Barcelona Supercomputing Center, Barcelona, Spain, oriol.lehmkuhl@bsc.es

[4] Universitat Politècnica de Catalunya and SEAT, Terrassa, Spain,
rocio.martin@upc.edu

[5] Universitat Politècnica de Catalunya, Terrassa, Spain, manel.soria@upc.edu

Introduction

Aeroacoustics is a topic of research with increasing relevance due to its technological and societal implications ([1, 2, 3]). The present work is focused on the flow over an open cavity at low Mach number, that is of interest to understand noise generation mechanisms in wall-bounded separated flows. While this configuration has been extensively studied ([4, 5, 6]), most of the works assume the flow to be two-dimensional (2D). However, for Reynolds numbers above ≈ 1200, the flow is three-dimensional (3D) [7]. This might result in significantly different sound sources. The purpose of the present work is to study the sound radiated by a 3D open cavity at Re=1500, M=0.15, and compare it with the results obtained assuming a 2D flow. To do so, two approaches will be used: Curle integral, evaluated as a post-process of an incompressible solution obtained with Alya [8] and Direct Simulation (DS), evaluated with NOISEtte code based on EBR schemes [9].

In the case of the first approach, a low dissipation methodology [10] strategy based on the recently proposed conservative EMAC scheme [11] will be used with a Galerkin approximation for space discretization together with a non-incremental fractional step method to stabilise pressure. Temporal discretization will be performed through a conservative explicit third-order Runge-Kutta scheme [12]. The solution obtained from this CFD formulation will then be used to evaluate the acoustic signal with the Curle method. For low Mach numbers, this formulation can be expressed as a surface integral [13]:

$$p(\boldsymbol{x},t) = \frac{1}{4\pi}\int_S -l_i n_j \left(\frac{1}{ra_0}[\dot{p}_{ij}] + \frac{1}{r^2}[p_{ij}]\right)dS \qquad (1)$$

where [*] means the evaluation of the expression at the retarded time $\tau = t - \frac{r}{a_0}$ and the surface S is the boundary of the solid body immersed in the fluid.
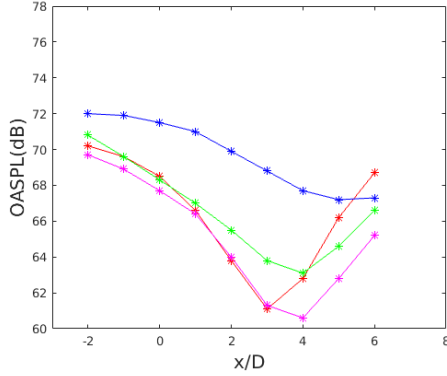
Fig. 1. SPL for nine observers: —— present Results, —— [4] DS, —— [4] Curle and —— [5] Curle

Problem Statement

Consider a two dimensional open cavity indefinitely extended along the z direction with geometrical parameters L/D=4, where L and D are the length and depth of the cavity respectively. The Reynolds number is Re=1500 and the Mach number is M=0.15.

When a two dimensional CFD simulation is considered, expression (1) is evaluated extending the integral domain along z/D assuming uniform p and $\dot{p}$ values until its contribution is negligible due to its inverse dependence with distance. Similarly, the integral also converges in the x-direction. Fig. 1 shows the calculated Sound Pressure Level for nine observers located at y/D=7.18 and x/D $\in$ [-2,-1,0,1,2,3,4,5,6] compared with the results from [4] and [5] when considering two dimensional flow behavior.

As previously stated, it is thought that these results will be significantly different when a 3D CFD simulation is taken as source terms for the integrands in expression (1). Figure 2 displays the streamlines in the 2D simulation. Due to the nonexistence of vortex stretching in two dimensions, the vortices do not vanish. This fact will generate larger pressure fluctuations on the integration surface. On the other hand, Fig. 3 shows the vortex structures defined by the *Q*-criterion, which exhibits the three dimensional flow behavior expected.

This paper will compute expression (1) using the results coming from a three dimensional CFD simulation and will compare them with the ones shown in Fig. 1. A direct simulation solution will be taken as the reference solution.
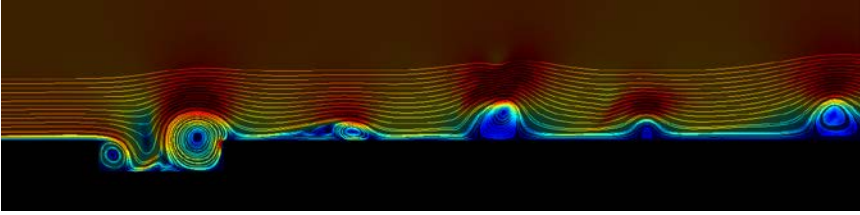
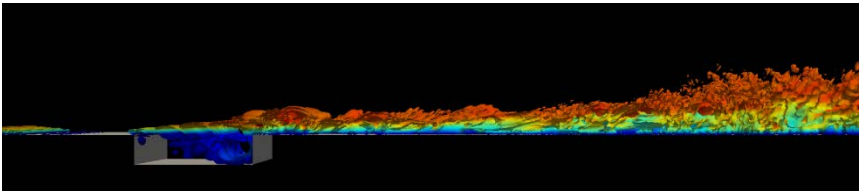Fig. 2. Streamlines for instantaneous velocity in the 2D case

Fig. 3. Vortices in the 3D case using the Q -criterion

References

1. Hua-Dong Yao, Lars Davidson, Lars-Erik Eriksson, Shia-Hui Peng, Olof Grundestam, and Peter E Eliasson. Surface integral analogy approaches for predicting noise from 3d high-lift low-noise wings. Acta Mechanica Sinica, 30(3):326–338, 2014.
2. Hua-Dong Yao, Lars Davidson, and Lars-Erik Eriksson. Noise radiated by low-reynolds number flows past a hemisphere at ma= 0.3. Physics of Fluids, 29(7):076102, 2017.
3. Michael Hartmann, Joerg Ocker, Timo Lemke, Alexandra Mutzke, Volker Schwarz, Hironori Tokuno, Reinier Toppinga, Peter Unterlechner, and Gerhard Wickern. Wind noise caused by the side-mirror and a-pillar of a generic vehicle model. In 18th AIAA/CEAS Aeroacoustics Conference (33rd AIAA Aeroacoustics Conference), page 2205, 2012.
4. Johan Larsson, Lars Davidson, Magnus Olsson, and Lars-Erik Eriksson. Aeroacoustic investigation of an open cavity at low mach number. AIAA journal, 42(12):2462–2473, 2004.
5. Jonas Ask and Lars Davidson. Sound generation and radiation of an open two–dimensional cavity. AIAA J, 47(6):1337–1349, 2009.
6. X Gloerfelt, C Bailly, and D Juvé. Direct computation of the noise radiated by a subsonic cavity flow and application of integral methods. Journal of Sound and Vibration, 266(1):119–146, 2003.
7. Guillaume A Bres and Tim Colonius. Three-dimensional instabilities in compressible flow over open cavities. Journal of Fluid Mechanics, 599:309–339, 2008.

8. Mariano Vázquez, Guillaume Houzeaux, Seid Koric, Antoni Artigues, Jazmin Aguado-Sierra, Ruth Arís, Daniel Mira, Hadrien Calmet, Fernando Cucchietti, Herbert Owen, et al. Alya: Multiphysics, engineering simulation toward exascale. Journal of Computational Science , 14:15–27, 2016.

9. Pavel Bakhvalov and Tatiana Kozubskaya. Ebr-weno scheme for solving gas dynamics problems with discontinuities on unstructured meshes. Computers & Fluids, 157:312–324, 2017.

10. O. Lehmkuhl, G. Houzeaux, M. Avila, H. Owen, M. Vazquez, and D. Mira. A low dissipation finite element scheme for the large eddy simulation on complex geometries. 19h International Conference on Finite Elements in Flow Problems - FEF 2017, Rome 2017, pages 1–10, 2017.

11. S. Charnyi, T. Heister, M. A. Olshankii, and L. G. Rebholz. On conservation laws of Navier-Stokes Galerkin discretizations. J. Comput. Phys., 337:289–308, 2017.

12. F. Capuano, G. Coppola, L. Rández, and L. de Luca. Explicit Runge-Kutta schemes for incompressible flow with improved energy-conservation properties. Journal of Computational Physics, 328:86–94, 2017.

13. Stewart Glegg and William Devenport. Aeroacoustics of Low Mach Number Flows: Fundamentals, Analysis, and Measurement. Academic Press, 2017.

PREDICTION OF TURBULENCE-CASCADE INTERACTION NOISE USING MODAL APPROACH

P. Chaitanya, P. Joseph

University of Southampton, UK

The turbulent wakes generated by a rotor interacting with outlet guide vanes is one of the dominant broadband noise sources in a turbofan engine. This present paper deals with the prediction of the broadband noise due to the interaction of rotor wake turbulence with the OGV. The approach proposed in this paper aims to reproduce the two-point cross spectral statistics of the turbulent velocity fluctuations at the OGV leading edges, which provides a complete specification of the rotor wake turbulence for broadband noise predictions. The approach proposed here is based on a superposition of vortical modes with the appropriate amplitudes. Three different vortical modes are investigated: 1) Fourier modes, 2) Proper Orthogonal Decomposition (POD) modes, 3) Normal modes of Linearized Euler Equations (LEE). A linearized unsteady Navier-Stokes solver can be used to predict the aerofoil response due to each incoming vortical mode.

ACOUSTIC DETECTION OF HELICOPTER ROTOR ICING

X. Chen[1], Q. Zhao[1], **G.N. Barakos**[2], A. Kusyumov[3]

[1]*Nanjing University of Aeronautics and Astronautics, Nanjing, China*
[2]*A University of Glasgow, Glasgow, UK, George.barakos@glasgow.ac.uk*
[3]*Laboratory 1, Kazan National Research Technical University, Kazan, Russia*

In this work, rotors with artificial iced shapes are studied to develop insight in the potential of acoustics-based ice detection. Using the Helicopter Multi-Block CFD solver, approximate iced shapes are added to the blades and the results are analyzed using the FW-H method. Several candidate monitoring positions are assessed for acoustic sensors to be placed on the helicopter fuselage. The influence of ice on the aero-acoustic characteristics of a rotor is calculated, and parameters such as the ice amount and the icing position on the blade are quantified..
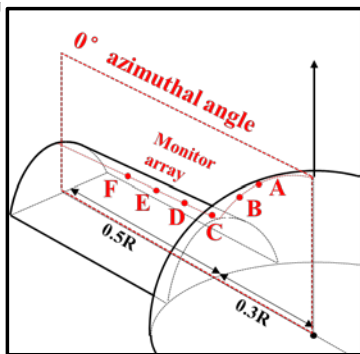
Fig. 1. Locations of microphones on the rear helicopter fuselage and tail-boom

The adopted method in this paper used the HMB3 CFD solver of the University of Glasgow [1, 2] and simulates the flow around helicopter blades in hover and forward flight. The established FW-H method [3] for acoustics is also used and the noise signals from iced rotor blades received on the helicopter fuselage, are compared with the signals of clean blades. The location and size of ice are both investigated and an appropriate array of microphones is designed. The array can sit on the rear helicopter fuselage and along the tail-boom so that ice occurring at any location on the blade can be detect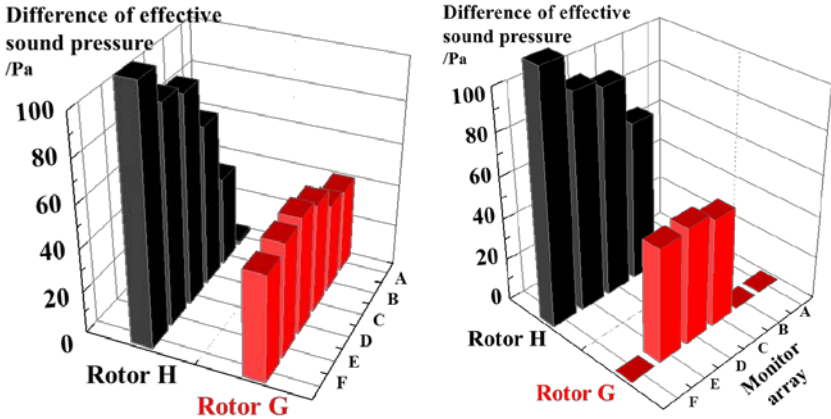ed. Several criteria for ice detection are established taking into account the sensitivities of real-world microphones that can be used during potential flight trials. Figure 1 shows the potential location of the microphones. empennage of a helicopter. Figure 2 presents results for the Caradonna-Tung [4] rotor in hover and for the UH60A rotor in forward flight [5]. The results show which microphone (A to F) is activated by a small amount of ice located near the 75% of the blade radius. Several cases have been investigated and it appears that the proposed 6-microphone array is adequate for the flight regime of the studied rotor.

The paper presents the validation of the employed method and a detailed account of the findings.

Fig. 2. Activated microphones in hover and forward flight by a small amount of ice near the 75%R of the UH60A rotor blade.

References

1. G. Barakos, R. Steijl, K. Badcock, A. Brocklehurst, Development of CFD capability for full helicopter engineering analysis, 31st Eur. Rotorcr. Forum. (2005) 1–15.M.E. Goldstein. Aeroacoustics. McGraw-Hill, New York, 1976.
2. R. Steijl, G.N. Barakos, CFD analysis of complete helicopter configurations - Lessons learnt from the GOAHEAD project, Aerosp. Sci. Technol. 19 (2012) 58–71. doi:10.1016/j.ast.2011.01.007.
3. K.S. Brentner, F. Farassat, Analytical comparison of the acoustic analogy and kirchhoff formulation for moving surfaces, AIAA J. 36 (1998) 1379–1386. doi:10.2514/2.558.
4. F.X. Caradonna, G.H. Laub, C. Tung, An experimental investigation of the parallel blade-vortex interaction, in: NASA/TM 86005, 1984.
5. I. Chopra, J. Sitaraman, J.D. Baeder, Validation of UH-60A rotor blade aerodynamic characteristics using CFD, Am. Helicopter Soc. 59th Annu. Forum. (2003)

BROADBAND NOISE PREDICTION OF A DUCTED AXIAL FAN BY MEANS OF A DISCONTINUOUS GALERKIN BASED CAA SOLVER

Jan W. Delfs, Roland Ewert, **Lev Liberson**, Markus Lummer, Michael Mössner

Institute of Aerodynamics and Flow Technology, Technical Acoustics, German Aerospace Center (DLR), Braunschweig, Germany, Lev.Liberson@dlr.de

To obtain a low-noise fan design in a justifiable amount of time, efficient computational aeroacoustic (CAA) methods are necessary for the prediction of aerodynamically generated noise. To bridge the gap between the high computational effort of scale resolving simulations and the limited predictability of semi-empirical models, a first principle based approach for broadband noise prediction is developed at the Department of Technical Acoustics of the German Aerospace Center (DLR).

The applied concept is a hybrid approach, where an unsteady acoustic simulation is performed based on a precomputed steady flow solution (mostly RANS). The acoustic computation relies on a coupled run of a propagation code and a synthetic turbulence generator, providing the necessary acoustic source information. Those stochastically generated sources are calculated by the Fast Random Particle Mesh method (FRPM) [1] while the CAA solver DISCO++ is used for sound propagation.
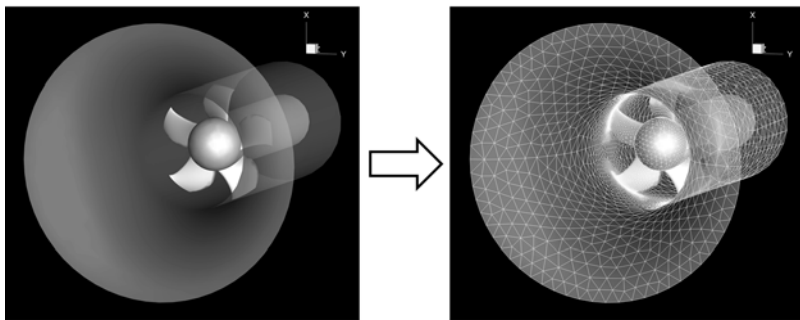

Fig. 1. 3-D geometry of a ducted axial fan discretized by an unstructured tetrahedral mesh

Since dealing with complex three-dimensional geometries and flow conditions an unstructured meshing approach is deemed to be beneficial. Local refinement often required due to small features of the geometry or high gradients in the flow field can be easily achieved using tetrahedral elements in an unstructured mesh. Fig. 1 depicts the surface mesh for a ducted axial fan, where vari-

ous levels of refinement are depicted. The spatial discretization used by DISCO++ is based on the 4th order discontinuous Galerkin (DG) method to solve the Acoustic Perturbation Equations (APE-4) [2].

For validation purposes the noise generation and propagation of a generic test case is computed and juxtaposed to measurement data. The case chosen is known as the "USI7" rotor which was designed and investigated at the University of Siegen to serve as a benchmark case for future studies on ventilator aerodynamics and acoustics. The setup consists of a five bladed, low pressure axial fan placed in a duct with an attached nozzle. A detailed description of the test rig as well as experimentally obtained data is provided by Carolus et al. [3] and is used within this study as reference.
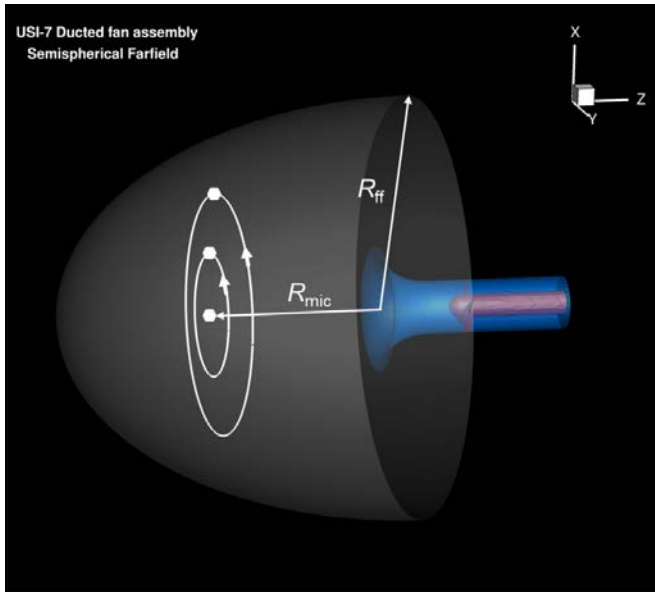

Fig. 2. CAA domain used for the acoustic simulations; half ellipsoidal-shaped domain to accommodate virtual microphones located along circles

The CAA domain chosen for the test case is depicted in Fig. 2. It is shaped half ellipsoidal upstream of the intake to accommodate the virtual microphones. For the datum problem the precomputed RANS mean flow solution does not account for any inhomogeneous inflow disturbances upstream of the fan. This allows reformulating the simulation problem in a rotating frame of reference, co-rotating with the fan with a constant angular velocity. It is found that the APE equations are covariant against general coordinate transformation, i.e. they remain formally unmodified in a rotating frame of reference.

Due to the rotating frame of reference, the sampling position of a microphone in the CAA domain is rotating as well. A further post processing step is required to counteract the rotation, i.e. extract data for a fixed position in the non-rotating frame of reference.

In this study two variations of the tip gap are simulated, i.e. $s_{A1} = 0.3$ mm and $s_{A2} = 3.0$ mm. The former is referenced to as case A1, the latter – case A2. For the A1 configuration, the tip gap is not resolved by the CAA grid, since very small element sizes are required – leading to extensive computational effort. Nonetheless, the impact of the gap on the noise generation of the ventilator is captured through the acoustic source terms computed by FRPM.

The instantaneous pressure field at the final time step of the simulation is presented in Fig. 3 for the A1 setup. The two slices in the colour plot show the pressure waves radiate spherically from the nozzle.
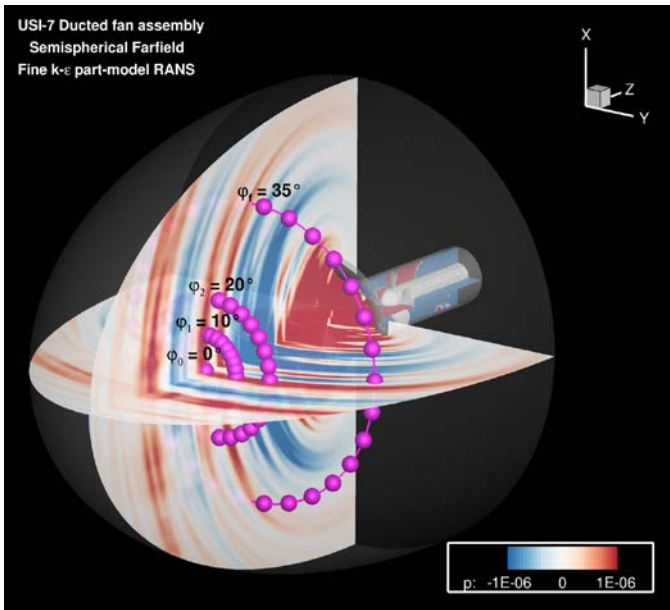

Fig. 3. Color plot of the instantaneous pressure field for the case A1

Notably, acoustic sources are computed only for one of the five blades, assuming the broadband noise sources of the different blades to be statistically independent. Since a linear acoustic problem is solved, the noise generation of the total assembly is the spectral sum of all five independent blades. This procedure allows to restrict the higher mesh resolution necessary to resolve the turbulence related sound sources to just one blade whereas the other blades can be meshed based on relieved aeroacoustics constraints.

A comparative evaluation of the sound pressure level spectra for the two cases A1 and A2 is presented in Fig. 4. Here, the sound pressure level recorded by the $\varphi = 35°$ virtual microphone position is compared to corresponding experimental data. Over a wide range of frequencies, the simulation is in good agreement with the measurement while some deviations can be found in the low frequency range. The expected increase in sound pressure level for a greater tip clearance (A2) is well predicted in terms of relative SPL, since no calibration for absolute levels is yet performed. Further studies concerning both the CFD and acoustic part are planned for the test case to increase the accuracy of the prediction as well as to assess and improve the efficiency of the method.
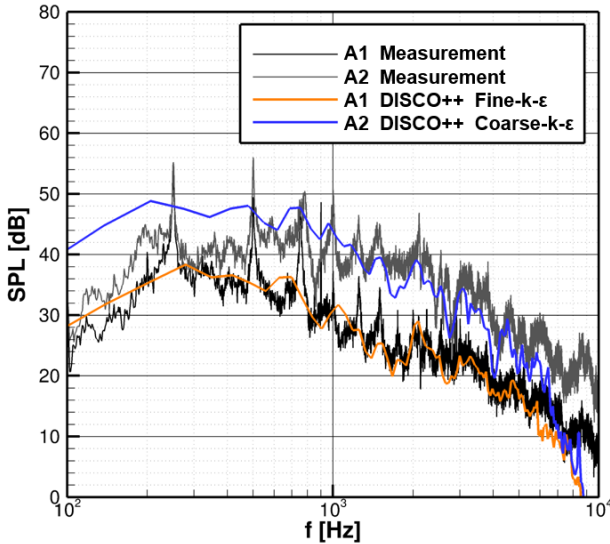

Fig. 4. Comparison of small tip gap (A1) with large tip gap (A2) setup

References

1. R. Ewert - Broadband slat noise prediction based on CAA and stochastic sound sources from a fast random particle-mesh (RPM) method - Computers & Fluids, 37, 2008
2. R. Ewert, W. Schröder - Acoustic perturbation equations based on flow decomposition via source filtering - Journal of Computational Physics, 188, 2003
3. T. Carolus, T. Zhu, M. Sturm - A low pressure axial fan for benchmarking prediction methods for aerodynamic performance and sound - Noise Control Engineering Journal, 63 (6), 2015

EXPERIMENTAL AND THEORETICAL INSTABILITY WAVE NOISE SHIELDING INVESTIGATIONS

Stanislav L. Denisov, Nikolay N. Ostrikov
TsAGI, Moscow, Russia, stanislav.denisov@tsagi.ru

Investigation of various aspects of external noise reduction with the help of engine placement over the airframe began in the 70s of the last century. The calculations which carried out in [1, 2] demonstrated a high potential for noise reduction of the external noise with the aid of similar layouts that realize the shielding effect. However, it should be noted that the shielding efficiency calculation performed in [1, 2], simple methods for diffraction calculation were used: the physical optic approximation, the Fresnel approximation [3] or the Maekawa method [4]. In these calculations the aircraft power plant was modeled by a point source with a directional pattern measured in the far field, but in fact aircraft power plant is a noncompact noise source,.

The incorrectness of modeling a noncompact source by a monopole source with a directivity pattern described by a set of spherical functions was demonstrated in [5]. In [6–8] the question of noncompactness was thoroughly studied and it was shown that the application of simple diffraction theories together with the replacement of a noncompact source by a point source with a directivity diagram based on measurements in the far field leads to an error in the prediction of the shielding efficiency in the geometric shadow zone to 20-30 dB and even more.

As shower in [6, 7] the reason for such a significant error is that the phase characteristics in the far field from the noncompact source are formed at a significant distance from the source and the simplified methods of diffraction calculating are extremely sensitive especially to the phase characteristics of the acoustic field near the source. Since the shielding surface of the airframe is placed in the immediate vicinity of the source in the near zone (or induction zone) the phase distribution inherent to approximate theories of diffraction calculation does not forming which leads to significant errors.

Based on the results of comparative calculations performed in [6, 7] the Geometric Theory of Diffraction (GTD) proved to be the most promising method of shielding efficiency calculation. The GTD allows one to accurately calculate not only the amplitude but also the phase of the sound field which is an extremely important property for noncompact sources. Performed experimental validation of the GTD method by means of maximum length sequence method [9] demonstrated not only the high accuracy of the sound field calculation in the geometric shadow zone, but also showed the applicability of the GTD to the investigation of the sound diffraction on the plane rectangular

and polygonal screens. Thus GTD was chosen to perform the shielding efficiency calculation of aircraft non-compact sources.

In the present paper as a noncompact aircraft noise source considering the problem of shielding efficiency calculation of acoustic radiation from a high-speed jet described by set of instability waves downstream developing [10] – experimentally confirmed large-scale coherent structures [11, 12]. Earlier such a representation made it possible to explain and calculate the main characteristics of sound radiation by round supersonic jets [10].

The proposed work generalizes the methods and approaches developed in [11] for the case of calculation of the noise efficiency radiated by the instability waves [13]. In this work the instability waves are considered as elementary sound sources and represent harmonic in time vibrations of the jet which have the form of wave packets. The perturbation amplitude in these packets exponentially grows downstream in the initial part of the jet. Then the thickness of the mixing layer increases the growth rate of the perturbation amplitude decreases. At the final stage from some section of the jet the amplitude of the wave packet begins to decrease. For each given frequency, the jet has a family of instability waves having a different structure in the azimuthal and radial directions. The total noise of the jet is found as a stochastic sum of the contributions of various instability waves.

For wave packet form determination used the fact that among of all possible perturbations in the initial part of the jet, spatially unstable perturbations (instability waves) are isolated. The amplitude of these instability waves exponentially grows downstream as long as the mixing layer remains thin enough (the Kelvin-Helmholtz instability). Thus, the evolution of perturbations in the jet is determined not by the entire infinite set of natural oscillations of the jet but only by its small part calling instability waves.

Each individual instability wave is modeled by the aggregate of point sources which amplitude and phase distribution is given by means of a model wave packet and the power density spectrum took from experimental data analysis.

It is shown that the developed method for shielding efficiency calculation of high-speed jets allows generalization to arbitrary flat polygonal screens. This fact make it possible to carry out shielding efficiency of noise emitted by noncompact sources such as instability waves to a wide class of layouts of aircraft with an upper engine arrangement.

References

1. U. Von Glahn, D. Groesbeck, and M. Reshotko. "Geometry Considerations for Jet Noise Shielding with CTOL Engine-Over-The-Wing Concept" // AIAA Paper 1974-568, June 1974.
2. U. Von Glahn, D. Groesbeck, and J. Wagner. "Wing Shielding of High-Velocity Jet and Shock – Associated Noise with Cold and Hot Flow Jets" // AIAA Paper 1976-547, July 1976.
3. M. Born, E. Wolf. "Principles of Optics" // Pergamon, Oxford, 1959.
4. Z. Maekawa "Noise Reduction by Screens" // Journal of Applied Acoustics, 1968, pp. 157 – 173.
5. D. Papamoschou. "Prediction of Jet Noise Shielding" // AIAA Paper 2010 – 653, 2010.
6. S. L. Denisov, N. N. Ostrikov. "Comparison of the methods for noncompact aviation noise sources shielding calculation" // The 22nd International Congress on Sound and Vibration, 12 – 16 July 2015, Florence, Italy.- Book of abstracts. P. 196.
7. N. N. Ostrikov, S. L. Denisov. "Airframe Shielding of Noncompact Aviation Noise Sources: Theory and Experiment" // AIAA Paper 2015 – 2691, 2015.
8. N. N. Ostrikov, S. L. Denisov. "Mean Flow Effect on Shielding of Noncompact Aviation Noise Sources" // AIAA Paper 2016 – 3014, 2016.
9. S. L. Denisov, A. I. Korolkov "Investigation of Noise-Shielding Efficiency with the Method of Sequences of Maximum Length in Application to the Problems of Aviation Acoustics" // Acoustical Physics, 2017, Vol. 63, No. 4, pp. 462–477.
10. C. K. W. Tam, D. E. Burton "Sound generated by instability waves of supersonic flows: Part 2. Axisymmetric jets" // Journal of Fluid Mechanics, 1984, Vol. 138, pp. 273-295.
11. V.F. Kopiev, S.A. Chernyshev, M.Yu. Zaitsev, V.M. Kuznetsov "Experimental validation of instability wave theory for round supersonic jet" // AIAA Paper 2006 – 2595.
12. J. Vera, L. T. Lawrence, S. Sinayoko, R. H. Self, M. J. Kingan "Hydrodynamic Pressure Field Ppropagation Model for the Prediction of the Far-Feld Sound Produced by Jet-Wing Interaction" // AIAA Paper 2016 – 2859.
13. O.V. Bychkov, G.A. Faranosov, S.L. Denisov, N.N. Ostrikov. "Theoretical Modeling of the Excess Noise Due to Jet-Wing Interaction" // AIAA Paper 2016 – 2932, 2016.

THE APPLICATION OF HARMONIC METHODS FOR THE CALCULATION OF THE TONE NOISE PROPAGATION THROUGH INLETS AND NOZZLES OF TURBOFANS

I.M. Druzhinin, V.I. Mileshin, **A.A. Rossikhin**

Central Institute of Aviation Motors (CIAM), Moscow, Russia, rossikhin@ciam.ru

In the process of the turbomachinery tone noise simulation the calculation of interactions between different blade rows should be performed and also the propagation of acoustic disturbances, generated by the interactions of rows, outside the turbomachine duct should be calculated. Though it is possible and even desirable to solve these two problems in one computation, for the sake of economy of computational resources, often the so called hybrid approach for the tone noise simulation is used. According to this approach the computation is divided into two parts – first the rotor-stator (rotor-rotor) computation is carried out, and then its results serves as a base for the separate computation of noise propagation [1].

Modeling of the interaction of rows in turbomachines remains currently a task, demanding to computational resources, especially if a turbomachine under consideration is multistage. The simplest and the most widespread approach is the direct full annulus time-domain unsteady calculation; however it is extremely expensive in terms of computational resources if the number of stages is more than two. One of the possible approaches for the acceleration of the computations is the transition from unsteady calculation of evolution of a flow-field in time to stationary calculation for the specified set of harmonics. Frequency-domain harmonic methods are proved to be computationally efficient for the computation of fan tone noise [2], reducing computational domain to a single blade passage for each row. Also, as it was shown in number of works, some of them written with the participation of the authors of this one, harmonic methods allow to perform approximate calculations of interactions between rows in a multistage turbomachine with acceptable accuracy and computational expense [3]. Calculations in the frequency-domain can be performed using either linear or nonlinear equations both for single stage and multistage turbomachines.

Modeling of the propagation of disturbances, generated in the inter-row interactions, through an inlet or a nozzle also generally represents a task, demanding to computational resources. However in the case when an inlet or a nozzle can be treated as axisymmetric, (which is common for test rigs), harmonic methods makes possible to significantly increase the speed of calculations. In this case the flow field can be decomposed into circumferential modes (harmonic functions of time and azimuth angle characterized by the frequency and the circumferential number). Then the calculation of noise propagation can be performed independently for each of these circumferential modes in the 2D com-

putational domain, corresponding to the longitudinal section of initial 3D geometry. Such approach is commonly called 2.5D. In many cases the solution can be described by a small number of circumferential modes, thus the reduction of 3D equations to the set of 2D equations can lead to the acceleration of the aeroacoustic calculation.

In the current work the implementation of the corresponding method in 3DAS (3 Dimensional Acoustics Solver) CIAM in-house solver [4] is described. The method can be used either in the linear approximation, which is appropriate approach for the calculation of the propagation of an interaction noise, or it can be used in the nonlinear statement. In the latter case it can be used for the calculation of the propagation of shock waves, arising in the blades of the fan operating at supersonic tip speed, through the inlet. Also the method can be used for the calculation of pure multiple tone noise. The comparisons between the results of linear and nonlinear computations in the frequency domain performed with the method under consideration and the results of direct unsteady calculations of noise propagation through an inlet and a nozzle are presented. It is shown that the usage of harmonic methods makes possible to increase the speed of calculations retaining acceptable precision both in the linear and nonlinear statements.

With the usage of 3DAS solver it is possible to combine 2D and 3D computations in one calculation. Special interfaces preserve the continuity of the solution on the boundary for the specified set of circumferential modes. This approach makes possible, for example, to perform the simulation of tone noise generation due to rotor-stator (rotor-rotor) interactions in the 3D setup and at the same time to model the propagation of disturbances through the inlet in the 2D setup. Such approach owing to a direct connection of calculations of interaction and propagation should provide the higher accuracy of the overall calculation, than the standard hybrid approach. Moreover the computational costs for carrying out of the given calculation not considerably surpass costs for carrying out of calculation of interaction between rows. The example of such a calculation for a counter-rotating fan is presented in the work.

References

1. Rumsey C. L., Biedron R. T., Farassat F. Ducted-fan engine acoustic predictions using a Navier-Stokes code, Journal of Sound and Vibration, Vol. 213, No. 4, pp. 643-664, 1998
2. Verdon, J.M. Linearized Unsteady Aerodynamic Analysis of the Acoustic Response to Wake/Blade-Row Interaction, NASA/CR—2001-210713, 2001.
3. Rossikhin A.A., Pankov S.V., Mileshin V.I., Numerical Investigation of The First Booster Stage Tone Noise of a High Bypass Ratio Turbofan,

GT2016-57352, ASME Turbo Expo 2016, Seoul, South Korea, June 13-17, 2016.

4. Nyukhtikov, M.A., Rossikhin, A.A., Sgadlev, V.V., Brailko, I.A. Numerical Method for Turbo-Machinery Tonal Noise Generation and Radiation Simulation Using CAA Approach, GT2008-51182, ASME Turbo Expo 2008: Power for Land, Sea and Air, GT2008, Berlin, Germany, June 9-13, 2008

TOWARDS FORCED EDDY SIMULATION FOR INSTALLED NOZZLE-WING CONFIGURATIONS

Roland Ewert, **Andrej Neifeld**

Institute of Aerodynamics and Flow Technology, Technical Acoustics,
German Aerospace Center (DLR), Braunschweig, Germany

This contribution presents results for the computation of the noise radiated by a single stream jet and for an installed configuration with an UHBR nozzle installed at a high-lift wing considering the entire wind tunnel set up of a related DLR experiment in the Acoustic Windtunnel Braunschweig (AWB). The direct noise computation (DNC) is performed solving the Navier-Stokes equations in perturbation form over a given background RANS flow in the framework of a zonal RANS/LES simulation with Non-Linear Disturbance Equations (NLDE) as first proposed by Morris et al. [1], and further developed in the works of Sagaut & Labourasse [6, 7], Batten et al. [8, 9] and Terracol et al. [10, 11].

In the Forced Eddy Simulation (FES) approach, besides a dissipative sub-filter model, forcing in space in time is applied using the so-called Fast Random Particle-Mesh Method (FRPM) to realize a stochastic backscatter method (stochastic volume forcing method) for technical applications and such avoiding grey areas. Compared to the NLDE system as proposed by Morris et al. [1], where all viscous fluctuations are neglected, the present approach is accounting for the shear-stress in the momentum equation but neglecting the contribution of viscous fluctuations to the energy equation. The viscous terms in the momentum equation are modelled as the resulting vector force rather than the entire shear-stress tensor. Hence, the governing equations read

$$\frac{\partial \rho'}{\partial t} + \frac{\partial}{\partial x_i}\left(\rho'\widetilde{v}_i + \rho^0 v_i'\right) = 0$$

$$\frac{\partial v_i'}{\partial t} + \widetilde{v}_j \frac{\partial \widetilde{v}_i}{\partial x_j} + \frac{1}{\overline{\rho}}\frac{\partial \overline{p}}{\partial x_i} - \frac{1}{\overline{\rho}}\widetilde{f}_i = \frac{1}{\overline{\rho}}\widetilde{f}_i^s$$

$$\frac{\partial p'}{\partial t} + \frac{\partial p'}{\partial x_i}\widetilde{v}_i + \frac{\partial p^0}{\partial x_i}v_i' + \gamma p'\frac{\partial \widetilde{v}_j}{\partial x_j} + \gamma p^0 \frac{\partial v_j'}{\partial x_j} = 0$$

with the right hand side term

$$\boldsymbol{f}^s = \underbrace{-\boldsymbol{\nabla} \times (\overline{\rho}\nu_r\, \widetilde{\boldsymbol{\omega}})}_{\boldsymbol{f}_D} + \underbrace{\boldsymbol{\nabla} \times \boldsymbol{q}}_{\boldsymbol{f}_F}$$

The stochastic forcing on the right hand side of momentum equations is based on DHIT calibrated backscatter model and comprises similar features as for example described by Leith [2] or Marstorp et al. [3]. On the other hand, the dissipation is modelled as a vortex force based on residual eddy viscosity, which is dynamically adjusting to growing, equilibrium or decaying turbulence

with the ratio between resolved and residual turbulent kinetic energy. The combined effect of forcing and dissipation which removes the energy at low wave numbers and feeds in energy at high wave numbers establishes the desired energy transfer as driving mechanism for the energy cascade (refer to Fig. 1).
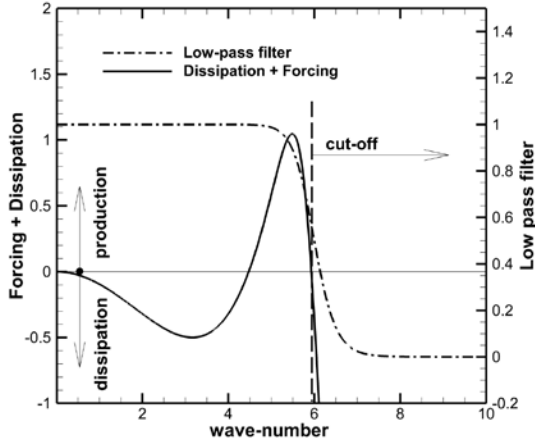

Fig. 1. Energy transfer caused by forcing and dissipation term

The above described methodology has been recently implemented in DLR's PIANO/FRPM code. A cold isolated single stream jet with nozzle exit Mach number of 0.9 in static condition is used for validation of the FES approach. The computational domain is resolved with approx. 10 million grid points with cylindrical grid topology. The grid cell width is in axial and radial directions rather constant. In circumferential direction the resolution is getting coarser with growing radius by nature of O-topology.
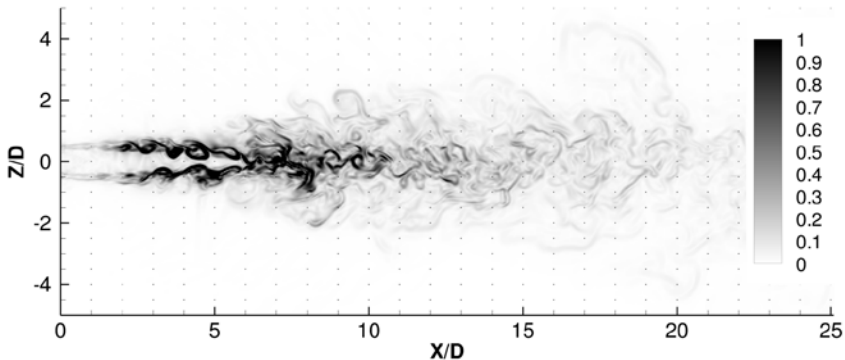

Fig. 2. Numerical Schlieren plot for cold isolated single stream jet with Ma=0.9

The study with this computational case is still ongoing, but has already shown encouraging results. Fig. 2 is showing an instantaneous plot of density gradient magnitude, i.e. as a numerical Schlieren plot. It can be observed that after nozzle exit the coherent structures start to grow which become after potential core rather chaotic and slowly decaying.
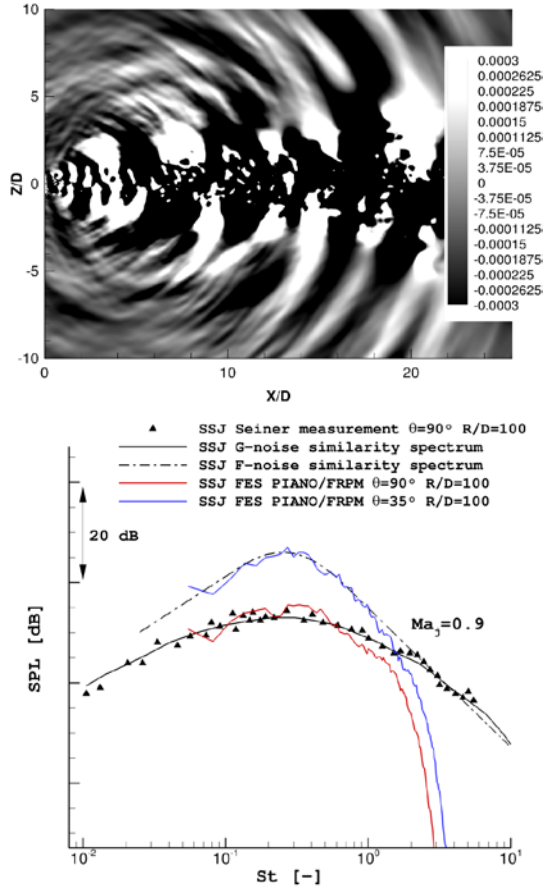

Fig. 3. (top) Contour plot of pressure fluctuations; (bottom) Comparison of spectra between measurement, similarity spectra and FES computation for polar angle of 90° and 35°

The contour plot of pressure fluctuations in Fig. 3 (top) is also showing the expected distribution, i.e. broadband radiation in polar angle range 90°-60° and Mach wave radiation for smaller polar angles. The corresponding spectra for two representative polar angles of subsonic high speed jet are plotted as a

comparison with measurement of Seiner and similarity spectra of Tam in Fig. 3 (bottom). The agreement of spectrum form for microphone position with Mach wave radiation with the F-noise similarity spectrum is considerably good. Also the spectrum at 90° fits to the both reference spectra, but let still room for improvement in high frequency range where the noise contribution appears to be slightly weaker. Thus, computations with adjustment of calibration parameters are planned in subsequent work.

With the aim to study the installation effect, a wing-nozzle configuration from LIST project is applied to FES approach, too. Since the above described validation with the single stream jet is not yet accomplished, the results of this computation should be considered as preliminary. Also the obtained time signal length is not yet long enough for a quantitative evaluation. Nonetheless, the applicability of this approach has been approved for more complex configurations than single stream jet. A contour plot of pressure fluctuations for this computation is depicted in Fig. 4. For this case, the highest noise contribution appears to come from the flap trailing edge, which is attributed to jet flow induced noise generation mechanism.
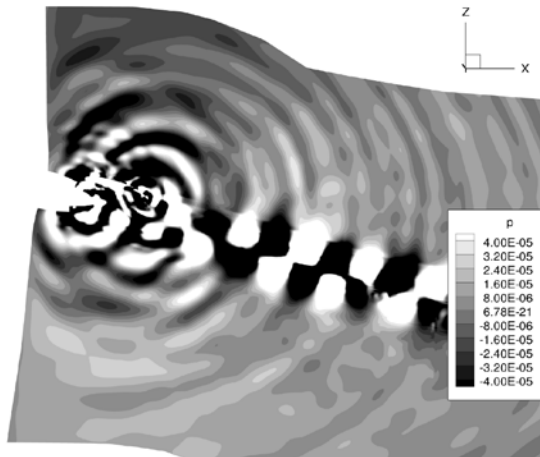

Fig. 4. Contour plot of pressure fluctuations for installed UHBR configuration with nozzle exit Mach number of 0.4 and ambient co-flow of 0.2

References

1. P.J. Morris, L.N. Long, A. Bangalore, Q. Wang. A Parallel Three-Dimensional Computational Aeroacoustics Method Using Nonlinear Disturbance Equations, J. Comput. Phys., v.133, 1997, pp.56–74.
2. C.E. Leith. Stochastic backscatter in a subgridscale model: Plane shear mixing layer. Phys. Fluids A, v.2, 1990, pp.297–299.

3. L. Marstorp, G. Brethouwer, A.V. Johansson. A stochastic subgrid model with application to turbulent flow and scalar mixing. Physics of Fluids, v.19, 2007.
4. J. Fröhlich, D. von Terzi. Hybrid LES/RANS methods for the simulation of turbulent flows. Progress in Aerospace Sciences, v.44, 2008, pp.349-377.
5. A. Neifeld. R. Ewert. Towards Forced Eddy Simulation of Airframe Induced Noise Radiation from Coherent Hydrodynamic Structures of Jet Flow. AIAA Aviation 2018, Atlanta.
6. Labourasse, E. and Sagaut, P., Reconstruction of Turbulent Fluctuations Using a Hybrid RANS/LES Approach, Journal of Computational Physics, Vol. 182, No. 1, 2002, pp. 301-336.
7. Labourasse, E. and Sagaut, P., Advance in RANS-LES coupling, a review and an insight on the NLDE approach, Archives of Computational Methods in Engineering, Vol. 11, No. 3, Sep 2004, pp. 199-256.
8. Batten, P., Ribaldone, E., Casella, M., and Chakravarthy, S., Towards a Generalized Non-Linear Acoustics Solver, AIAA Paper 2004-3001, 2004.
9. Batten, P., Spalart, P., and Terracol, M., Use of Hybrid RANS/LES for Acoustic Source Predictions, Cambridge University Press, 2007.
10. Terracol, M., A Zonal RANS/LES Approach for Noise Sources Prediction, Flow, Turbulence and Combustion, Vol. 77, No. 1, Nov 2006, pp. 161-184.
11. Terracol, M., Manoha, E., and Lemoine, B., Investigation of the Unsteady Flow and Noise Generation in a Slat Cove, AIAA Journal 54(2), 2016.

ACOUSTICS DESIGN SENSITIVITY ANALYSIS FOR THE NOISE CONTROL AND MINIMIZATION ON LANDING GEARS

Amine Ghouali[1], Antoine Boillot[1], Maxime Lebrun[1],
Neil Price[2], Quentin Bouvy[1]

[1] *Safran Landing Systems, Vélizy, France, amine.ghouali@safrangroup.com*
[2] *Safran Landing Systems, Gloucester, UK, neil.price@safrangroup.com*

This paper provides a new acoustics design sensitivity approach for the minimization of noise on landing gear parts. The idea consists of direct differentiation with respect to the gear design parameters X of the far-field Sound Pressure Level (**SPL**) of the landing gear during flyover [1]:

$$SPL = 10log_{10}\left(D_w\left(\sum_s P_s^2 + P_w^2 + P_g^2 + P_h^2 \right) \right) + \underbrace{10log_{10}(C) + R\alpha - 94}_{x_{noise}} \qquad (1)$$

Here, C is the convective amplification factor. α is the atmospheric attenuation and D_w the directivity function accounting for installation effects. P^2_i is the mean square far-field pressure of an individual component source at an observer radius R:

$$P^2_i = H_i(\rho, V, X) \times F(St) \qquad (2)$$

$H_i(\rho, V, X)$ is a function depending on the air density ρ, the air velocity V and the design parameters X. $F(St)$ is the *spectral function* expressed with respect to the Strouhal parameter as:

$$F(St) = \frac{a_1^i \times St^N}{a_2^i + a_3^i \times St^N + a_4^i \times St^{2N}} \qquad (3)$$

a^i and N are the experimental coefficients of the ith component correlated from wind tunnel test [1]. The Strouhal is defined in terms of the frequency f and the component diameter d as: $St = (f \times d)/V$.

Assuming that D_w and χ_{noise} are independent of design parameters, the Acoustics Design Sensitivity of the SPL level (1) is obtained by the following differentiation forms [2]:

$$\frac{dSPL}{dX} = \frac{10 \times \sum_i \frac{\partial P_i^2}{\partial X}}{\ln(10) \times \left(\sum_i P_i^2 \right)} \qquad (4)$$

$$\frac{\partial P_i^2}{\partial X} = \frac{\partial H_i(\rho, V, X)}{\partial X} \times F(St_i) + H_i(\rho, V, X) \times \frac{\partial F(St_i)}{\partial X} \qquad (5)$$

$$\partial F(St)/\partial X = \partial F(St)/\partial d = f/V \qquad (6)$$

The numerical implementation of the proposed Acoustics Design Sensitivity analysis (4)–(6) has been performed using SCILAB code and its open sources [3]. The obtained sensitivities are used to control and minimize noise objective $A(X)$ such as:

$$\text{Min}_{\{X\}}[\![A(X)]\!]$$
$$X_{min} \leq X \leq X_{max} \tag{7}$$

X_{min} and X_{max} are the lower and the upper limits of the design parameter sets. The acoustics objective $A(X)$ may concern the Overall Sound Pressure Level (**OASPL**) [measured for one given microphone position] or its average Level $\overline{\mathbf{A}}$ [OASPL integrated on the total number of microphones].
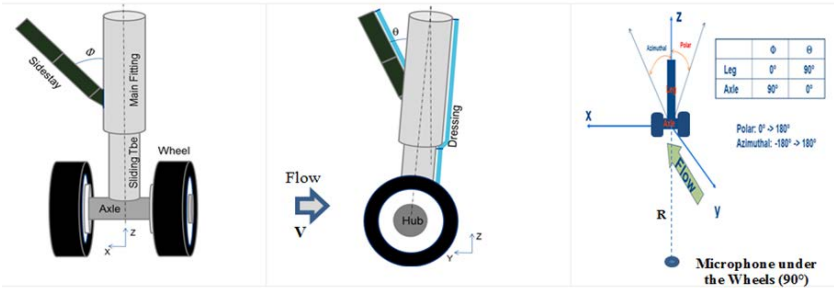

Fig. 1. Components definition of the Generic Landing Gear (*GLG*)

The numerical illustration will be carried out on the *Generic Landing Gear* (*GLG*) represented in Fig. 1 by 2 *wheels*, the wheel *hubs,* and the *strut cylindrical parts* (main fitting, sliding tube, sidestay and axle).

The sensitivity computations have been performed with respect to the following design parameters: **Diameters d_S** (Struts), **d_W** (Wheels), **d_H** (Hubs) and **d_D** (Dressing); **Lengths l_S** (3 Struts), and **l_D** (Dressing); **Azimuthal angles Φ_S** (3 Struts); **Width W_W** (Wheels); **Depth h_H** (Hubs); **Numbers N_H** (number of Wheels) and **N_H** (number of Hubs). Fig. 2a gives estimates of the sensitivities under the wheels; at 90° location. It is demonstrated that 82% of the far-field OASPL is sensitive to only *six parameters (d_{MF}, d_{SS}, w_W, d_A, h_H, and d_W)* instead of the (fifteen) initially predefined ones. Moreover, almost 65% of the noise is controlled by the *main-fitting* and the *sidestay* design parameters.

The above (ADS) sensitivities correspond to an overall reduction of **1.45dB** of the landing gear (OASPL) noise. The attenuation performed on the *main-fitting* and *sidestay* is about **0.97dB** representing the bulk of the overall noise attenuation on the landing gear. The first optimization problem consists of minimizing the (OASPL) overall noise objective. Fig. 3a illustrates the evolution of the r*eference* and *optimized* landing gear noise directivity witch shows an average attenuation of 1.35dB.
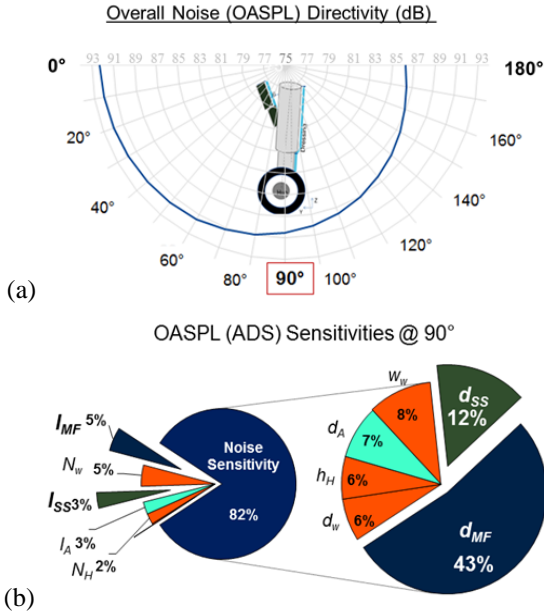
Fig. 2. a) GLG reference noise directivity,
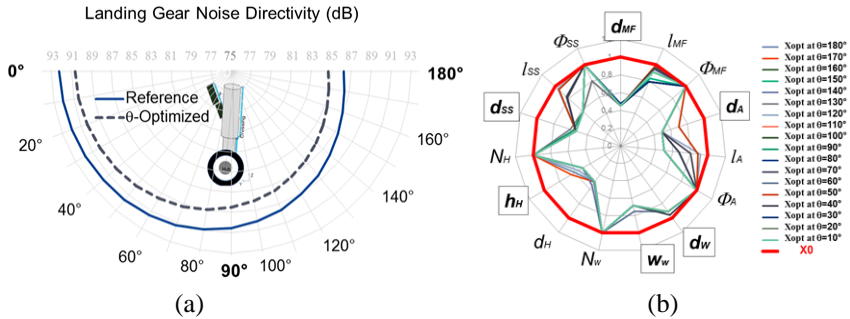b) Acoustics Design Sensitivities at 90°

Fig. 3. a) Reference and θ-Optimized directivity,
b) Optimized shape design parameters

Furthermore, the **OASPL** shape optimization is carried out for each angular θ-position and therefore will lead to a different set of optimized parameters (Fig. 3b) for each different position ($0° < \theta < 180°$). From a design point of view, this solution will not acceptable because they correspond to new landing gear design architecture for each θ position.

A suitable formulation of the noise objective as an average level ($\overline{\mathbf{A}}$) will help to overcome the above situation and will lead to a unique converged optimum solution $\mathbf{X_{OPT}}$ of the landing gear shape parameters. Figure-4.b shows the evolution of unique set of optimum parameters with respect to the initial set of design values. The new ($\overline{\mathbf{A}}$) optimized directivity is similar to the previously (**OASPL**) optimized one because the control parameters (d_{MF}, d_{SS}, w_W, d_A, h_H, and d_W) - previously identified for θ=90° - converge always to the same optimum value and remain unchanged for all θ-position (Fig. 4a).
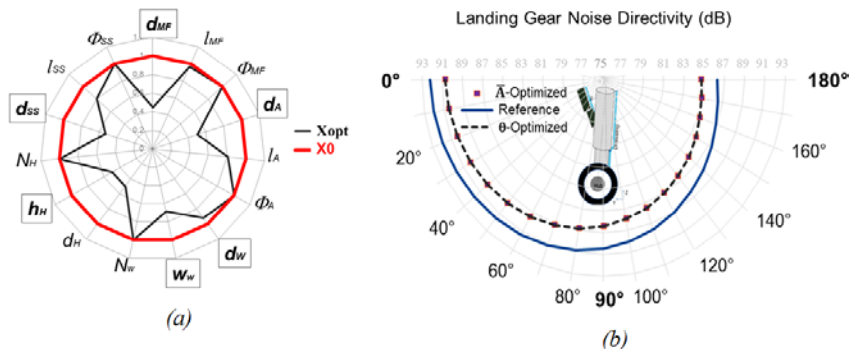

Fig. 4. a) Reference and Optimized directivities,
b) Optimized shape design parameters

References

1. M.C. Smith, L.C. Chow. Validation of a Prediction method for Aerodynamic Noise from Aircraft Landing Gear, AIAA-2002-2581, 2002.
2. A. Ghouali, N. Price. Acoustics Design Sensitivity Analysis for the Noise Optimization of Landing Gears, Applied Acoustics, Submitted, 2018.

THE CHARACTERISTICS AND SPATIAL STRUCTUIRE OF WALL PRESSURE FLUCTUATIONS IN A FLOW OVER STEPS

A.Yu. Golubev, **S.V. Kuznetsov**

Moscow Scientific Research Centre of TsAGI, Moscow,
alexeygolubev@yandex.ru, international44@yandex.ru

Wall pressure fluctuations on the surface of fuselage are a substantial source of noise inside an airliner, as their impact on the covering leads to vibrations of the elastic construction, followed by sound radiation into the cabin. At the same time, the problem of internal noise reduction is complicated due to the strict limitations of size and weight of the airplane constructions. Thereby, precise information about the characteristics and spatial structure of wall pressure fluctuations is a key issue concerning the reduction of internal noise of the aircraft.

In the acoustic Department of TsAGI have been conducted series of flight and laboratory experiments, which have allowed to obtain the characteristics of wall pressure fluctuations in a turbulent boundary layer on a smooth surface with small gradients of mean pressure and to develop empirical equations to calculate them [1, 2].

However, due to design features, on the surface of the aircraft there are some additional disturbances apart from the uniform wall pressure fluctuations of the undisturbed boundary layer on a smooth surface. One particular source of such disturbances is local separation flows which occur in the vicinity of surface discontinuities. The characteristics of the additional disturbances vary in space to a much greater extent than the characteristics of the pressure fluctuations of the undisturbed turbulent boundary layer.

A typical example of the surface discontinuities on the fuselage of an airliner are steps of various configurations. Perturbations produced by such obstacles are the subject of active experimental and computational studies [3–7].

It was found out, in particular, that exactly in front of a step, the excess value is 20-30 dB in the low frequency range. Behind the step, this excess is 15-20 dB at low and medium frequencies, but the spatial area of high pressure fluctuations is significantly greater than in front of the step. As a result of parametric studies, the main patterns of spectral density, correlation scales and phase velocity of non-uniform fields in front and behind the step were obtained depending on the Mach and Reynolds numbers, dimensionless height of the step, geometry of the non-uniformity zone. It was shown that the influence of the Mach number is an increase of the dimensionless spectral density in the region of transonic regimes (M=0,8-1,5) with the formation of a local maximum in the vicinity of M=1.2. Also noted the transformation of the wall pressure fluctuations field behind backward-facing step with M>1.

When the size of the combination of forward- and backward-facing steps change (which affects the mutual arrangement of recirculation zones – in front of the configuration, behind the configuration and at the side edge), a significant change of the local characteristics of the wall pressure fluctuations in its vicinity can be observed.

The results of experimental studies show that under certain conditions wall pressure fluctuations in front and behind of the combination of forward- and backward-facing steps can be significantly correlated. That correlation can be substantially higher than the one in the undisturbed turbulent boundary layer (TPS) with the same distance between the transducers. Thus, in a sufficiently long range of low frequencies, the correlation between the pressure fluctuations in front of the forward-facing step and behind the backward-facing one was significantly higher than the correlation observed in the undisturbed turbulent boundary layer. A distinctive feature of this phenomenon is that the formation of an additional (in relation to noise in the cabin) non-uniform wall pressure fluctuations field occurs in the interaction of already existing fields, those local characteristics does not notably change in a wide range of variations of the parameters.

Generalizing the results of laboratory and flight experiments, has been developed an empirical model of wall pressure fluctuation fields in the vicinity of the combined forward- and backward-facing steps configuration. It was shown that the spectrum of spatial correlations can be represented with three components: the spectrum of spatial correlations in front of the forward-facing step, behind the backward-facing step and their combined configuration.

Further efforts were made to reveal the structure of wall pressure fluctuations directly on the step surface.

Fig. 1, given as an illustration, represents the difference between the spectral levels of pressure fluctuations on the surface of a step and the spectral pressure fluctuation levels of the undisturbed turbulent boundary layer (TBL). The observation points are located on various distances from the leading edge. The results are presented for the height of the step h = 5mm and the speed of the upcoming flow U = 45m/s. It is evident that in the vicinity of the edge observed spectral levels are more than 20 dB above the levels of the undisturbed TBL at all frequencies and almost 30 dB higher at the low frequencies. As the distance from the edge increases, there is a significant decrease in both the low-and high-frequency parts of the spectrum. Already at a distance of 3h there is a decrease in the spectral levels of pressure fluctuations in these frequency ranges by about 10 dB. At the same time, in the mid-frequency part of the spectrum there is a significantly slower decline in spectral levels and at a distance of 3h in this area of Strouhal numbers there is a maximum, the spatial position of which corresponds to the relative position of 1.5 step heights. Since $x/h > 3$ there is a uniform

frequency reduction in the spectral levels, with the maximum shifting to the lower frequencies while receding from the edge.
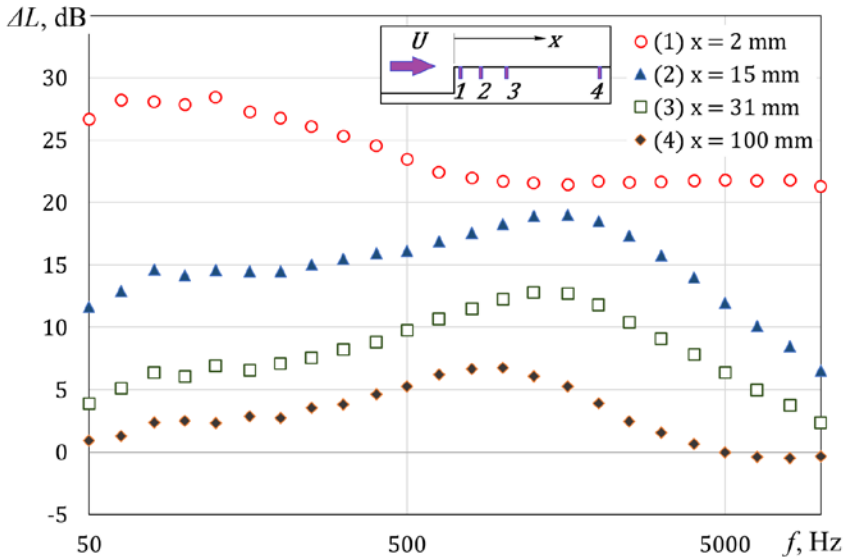

Fig. 1. The excess of the wall pressure fluctuations spectrum above the level of undisturbed turbulent boundary layer on the step surface with a height of 5 mm; the flow velocity U=45 m/s

It was showed that for this configuration there is a significant increase in the spectral levels of wall pressure fluctuations in comparison with the undisturbed turbulent boundary layer. A small dependence of the spectral levels on the thickness in the boundary layer for the steps with the relative height h/δ>0.03 has been demonstrated. At the same time, a substantial transformation of the spectra at the distance of 3 heights of the step with further uniform decline in all the range of Strouhal numbers reveals a much more significant influence of step height on the wall pressure fluctuation characteristics.

The results of experimental studies of wall pressure fluctuations on the surface of swept steps were represented. It was shown that the three-dimensional nature of the upcoming flow does not significantly affect the spectral levels of pressure fluctuations at the angles less than 30 degrees. The further increase of the angle is accompanied by a progressive decrease in the spectral levels of pressure fluctuations throughout the frequency range.

As a result of experimental studies has been developed a computational model of the wall pressure fluctuations field on the surface of the step. Contribution of different fields in the vicinity of the step to the acoustic radiation is

numerically evaluated on its basis. It is shown that the contribution of the wall pressure fluctuation field on the surface of the step is comparable with that of the other non-uniform fields in the vicinity of the step, but it is not dominant in case of small steps.

The calculation estimation demonstrates that presence of steps on the surface of a fuselage may be a reason of increased local noise generation inside an aircraft.

References

1. Efimtsov B.M. Wall pressure fluctuation field characteristics at large Reynolds numbers // Akustichesky zhurnal, 1982, Vol. 28, № 4, pp. 491-487.
2. Efimtsov B.M. Similarity criteria of wall pressure fluctuation spectra of the turbulent boundary layer // Akustichesky zhurnal, 1984, Vol. 30, № 1, pp. 58-61.
3. Awasthi M, Forest J.B., Morton M.A., Devenport W., Glegg S. The Disturbance of a High Reynolds Number Turbulent Boundary Layer by Small Forward Steps // AIAA paper 2011. №2777. 26 p.
4. Ji M., Wang M. Sound generation by turbulent boundary layer flow over small steps // Journal of Fluid Mechanics. 2010, vol. 654, pp. 161-193.
5. Efimtsov B.M., Kozlov M.N., Kravchenko S.V. Andersson A.O. Wall pressure-fluctuation spectra at small forward-facing steps // AIAA paper 99-1964. 11p.
6. Efimtsov B.M., Kozlov M.N., Kravchenko S.V. Andersson A.O. Wall pressure-fluctuation spectra at small backward-facing steps // AIAA paper 2000-2053. 10p.
7. Golubev A.Yu. Specific Features of Pressure-Fluctuation Fields in the Vicinity of a Forward-Facing Step – Backward-Facing Step Configuration // Acoustical Physics, 2018, Vol. 64, № 1, pp. 64-69.

A PECULIAR CASE OF FAN-WING ACOUSTICS

Vladimir V. Golubev, Stanislav Karpuk, Marina Kazarina
Embry-Riddle Aeronautical University, Daytona Beach, USA,
golubd1b@erau.edu

This work presents a numerical study of the acoustic signature of NACA 65_4221 airfoil featuring a leading-edge-embedded Cross-Flow Fan (CFF) used as an Active Circulation Control (ACC) device. Such fan-wing design has been proposed and recently investigated [1] for a prospective medium-size Extremely Short Take-Off and Landing (ESTOL) UAV concept. Three different configurations are analyzed and compared to determine the acoustic impact of the fan-wing concept: the conventional airfoil with a single-slotted Fowler flap, the fan-wing airfoil with the Fowler flap and non-operating fan, and the fan-wing airfoil with the rotating fan. Far-field noise levels are predicted based on the near-field CFD data using an integral technique, with several interfering noise sources identified.

The CFF technology, first patented in 1893 by Mortier, is now actively used for heating, ventilation, and air conditioning. Such fan consists of three major parts: the inlet, the impeller with forward-curved blades located inside the housing consisting of rear and vortex walls, and the outlet (Figure 1*(a)*). For almost four decades, the fan has been discussed as a potential Active Flow Control (AFC), distributed-propulsion, high-lift, and VTOL device. Kummer and Dang [2], Chawla [3], Lin [4] and Nieh [5] studied CFF flow physics when the fan is embedded in the airfoil. Kummer and Dang [2] also considered CFF as a novel propulsion device that could improve the aircraft performance in order to reduce the fuel burn and decrease the operational cost of the aircraft. Numerical and experimental investigations showed significant increase in airfoil lift and increase of the stall angle of attack. In addition, Ref. [2] demonstrated the thrust capabilities of the fan embedded close to the wing trailing edge by building a number of scaled UAV prototypes. Application of CFF as a VTOL device was studied by Gossett [6] and included a conceptual design of a VTOL aircraft.

Application of CFF to a commercial aircraft was studied by Kramer et al. [7] and showed a promising result. It was determined that an optimized Goldschmied wing with the fan embedded at the trailing edge of the transonic commercial aircraft could reduce fuel consumption comparing to Boeing SUGAR aircraft by 12% percent.

The research on using CFF as a high-lift device was conducted by Gologan et al. [8] and Phan [9]. Ref. [8] used the same fan configuration used by Kummer and Dang [2] to investigate the power requirements for the fan installed in a commercial regional STOL aircraft. Although the model was not optimized, the wing-embedded CFF showed potential to be a strong high-lift

70

device for a commercial aircraft. Phan [9], on the other hand, investigated a different configuration, with CFF embedded into the leading edge of the wing, as shown in Figure 1*(b)*. He applied his results to examine flight performance data based on Piper PA-18 aircraft. The results demonstrated reduction of the take-off run by 50%. In addition, three-dimensional CFD analysis was performed on a wing featuring a cross-flow fan embedded along the entire span.
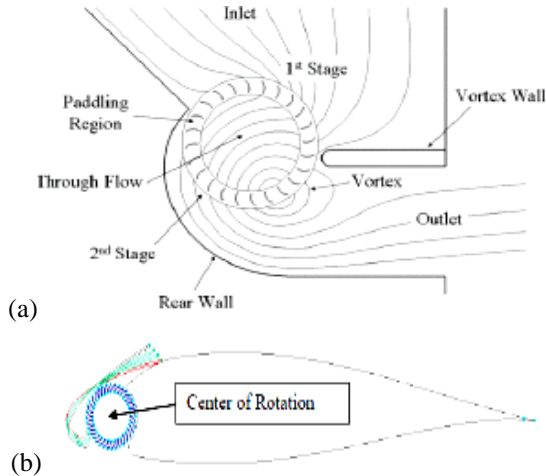

(a)

(b)

Fig. 1. (a) CFF schematic; (b) airfoil geometry with LE-embedded CFF

The feasibility of the leading-edge-embedded CFF high-lift technology applied to a multi-purpose transport aircraft was studied by Karpuk et al [1]. An aircraft with the CFF technology was designed and compared to a similar airplane featuring conventional high-lift devices. For a 16,000 lb aircraft, the take-off distance reduction and a payload reduction due to the fan mechanical system were 18% and 13.6% respectively.

Although significant work was done regarding CFF physics and its aerodynamic ACC impact when embedded in the aircraft wing, the acoustic behavior of the fan-wing concept was never addressed. The present work focuses on the numerical aeroacoustic investigation of the CFF airfoil. Three cases were simulated: an airfoil with a single-slotted Fowler flap and without the fan, a CFF airfoil with the flap and non-operating fan, and a CFF airfoil with the flap and operating fan.

Numerical simulations employed a conventional NACA 65_4221 airfoil with the flap-to-chord ratio is 30% and the flap deflection of 30^0. For the baseline airfoil (Case 1), the slot gap was equal to 6%, but the gap for the CFF airfoil embedding 36-blade fan was reduced to 1% to ensure attachment of the jet flow from the fan.
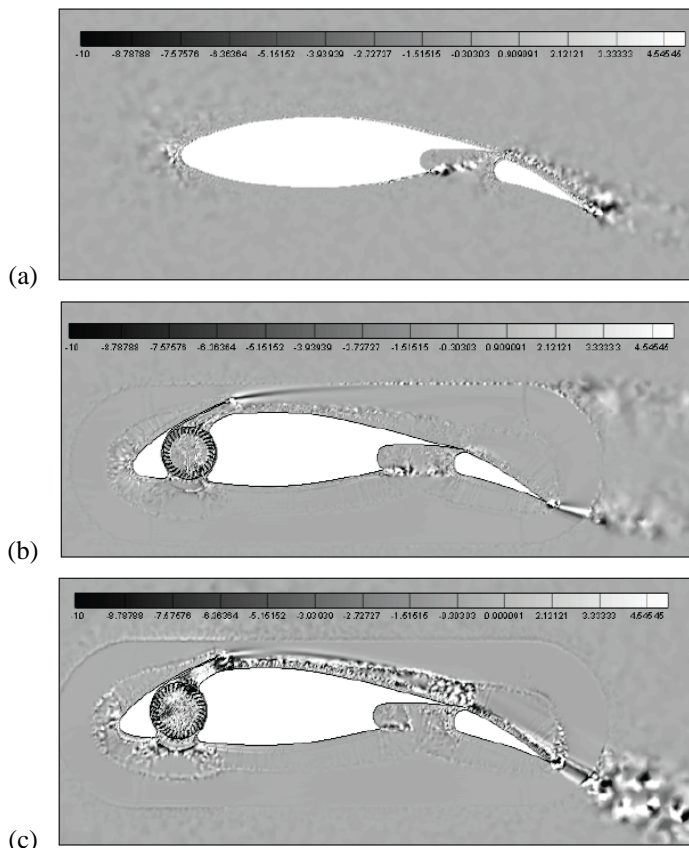
(a)

(b)

(c)

Fig. 2. Dilatation contours: (a) baseline case; (b) CFF airfoil with stationary fan;
(c) CFF airfoil with rotating fan

Pointwise [11] T-REX mesh generator for accurate resolution of the boundary layer was used for all cases, with the maintained value of y+=1. The computational-domain far-field was located 70 chords away, with imposed far-field non-reflecting boundary conditions. All computational cases have 450000-500000 cells.

ANSYS Fluent [12] with embedded FW-H algorithm was used to estimate the far-field acoustics of the airfoils. Unsteady RANS with Spalart-Allmaras turbulence model was used. The airfoils were simulated with the free-stream velocity of 15 m/s at $\alpha=0^0$. 30 virtual microphones were located 15 chords away to capture the far-field pressure around the airfoil.

Preliminary results obtained for the dilatation fields for each case are shown in Fig. 2. It appears that the acoustic sources for the Case 1 baseline air-

foil configuration (without the fan) are localized at the slot region to contribute to the expectedly dominating trailing-edge noise components. Similar results are observed in Case 2 for the CFF airfoil with non-operating fan. Furthermore, the slat lip and the unsteady flow disturbed by the stationary fan generate additional acoustic components. However, the most severe noise appears induced by the rotating fan in Case 3. The major additional noise source is attributed to the wall jet generated by the fan from the slat exit on the suction side of the airfoil. The final presentation will include comparison of acoustic directivities and acoustic spectra at the selected monitor points to clearly identify the contribution of the dominating fan-wing acoustic sources.

References

1. Karpuk. S., Kazarin. P., Gudmundsson. S., Golubev. V., "Preliminary Feasibility Study of a Multi-Purpose Aircraft Concept with a Leading-Edge Embedded Cross-Flow Fan", 2018 AIAA Aerospace Sciences Meeting, Kissimmee, FL, January 2018.
2. Kummer, J. D., Dang, T. Q, "*High-Lift Propulsive Airfoil with Integrated Crossflow Fan*," AIAA Journal, Vol. 43, No. 4, 2006, pp. 1059-1068.
3. Chawla, K., "*Optimization of Cross Flow Fan Housing for Airplane Wing Installation*," M.S. Thesis, University of Texas at Arlington, Arlington, TX, 1984.
4. Lin, C.-H., "*A Wind Tunnel Investigation of the External Aerodynamics of an Airfoil with an Internal Cross Flow Fan*," M.S. Thesis, University of Texas at Arlington, Arlington, TX, 1986.
5. Nieh, T.-W., "*The Propulsive Characteristics of a Cross Flow Fan Installed in an Airfoil*," M.S. Thesis, University of Texas at Arlington, Arlington, TX, 1988.
6. Gossett, D. H., "*Investigation of Cross Flow Fan Propulsion for a Lightweight VTOL Aircraft*," M.S. Thesis, Naval Postgraduate School, Monterey, CA, Dec. 2000.
7. Kramer, B., Ansell,P., D'Urso, S., Ananda, G., Perry, A., "*Design, Analysis, and Evaluation of a novel propulsive Wing Concept,*" Final Report, Rolling hills Research Corporation, June 30th, 2016.
8. Goland, C., Mores, S., Steiner, H., Seitz, A*., "Potential of the Cross-Flow Fan for powered-Lift Regional Aircraft Application"*, 9th AIAA Aviation Technology, Integration, and Operations Conference (ATIO), 21-23 September 2009, Hilton Head, South Carolina.
9. Phan., N, H., *"Leading Edge Embedded Fan Airfoil Concept – a new powered High Lift Technology"*, PhD Dissertation, Syracuse University, Syracuse, NY, 2015.
10. Pointwise Grid Generator, http://www.pointwise.com/.
11. ANSYS FLUENT 12.0 Users Guide, April, 2009.

COMPARISON OF SOME POPULAR LOW-ORDER JET NOISE PREDICTION SCHEMES FOR HEATED AND UNHEATED JETS

V. Gryazev, S. Karabasov

Queen Mary University of London, London,
v.gryazev@qmul.ac.uk, s.karabasov@qmul.ac.uk

Hybrid methods for jet noise prediction based on some form of linearisation of the governing Navier-Stokes equations have been around since the pioneering work of Lighthill [1]. Since the classical Lighthill acoustic analogy, a number of researchers contributed to the development of models with increasingly more accurate decomposition of the governing equations into a linear sound propagation and a nonlinear sound generation part. Most notable are the contributions by Lilley [9] and Goldstein [3].

Following the original introduction of the Goldstein generalized acoustic analogy [3], it has been used in several subsequent works including [4, 5, 8]. Also based on the Goldstein analogy, in a series of works [6, 7] a spectral method for noise prediction from heated subsonic axisymmetric jets was developed. The sound pressure density is calculated using an acoustic integral, which includes two distinct noise sources. One source is based on the covariance of the fluctuating Reynolds stresses (typical of pure unheated jets) and the other is based on modelling the fluctuating enthalpy source (typical of heated jet noise). For each source a separate semi-empirical model was developed. For example, the isotropic turbulence model [2] was applied to estimate the covariance of the fluctuating Reynolds stresses. For sound propagation, the Green's function method was used that is based on solving the Lilley equation [9] under the conditions of constant jet pressure as well as the locally parallel mean flow, following the work of Tam and Auriault [10]. The entire formulation was adjusted to be able to operate with the time-averaged flow fields and fluctuation variances which can be obtained from solving the Reynolds Averaged Navier Stokes (RANS) equations. The full model was calibrated and verified using an extensive set of jet noise data from NASA. In parallel, the Green's function solution method, which was used for numerically solving the Lilley equation, was verified using analytical solutions for plug flow profiles.

One attractive feature of the Khavaran model [6, 7], which explicitly accounts for both the heated and the unheated jet sources, is the relatively small number of calibration parameters it uses. Our goal in this paper is to implement and test the Khavaran model for conditions of the heated and unheated jets of the SILOET experiment. Compared to original model [7], which was based on solving the standard Lilley equation which only includes the sound mean flow refraction effects, we also include the variable sound speed effect on sound propagation into account. The conditions of the heated and unheated SILOET

jet cases, the corresponding reference solutions based on the Large Eddy Simulation (LES) and the Ffowcs Williams –Hawkings (FW-H) method, as well as the (scaled) far-field microphone data from the SILOET experiment have already been published in [11]. In what follows the Khavaran jet noise model will be first implemented with the recommended calibration coefficients from [6, 7]. It will be then shown how the original source model needs to be recalibrated for good noise predictions in case of the SILOET jets. We will further compare the predictions of our best re-calibrated model's predictions with the predictions of the Tam and Auriault model [10] which has been implemented for the same two jet cases. Finally, a new model for heated and unheated jet noise predictions will be introduced based on combining the model from [3] for the noise source due to the fluctuating Reynolds stresses and the Khavaran model [7] for the fluctuating enthalpy noise. An outline of our work is given below.

The model of Khavaran [7] is considered with taking into account the variable sound speed on mean flow sound propagation. The jet flow field is represented by a piece wise constant function in the stream-wise direction and ignore the stream-wise derivatives, which corresponds to the locally parallel jet flow model. Following [6,7], the far-field sound pressure is defined,

$$\overline{p^2}(\mathbf{x}, \omega) = \int_V \overline{p^2}(\mathbf{x}, \mathbf{y}, \omega) d\mathbf{y},$$

where

$$\overline{p^2}(\mathbf{x}, \mathbf{y}, \omega) = \int_\xi \int_{-\infty}^{\infty} G^*(\mathbf{x}, \mathbf{y} - \xi/2, \omega) G(\mathbf{x}, \mathbf{y} + \xi/2, \omega) q(\mathbf{y}, \xi, \tau) e^{i\omega\tau} \, d\tau d\xi$$

is the far-field spectra density per unit volume of turbulence, G is the relevant Green's function, and q is two-point fourth-order space-time correlation between source points and separated by time and space. Far-field sound pressure is modelled as combination of two independent sources responsible for the fluctuating Reynolds stresses and the fluctuating enthalpy noise so that

$$\overline{p^2}(x, r, \omega) = AF_A + BF_B$$

where A and B are calibration coefficients. The calibration coefficients can be determined by the far field sound spectra calibration at 90° observer angle.

$$F_A = |\cos^2\varphi + Q\sin\varphi|^2 \, F, \quad F_B = (1 - M^s\cos\varphi)^2 \frac{15}{16} \frac{c_\infty^2}{\kappa} \frac{\overline{h_{t'}^2}}{\overline{h^2}} F,$$

$$F = \frac{\rho_\infty^2 I_{1111} k^4 (1 - M^s\cos\varphi)^2 |\cos^2\varphi + Q\sin\varphi|^2}{(4\pi R)^2 (1 - M_c\cos\varphi)^2} \sum_{n=0}^{\infty} (1 + \delta_{0n}) f_n f_n^*.$$

$$Q^2 = \Phi^2 - \cos^2\varphi, \quad \Phi^2 = \frac{\rho}{\rho_\infty} (1 - M^s\cos\varphi)^2$$

where $k = \omega / c_\infty$ is wave number, $M^s = U / c_\infty$ Mach number, $M_c = U_c / c_\infty$ convective Mach number, I_{1111} the source, f_n modes of the Green's function, $\overline{h_{i'}^2} / \widetilde{h^2}$ enthalpy factor which play significant role for heated jet.
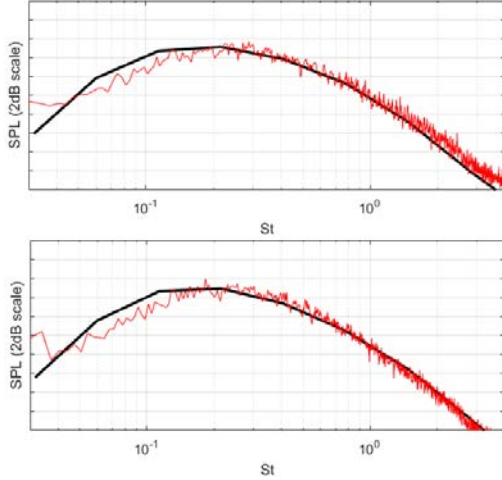

Fig. 1. Far-field noise spectra predictions vs the experiment for the heated SILOET jet case at 90° (top) and 60° (bottom)

Here we develop a novel acoustic analogy scheme which combines the Khavaran model of the enthalpy fluctuation noise source with the methodology based on the Goldstein generalised acoustic analogy formulation [3] which was implemented in [5]. The idea of Goldstein's acoustic analogy is to exactly re-arrange the fundamental Navier-Stokes equations in such a way that the left-hand side of the linear hyperbolic part of the original equations remains, while in the right-hand side there are the effective sources.

As a result, the noise in the far field zone can be calculated as a convolution of sources with the corresponding matrix Green's function responsible for the sound propagation in the jet.

$$\hat{P}(\mathbf{x}, \omega) = \int_{\mathbb{R}^3} \int_{\mathbb{R}^3} \hat{R}_{ijkl}(\mathbf{y}, \mathbf{\Delta}, \omega) \hat{I}_{ij}(\mathbf{y}, \omega; \mathbf{x}) \hat{I}_{kl}^*(\mathbf{y} + \mathbf{\Delta}, \omega; \mathbf{x}) d\mathbf{\Delta} d\mathbf{y},$$

where $\hat{I}_{ij}$ is second-rank wave-propagation tensor which includes the components of the adjoint vector Green's function and the mean flow gradients; $\hat{R}_{ijkl}$ is the Fourier transform of the temporal-spatial cross correlation of the turbulent sources.

$$\hat{R}_{ijkl}(\mathbf{y}, \mathbf{\Delta}, \omega) = \int_\tau R_{ijkl}(\mathbf{y}, \mathbf{\Delta}, \tau) e^{-i\omega\tau} d\tau = \int_\tau \overline{T_{ij}'(\mathbf{y}, \cdot) T_{kl}'(\mathbf{y} + \mathbf{\Delta}, \cdot + \tau)} e^{-i\omega\tau} d\tau$$

Integral formula, which involves the covariance tensor of the 4th rank in the (6+1) space-time is the main equation for far-field predictions in the Goldstein acoustic analogy. The fourth-order two-point velocity correlations can be approximated by a Gaussian function [10].

$$R_{ijkl}(\mathbf{y}, \mathbf{\Delta}, \tau) = A_{ijkl}(\mathbf{y}) \exp\left[-\frac{|\Delta_1|}{\tilde{u}\tau_s} - \frac{\ln 2}{\ell_s^2}\left((\Delta_1 - \tilde{u}\tau)^2 + \Delta_2^2 + \Delta_3^2 \right) \right],$$

where $A_{ijkl} = C_{ijkl}(2\overline{\rho}k)^2$, $\ell_s = C_\ell \kappa^{1.5}/\varepsilon$ and $\tau_s = C_\tau \kappa/\varepsilon$ are the turbulence length- and time-scales; C_{ijkl}, C_ℓ and C_τ are nondimensional constants and κ and ε are the usual turbulence length and time scales obtained from RANS calculations.

Results of the spectra predictions of the new combined model are compared with those of the Khavaran model [6, 7], the Tam & Auriault model [10], and the original Goldstein acoustic analogy model implemented in [5].

References

1. Lighthill, M.J. On Sound Generated Aerodynamically. I. General Theory. Philosophical Transactions of the Royal Society, 1952
2. Batchelor, G.K., "The Theory of Homogeneous Turbulence," Cambridge University Press, 1953.
3. Goldstein, M.E., "A generalized acoustic analogy," J. Fluid Mechanics, 488 (2003), pp. 315-333.
4. Goldstein, M. E. and Leib, S. J. 2008 The Aero-acoustics of slowly diverging supersonic jets J. Fluid Mech., 600, 291–337.
5. Karabasov, S.A., "Understanding jet noise," Phil. Trans. R. Soc. {368} (2010), pp. 3593-3608.
6. Khavaran, A., Kenzakowski, D.C., and Mielke-Fagan, A.F., "Hot jets and sources of jet noise," International J.Aeroacoustics, 9 (2010), pp. 491-532.
7. Khavaran, A., and Bridges, J., "An empirical temperature variance source model in heated jets," Technical Report, TM-2012-217743, NASA, 2012.
8. Leib, S. J. and Goldstein, M. E. 2011 Hybrid Source Model for Predicting High-Speed Jet Noise AIAA Journal, 49(7), 1324–1335.
9. Lilley, G.M., "On the noise from jets, noise mechanisms," AGARD-CP-131 (1974) 13.1-13.12.
10. Tam, C.K.W., Auriault. L., "Mean flow refraction effects on sound radiated from localized source in jets," J. Fluid Mechanics, 370 (1998), pp. 149-174.
11. Markesteijn, A.P., Semiletov, V.A., Karabasov, S.A. "GPU CABARET solutions for the SILOET jet noise experiment: Flow and noise modelling", AIAA-2016-296
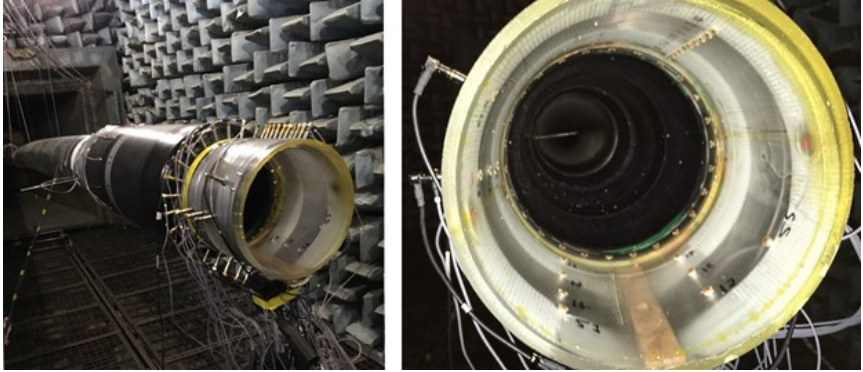
EXPERIMENTAL STUDY IN THE ANECHOIC CHAMBER DIFFERENCE IN DIAGRAMS OF SOUND RADIATION DIRECTIVITY FROM THE OPEN END OF THE AIR INLET WHEN MODELING STATIC AND FLIGHT CONDITIONS

M.S. Ipatov, V.F. Kopiev, A.E. Kruglyaeva, **N.N. Ostrikov**,
M.A. Yakovets

TsAGI, Zhukovsky, Russia

The numerical simulations carried out in the work [1] demonstrate a significant difference in directivity for the radiation of the same duct mode from an engine inlet when operating in static condition versus in the forward flight. It was shown that the large change in directivity is the result of the combined effects of diffraction and refraction realized near inlet orifice due to flow inhomogeneity in the static conditions.

The present work is aimed at an experimental investigation of this effect, for which an installation was assembled in the anechoic AK-2 chamber (the scheme and photograph of the assembled unit are shown in Fig. 1) consisting of a small-scale air inlet model in which the azimuthal rotating modes are generated with the help of 12 acoustic drivers installed flush on the inner surface of the duct with a uniform pitch in the azimuth direction, a radial fan Vesa Vran6-6,3 to create a suction flow inside the duct of an air inlet model, an internal diameter 200 mm air duct, which coincides with the duct diameter of the air inlet model, liners sections for damping the fan noise.

Fig. 1. Scheme (left) and photo (right) of the small-scaled inlet in chamber AK-2 experiment

Since the outer diameter of the small-scale model of the air inlet intended for testing is 270 mm, a nozzle with a diameter of 60 cm was used to realize the co-flow created by the outer contour of K3. The velocities of the co-flow and suction flow varied independently from 0 to 40 m/s, and measurements of the radiation directivity pattern were made.

Fig. 2. Location of the 48 microphone array with respect to the air inlet duct

To control the structure of the modes generated in the duct by 12 speakers, a 48 microphones array was developed (Fig. 2), containing an annular grid of 26 microphones, an axial array of 10 microphones, and 12 more microphones located at different axial and azimuthal coordinates. This array, capable of resolving sound modes in the range of azimuth numbers from $m = -12$ to $m = 13$, and also extracting the radial structure of the sound field, was established during the tuning of the mode generation system at the open end of the air inlet model, and after the adjustment was dismantled. For tuning the system of generation of modes, an algorithm developed earlier in work [2] was used, which allows generating modes with predefined azimuth numbers dominating the remaining modes by 20 dB or more, including generating only one dominant azimuth mode.

In the experiments carried out in the channel of the air intake model, a different structure of azimuth modes was generated in the frequency range 4-8 kHz, in which the azimuthal number of propagating modes does not exceed $|m| = 12$, and therefore the structure of the sound field is completely extracted by 48 microphone array.

Based on the results of experimental studies, the following results were obtained.

The implementation in the duct of only the suction flow with the 48 microphones array installed on its cutoff has shown that the tuning of the modes performed in the absence of a flow in the channel is retained even if there is a stream (in top Fig. 3, the setting for the dominant 5th azimuth mode all considered speeds).

During the test measurements, it was found experimentally and theoretically explained the hypersensitivity to the temperature regime of the radiation pattern emitted from the duct under the same operating mode of the sound source. It is shown that a change in the temperature in the anechoic chamber by

3°C leads, at some frequencies of sound generation, to a discrepancy of the sound pressure levels at some viewing angles by an amount of the order of 2 dB. According to the results of the test measurements, it was concluded that it is necessary to perform at least two repeated measurements in the same modes during the tests with a repeatability of the temperature regime within $T = \pm 0.5^{\circ}C$.
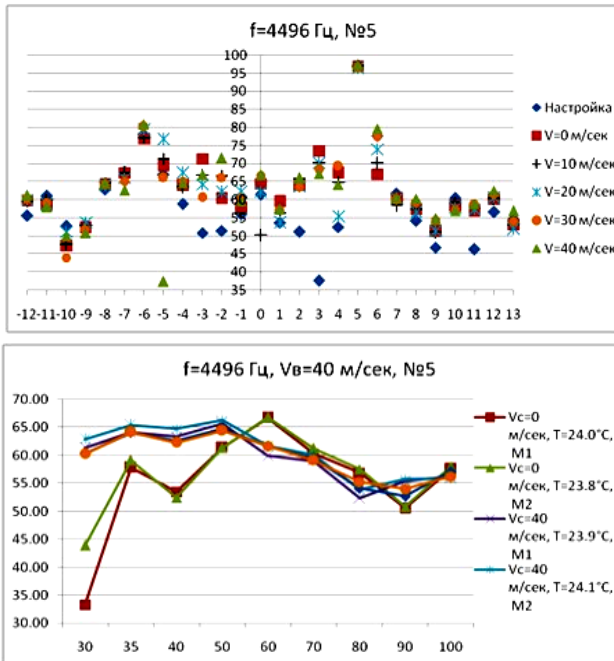
Fig. 3. Generation of the 5th target mode at a frequency of 4,496 Hz for different operating modes: the amplitude of the azimuth modes at different suction flow rates (top); the comparison of the directivity diagrams at different speeds of the co-flow at the velocity of the suction flow Vs = 40 m/s (bottom)

A smoke visualization of the flow near the open end of the air inlet duct was carried out for various ratios between the velocity of the suction stream and the rate of the co-flow, which showed that under the test conditions in the anechoic chamber AK-2, the shear layer of the co-flow stream is sucked at large excesses of the suction velocity of the flow into the air inlet duct above the nonzero velocity of the co-flow.

Studies have shown that the effect found in [1] for single-mode sound generation in a duct, as a whole, is experimentally confirmed. The analysis of the received sound field patterns shows their significant dependence on the

speed regime for the suction and co-flows selected in the tests with the same tuning of the generation system. Fig. 3 (bottom) shows an example of a change in the directivity diagram in the case of a single-mode structure of the sound field in the duct, and in the bottom Fig. 4 is the case of a multimode structure of the generated sound field. It is shown that at different observation angles, a change in the sound pressure level by 10 dB can be observed in the case of single-mode sound generation and by 20 dB in the case of multimode sound generation when the velocity regime for flows changes. It is found that the most frequently realized situation is the one at which the amplitude at the maximum of the radiation pattern in the absence of a co-flow is less than the corresponding amplitude in the case of equal velocities of the co-flow and suction flow by an amount of the order of 2-4 dB.
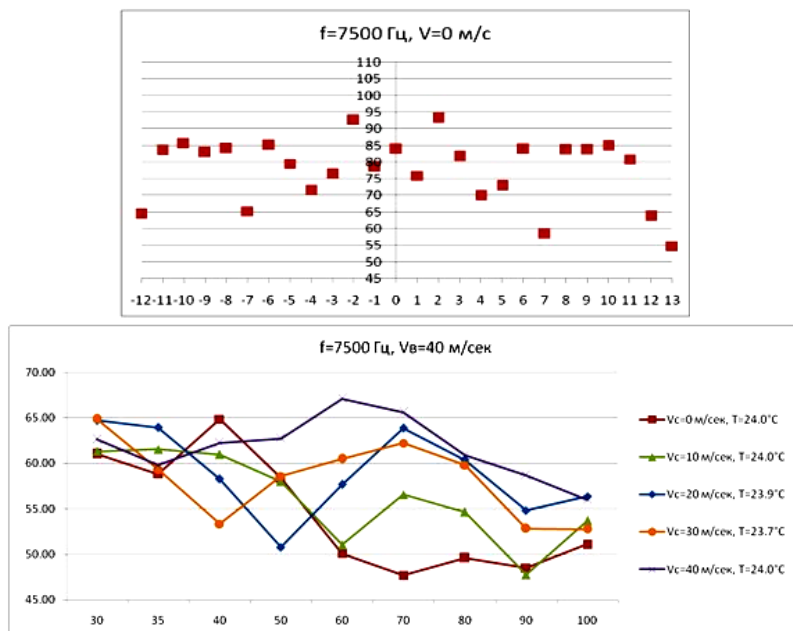
Fig. 4. Multimode generation at a frequency of 7500 Hz for various modes of operation: the amplitude of the azimuth modes in the absence of a flow (top); the comparison of the directivity diagrams at different speeds of the co-flow at the velocity of the suction flow Vs = 40 m/s (bottom)

Thus, the results of the studies show the need to make adjustments to the methods for recalculating the results of acoustic tests of aircraft engines under static conditions on flight conditions.

References

1. C.K.W. Tam, S.A. Parrish, E. Envia, E.W. Chien. Physics of Acoustic Radiation from Jet Engine Inlets. AIAA Paper 2012-2243.
2. Ostrikov N.N., Yakovets M.A, Ipatov M.S., Pankratov I.V., Denisov S.L. «Experimental study of the effect of flow velocity at the inlet on the azimuthal mode radiation: static and flight», Proceedings of 24th International Congress on Sound and Vibration, July 2017, UK.

A SPLITTING METHOD FOR AEROACOUSTIC SIMULATIONS

Yoshihiro Kato[1], **Igor Menshov**[2,3]

[1]Toyota Central Research & Development Labs., Inc., Aichi, 480-1192 Japan,
kato@cfd.tytlabs.co.jp
[2]Keldysh Institute for Applied Mathematics RAS, Moscow 125047, Russia
[3]SRISA RAS, Moscow 117218, Russia menshov@kiam.ru

A numerical approach to problems of aeroacoustics is considered. This approach is based on splitting the acoustic field from the flow field. Commonly, the level of acoustical fluctuations is much smaller than the flow fluctuation, therefore this method is well fit to deal with variables of different order in magnitude. The method has certain advantages over other methods that treat sound and flow fields in uncouple manner. In particular, numerical schemes for acoustic and fluid equations can be chosen properly to take into account basic features of these equations. In the first approximation, the flow equations are found to be unsplit from the acoustic equations, i.e., the generated sound does not affect the flow field. Feedback effects of acoustics upon fluid are taken into account by terms of higher orders that introduce a minor influence and can be neglected. In the present paper we use this assumption.

There are different flow/acoustic splitting methods that incorporate analytical solutions to Lighthill's equation [1]. All these methods are derived on the assumption that the solid surface is small enough in comparison with the propagating acoustic wave length, and the observation point is far from sound sources. However, in some situations one has to study near acoustic field so that the scale of the solid can not be considered as small as, e.g., an automobile rearview mirror. The above mentioned splitting methods are then not applicable.

In the present paper we develop a different approach. It is inspired by the study of Slimon et al [2]. We consider the solution to the compressible Navier-Stokes equations as an expansion in series with respect to a small parameter that is the squared Mach number. The leading terms in these expansions that define the base flow field is governed by the incompressible Navier-Stokes equations. Higher order terms are for the acoustic field, and are governed by a reduced system that depends on parameters of the base flow. Such an approach allows the acoustic equations to be applied not only in the far field, but in the near field also.

Let us consider the system of compressible Navier-Stokes equations and introduce non-dimensional flow variables by means of inflow parameters: $U = u / u_\infty$, $P = (p - p_\infty) / (\rho_\infty u_\infty^2)$, $R = (\rho - \rho_\infty) / \rho_\infty / M_\infty^2$, where M_∞ is the inflow Mach number. Then, the solution to the obtained non-dimensional system of equations we try to seek in the form of the following asymptotic expan-

sion: $\mathbf{Q} = \mathbf{Q}_* + M_\infty^2 \mathbf{q}' + O(M_\infty^4)$, where $\mathbf{Q} = (R, U, P)$, $\mathbf{q} = (\rho, u, p)$.

The system of equations that correspond to the leading terms is obtained by neglecting $O(M_\infty^2)$ terms. This system reads as the incompressible Navier-Stokes equations with respect to $\mathbf{Q}_*$, and an equation that describes the density perturbation R_*. By introducing $\theta_* = \mathrm{Re}(R_* - P_*)/(\gamma - 1)$, where Re is the Reynolds number and γ is the specific heats ratio, the latter is written as

$$D_*\theta_* / Dt = \Delta\theta_* / \mathrm{Re}/\mathrm{Pr} - \Delta P_* / \mathrm{Pr} - 2e_*e_* \tag{1}$$

where Pr is the Prandtl number, e_* is the strain rate tensor.

The acoustic field is described by terms of order $O(M_\infty^2)$ in the mass and momentum equations:

$$\partial\rho'/\partial t + \partial f_k/\partial x_k = -D_*\rho_*/Dt \tag{2}$$
$$\partial f_i/\partial t + \partial h_{ik}/\partial x_k = -D_*(\rho_* u_{*,i})/Dt$$

with

$$f_i = (1 + \rho_* + \rho')u_i' + \rho' u_{*,i}; \quad h_{ij} = f_i(u_{*,j} + u_j') + (1 + \rho_*)u_{*,i}u_j' + p'\delta_{ij}$$

Here $\rho_* = M_\infty^2 R_*$. We assume that the acoustic field is isentropic, and employ the following relation: $p' = C_*^2\rho'$, where $C_*^2 = \gamma(1 + \gamma M_*^2 P_*)/(\gamma M_*^2(1 + \rho_*))$.

It was shown in [3] that the r.h.-s. of (1) has small effect and can be neglected. With this assumption, there is no need to solve (2); it results in a simple relation $R_* = P_*$ which is used in the present paper.

The flow field equations are calculated with the LES model by Inagaki et al. [4] with the mixed-time-scale SGS model. The discretization method is the finite volume method on the collocated grid [5]. The spatial derivative is approximated by the second-order central difference; time integration is performed with the Crank-Nicolson implicit scheme. The pressure field is calculated by the SMAC scheme.
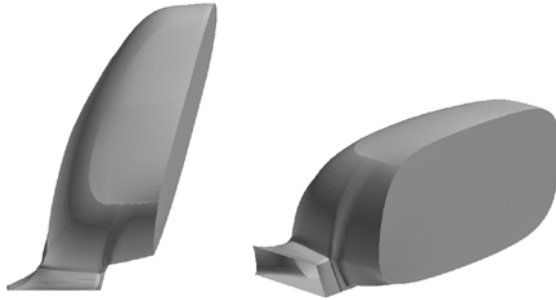
Fig. 1. Rear-view mirror model

The acoustic field is calculated by the finite volume method with the WENO scheme. The solution vectors on the both sides of the cell face are calculated by the fourth-order WENO scheme, and the HLLE approximate Riemann solver is applied to calculate the numerical flux. Time integration is performed with the two-step Runge-Kutta scheme.

The above numerical approach is applied to calculate the acoustic filed generated by the rear-view mirror of an automobile. We analyze a mirror with the shape supported by the short stay shown in Fig. 1. The flow field and the sound field are calculated around the rear-view mirror on a flat plate in uniform flow. A sketch of the computational domain with the boundary conditions used in the calculation of the flow field and the acoustic field is shown in Figs. 2a and 2b, respectively. In the flow field calculations, we use a single-block structured grid over the whole region. The grid spacing normal to the wall for the first point is 0.4mm. The number of the grid points is $309{\times}143{\times}159$ for x, y, z directions. The main flow velocity is 38.9m/s, and the Reynolds number based on a reference length of 0.1m and the main flow velocity is 253,000. Under these conditions, the Mach number is equal to 0.113.
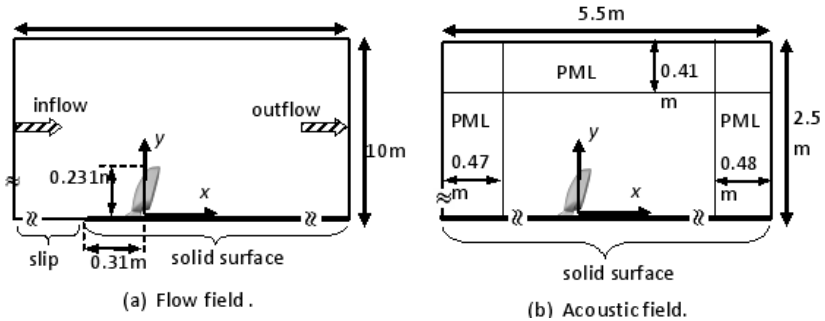
Fig. 2. Computational regions (x-y plane)

In the acoustic field calculations, the number of grid points is $283{\times}150{\times}160$ in x-, y-, z- direction. We implement the PML (Perfectly Matched Layer) approach that guaranties no reflection in the far field. The dumping function in the PML is proportional to square of the distance from the inner edges of the PML.

The Courant number 0.25 was chosen for acoustics, and 0.0625 for flow calculations. One time step calculated for the base flow corresponds to four steps acoustics calculations. To match the computed data, we use a cubic interpolating function that interpolates acoustic variables keeping continuous gradients. The time step for flow is $2.56{\times}10^{-6}$ seconds and that for acoustics is $0.64{\times}10^{-6}$ seconds. This time steps are reasonable as we are interested in the sound in the region 1-2 kHz ($5.0{\times}10^{-4}$ - 10^{-3} seconds).
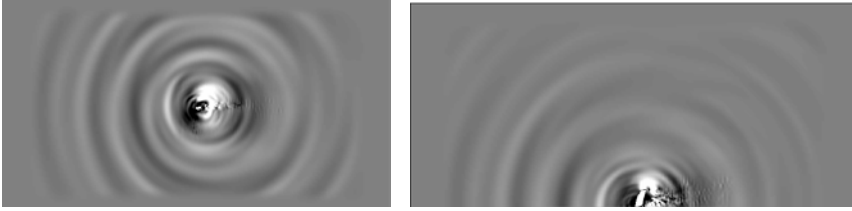
Fig. 3. Computed acoustic field: x-z plane, ground surface (left),
x-y plane (right)

Some numerical results related to the acoustic field are shown in Fig. 3. The distribution of pressure in the x-y plane near the central cross section of the rear-view mirror is shown on the right, and the distribution of pressure on the ground plane on the left.

References

1. M.J. Lighthill. On Sound Generated Aerodynamically I. General Theory. Proceedings of the Royal Society of London A, v.211, 1952, pp.564-587.
2. S.A. Slimon, et al. Development of Computational Aeroacoustics Equations for Subsonic Flows Using a Mach Number Expansion Approach. JCP, v.159, 2000, pp.377-406.
3. Y. Kato, I. Menshov, and Y. Nakamura. Aeroacoustic Simulation around a Circular Cylinder by the Equations Split for Incompressible Flow Field and Acoustic Field. Transactions of the Japan Society of Mechanical Engineers, Series B, v.71, No.711, 2005, pp.2694-2701.
4. M. Inagaki and K. Abe. A Mixed-time-scale SGS Model with Fixed Model-parameters for Practical LES. Journal of Fluids Engineering, v.127, 2005, pp.1-13.
5. M. Inagaki and K. Abe. An Improvement of Prediction Accuracy of Large Eddy Simulation on Colocated Grids. Transactions of the Japan Society of Mechanical Engineers, Series B, v.64, No.623, 1998, pp.1981-1988.
6. M.E. Goldstein. Aeroacoustics. McGraw-Hill, New York, 1976.
7. C.K.W. Tam, J.C. Webb. Dispersion-relation-preserving finite difference schemes for computational acoustics. J. Comput. Phys., v.107, 1993, pp.262–281.

DIRECT NUMERICAL SIMULATION OF SHOCK WAVE / TRANSITIONAL BOUNDARY LAYER INTERACTION

D.V. Khotyanovsky, A.N. Kudryavtsev

Khristianovich Institute of Theoretical and Applied Mechanics, Siberian Branch
of the Russian Academy of Sciences, Novosibirsk, Russia,
khotyanovsky@itam.nsc.ru

In this study, we perform the direct numerical simulation (DNS) of the effects of flow unsteadiness in the transitional supersonic flat-plate boundary layer on shock wave/boundary layer interaction. The DNS of the laminar-turbulent transition in the flat-plate boundary layer is performed with the CFS3D code at the free-stream Mach number $M = 2$. The flow parameters correspond to the experimental studies [1]. The computational procedure for the DNS of the transitional boundary layer follows the approach and the numerical techniques used in our previous studies [2] on supersonic boundary layer transition. The Navier–Stokes computations are performed in a 3D computational domain. Boundary conditions at the inflow boundary specify the self-similar basic laminar boundary layer flow with the superimposed unsteady disturbance in the form of the most unstable linear stability waves, which are two symmetrical three-dimensional Tollmien–Schlichting waves propagating at equal and opposite angles $\pm 55°$ to the flow in the transverse direction. The unstable waves generated by the inflow forcing grow in the streamwise direction (along the *x*-axis), which ultimately triggers the laminar-turbulent transition in the boundary layer further downstream. The shock wave boundary layer (SWBL) interaction is initiated by the incident shock impinging on the transitional boundary layer from the external flow. In experiments [1] the incident shock wave was generated by a wedge located at some distance above the plate. In our computations, the incident shock is set up as a jump in the boundary conditions on the upper boundary of the computational domain. The shock wave angle is $36.2°$, which corresponds to the wedge angle $7°$.

Due to the interaction with the incident shock wave, the adverse pressure gradient is induced in the transitional boundary layer. This leads to boundary layer separation and formation of the reverse flow region, see Fig. 1. Large-scale turbulence structures evolving in the transitional boundary layer cause significant flow oscillations in the SWBL interaction region which manifests in fluctuations of the position and shape of separation and reattachment lines, and also in staggering of the reflected shock wave. The DNS results demonstrate that the instantaneous separation and reattachment curves has complicated, meandering shape, see Fig. 1b where the white curves mark zero skin friction coefficient C_f.
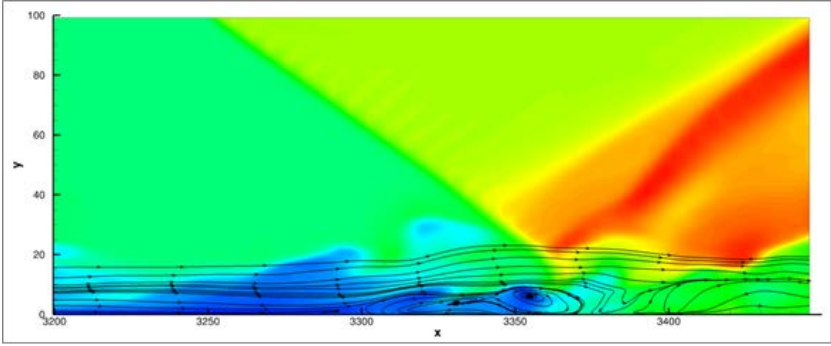
(a)
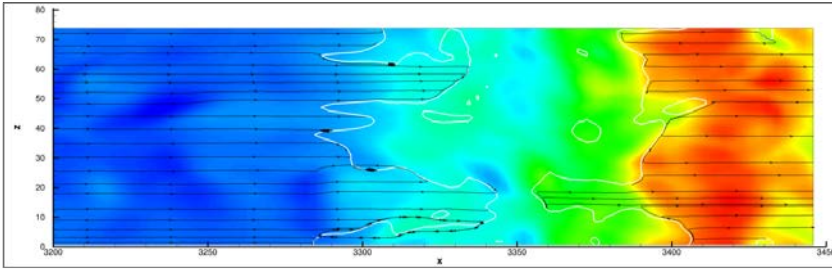
(b)

Fig. 1. Instantaneous visualization of the SWBL interaction; density contours and selected streamlines in the vertical (x, y) plane (a); density contours and the selected limit streamlines on the plate surface in (x, z) plane (b)

The unsteady SWBL interaction also causes substantial fluctuations of the shape and position of the reflected shock wave. Based on time histories of the oscillations of the gas dynamic quantities recorded in the computations behind the reflected shock, see Fig. 2, we can assume that the flow dynamics is determined by irregular fluctuations of various frequencies. The characteristic period of these fluctuations is $10\ldots12$ $\delta_{0.99}/U_\infty$. The maximum period recorded within the timeframe used in our computations is 30 $\delta_{0.99}/U_\infty$ that corresponds to the Strouhal number $Sh = 0.033$. This non-dimensional oscillation frequency is in accordance with the available experimental data.

Based on the DNS results, we can conclude that the flow dynamics is governed by the mutual influence of the separation zone induced by the incident shock wave and the large-scale turbulence structures evolving in the transitional boundary layer.
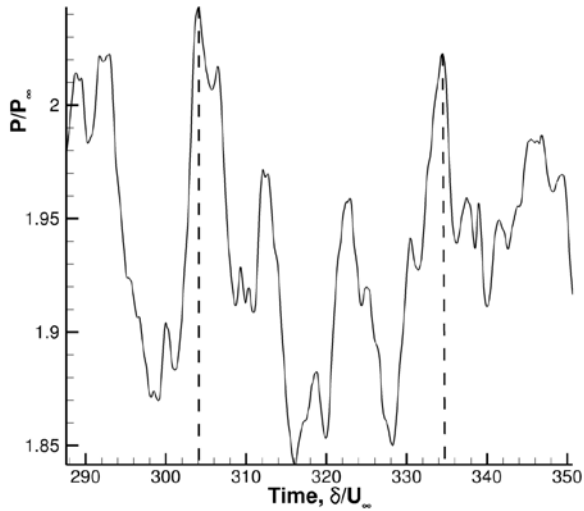
Fig. 2. Pressure fluctuation time history downstream of the SWBL interaction region

References

1. P.A. Polivanov, A.A. Sidorenko, A.A. Maslov. Correlations Study in Shock Wave/Turbulent Boundary Layer Interaction. Technical Physics Letters, v. 36, 2010, pp. 104–107.
2. A.N. Kudryavtsev, D.V. Khotyanovsky. Direct numerical simulation of transition to turbulence in a supersonic boundary layer. Thermophysics and Aeromechanics, v. 22, 2015, pp. 559–568.

MECHANISMS AND MODELLING OF UNDULATED LEADING-EDGE AEROFOILS

J.W. Kim, **J.M. Turner**

Aerodynamics & Flight Mechanics Research Group, University of Southampton, Southampton, United Kingdom, J.W.Kim@soton.ac.uk

It is well established that wavy leading edges (WLE) may offer substantial broadband reductions for the problem of aerofoil interaction noise. However, despite rapid growth in the field there still exists fundamental questions regarding the physical mechanisms by which these reductions are possible. In this work two of the leading explanations -- destructive interference and source strength reduction -- are investigated in order to determine their respective contributions to the noise reductions. In particular the focus is on two universal properties of the observed WLE noise reduction spectra. (1) The increase of noise reduction with frequency. (2) Almost zero noise reduction at low frequency. The findings raise important questions for future modelling approaches concerning which characteristics are critical for properly capturing the physics. Through application of a 1D leading edge (LE) model the interference mechanism is shown as the main driving force for the increasing noise reduction. However, it is found that approaches based solely on the LE lead to erroneous conclusions regarding the significance of source strength variation. This is made apparent from the surface pressure spectra, which shows the strength downstream of the LE is significant at high frequencies. As a consequence, an FW-H (Ffowcs-Williams and Hawkings) solver is used to demonstrate that the majority of the surface is required to accurately predict the noise reduction. Regarding low frequency noise reduction, it is found that despite previously observed reduced strength along the LE line [1, 2], the percentage of the surface with similar strength is similar for straight and wavy cases. This is caused by noise increase regions further downstream, leading to net zero noise reduction.

A description of the current problem is shown in Fig.1. (*a*) and (*b*). We consider the interaction of a prescribed spanwise vortex impinging on the leading edge of a zero-thickness aerofoil with an undulated leading edge (see [1]). The aerofoil has semi-infinite chord length focusing solely on the mechanisms associated with the LE interaction. Fig. 2 (*a*) and (*b*) shows the acoustic pressure and corresponding spectra at an observer directly overhead for SLE (straight leading edge) and two WLE aerofoils with different amplitudes. It is clear how the WLE obtains significant noise reductions compared to the baseline case particularly at high frequency. In Fig. 2 (*c*) the noise reduction spectra is plot against the Strouhal number based on LE amplitude. This demonstrates the approximately linear noise reduction trend associated with the undulated LE, which was first shown experimentally in [3].
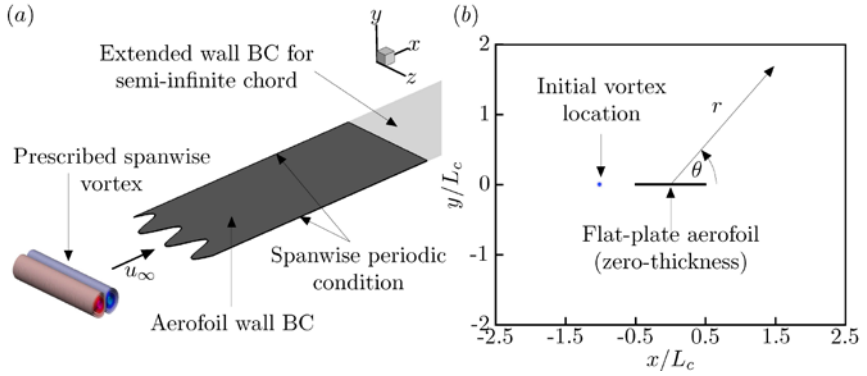
Fig. 1. (*a*) Schematic diagram of the aerofoil-vortex interaction simulations; (*b*) the initial condition viewed from the mid-span (z=0)
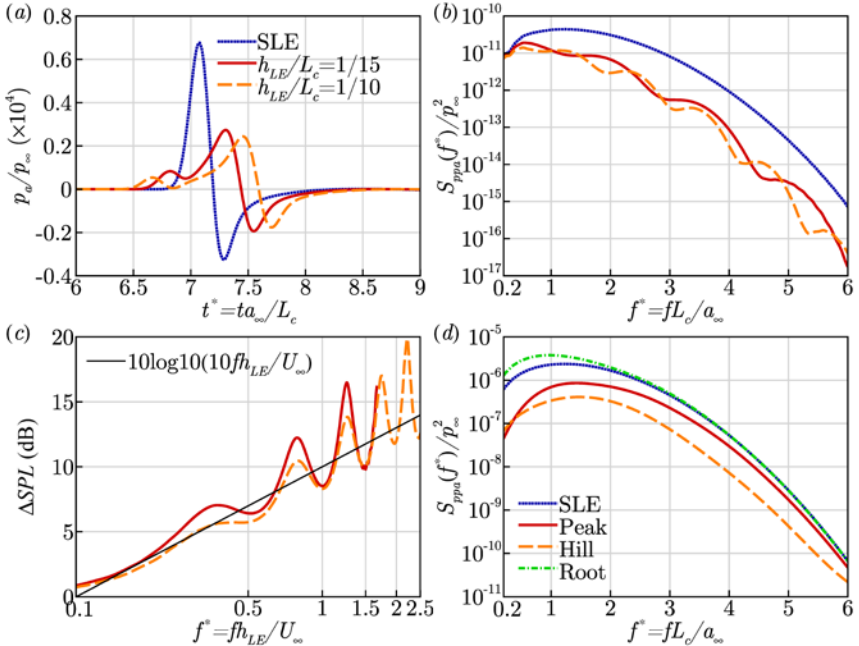
Fig. 2. Acoustic pressure data obtained at a far-field observer $\boldsymbol{x} = (0, 5L_c, 0)$ for SLE and two WLE geometries with differing amplitude: (*a*) time signals of acoustic pressure; (*b*) power spectra; (*c*) noise reduction spectra ΔSPL vs Strouhal number (based on WLE amplitude); (*d*) LE source strength (wall power spectra) vs normalised frequency

The mechanisms associated with this trend are the principle motivation of the current work. Additionally Fig. 2 (*d*) shows the source strength (surface pressure spectra) obtained one point downstream from the LE, revealing significant reductions at low frequency near the WLE peak and hill. The question also arises as to why this trend is not also observed at the far-field.
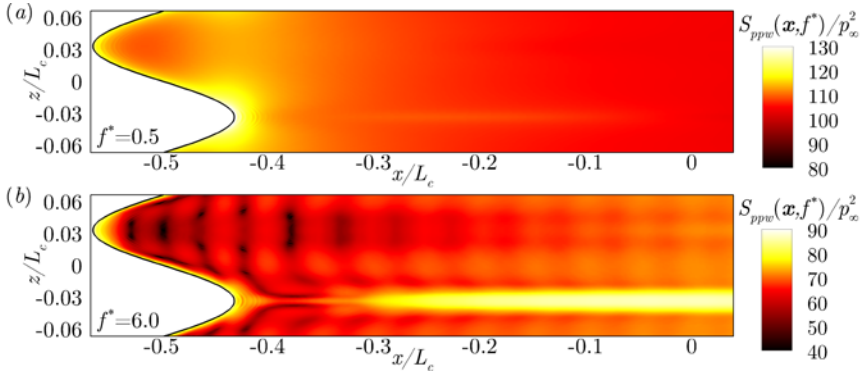
Fig. 3. Surface source strength distribution plot as SPL (dB scale):
(*a*) WLE f^*=0.5; (*b*) WLE f^*=6

Fig. 3 shows contour maps of the surface pressure spectra for a WLE aerofoil at low (f^*=0.5) and high (f^*=6) frequencies. At the lower frequency the source distribution is mostly as expected, concentrated near the leading edge and reducing rapidly further downstream. However at higher frequency the source strength is more distributed in the streamwise direction. In particular there is a prominent streamwise region directly downstream of the root which acts as the primary source. According to this result it is apparent that the full aerofoil surface (not just the LE) needs to be considered to properly capture the physics associated with the WLE. It is shown in the present work that one of the key factors governing the noise reduction is the percentage of surface area with significant source strength, which is found to decrease as a function of frequency.

An attempt has also been to decouple the spanwise destructive interference and source strength reduction mechanisms in order predict their individual contributions to the far-field noise reduction. This is achieved by modifying the input to an FW-H solver. The interference only prediction is obtained by mapping the SLE surface pressure data onto the WLE geometry. Meanwhile the source strength only prediction is obtained by eliminating the spanwise variation in retarded time from the WLE case. The result is shown in Fig.4, revealing that both mechanisms make significant contributions towards the WLE noise reduction, but phase interference is generally dominant.

92
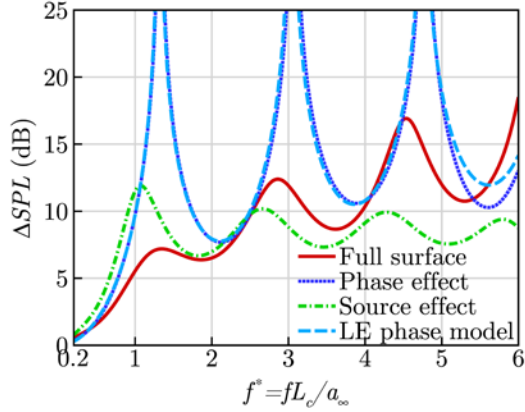
Fig. 4. Modified source FW-H noise reduction predictions highlighting contributions from destructive interference and source strength variation respectively. Comparison is also made with a 1D LE phase model

Acknowledgements

References

1. J.M. Turner, J.W. Kim. Aeroacoustic source mechanisms of a wavy leading edge undergoing vortical disturbances. J. Fluid Mech., v.811, 2017, pp.582-611
2. J.W. Kim, S. Haeri, P.F. Joseph. On the reduction of aerofoil-turbulence interaction noise associated with wavy leading edges. J. Fluid Mech., v.792, pp.526-552
3. C. Paruchuri, P. Joseph, S. Narayanan, C. Vanderwel, J. Turner, J.W. Kim, B. Ganapathisubramani. Performance and mechanisms of sinusoidal leading edge serrations for the reduction of turbulence-aerofoil interaction noise. J. Fluid Mech., v.818, pp.435-464

SECONDARY NOISE SOURCES IN A VORTICAL FLOW INTERACTING WITH AN UNDULATED AEROFOIL

J.W. Kim, **J.M. Turner**

Aerodynamics & Flight Mechanics Research Group, University of Southampton, Southampton, United Kingdom, J.W.Kim@soton.ac.uk

The noise generated by vortical disturbances impinging on an aerofoil has widely been studied in the past where the primary source mechanism is the vortical scattering at the leading edge (LE) of the aerofoil. In this work the secondary source mechanisms -- the subsequent vortical scattering at the trailing edge (TE) and the backscattering of the produced acoustic waves -- are investigated in detail particularly associated with an undulated aerofoil geometry. The present study is performed by employing high-fidelity numerical simulations in which a prescribed spanwise vortex impinges on a non-lifting flat-plate aerofoil with zero thickness situated in an inviscid mean flow. The current investigation provides new findings on the secondary sources and their influence on the noise reduction due to the LE undulation of the aerofoil. It is found that the secondary sources make substantial impacts on the acoustic power spectra and directivity profiles in the far field, which are not described by using the primary source only. One of the most profound observations made in this work is that the vortical scattering at the TE is the dictating source of noise at high frequencies at most of the observer directions irrespective of the LE undulation. Meanwhile the acoustic backscattering (from both the LE and TE) is significant at low frequencies in the downstream direction. When an undulated LE is used, the TE vortical scattering even exceeds the primary source in the upstream direction for the majority of frequencies. The dominance of TE vortical scattering results in the noise reduction (a beneficial effect of using an undulated LE) disappeared in the high-frequency range, which raises a couple of critical questions to address in the future.

The current problem of aerofoil noise generation due to interaction with a prescribed spanwise vortex impinging on the leading edge is depicted in Fig. 1 (*a*) and (*b*). Full details of the computational methodology are provided in reference [1]. Instantaneous contour plots of the acoustic pressure generated as a result of the interaction are shown in Fig 1 (*c*) to (*f*) for the aerofoil with a semi-infinite chord and with a finite chord compared against each other. The aerofoil is a flat plate with zero thickness and zero angle of attack against the mean flow. The semi-infinite-chord case shows the LE vortical scattering (LEVS) that is the primary source (denoted by S1) of the interaction noise generation. In the meantime the finite-chord case reveals additional acoustic waves generated due to the presence of a TE, which are herein referred to as the secondary source

(denoted by S2). The secondary source is subdivided into two: (1) "TE vortical scattering" (TEVS); and, (2) "acoustic backscattering" (ABS).
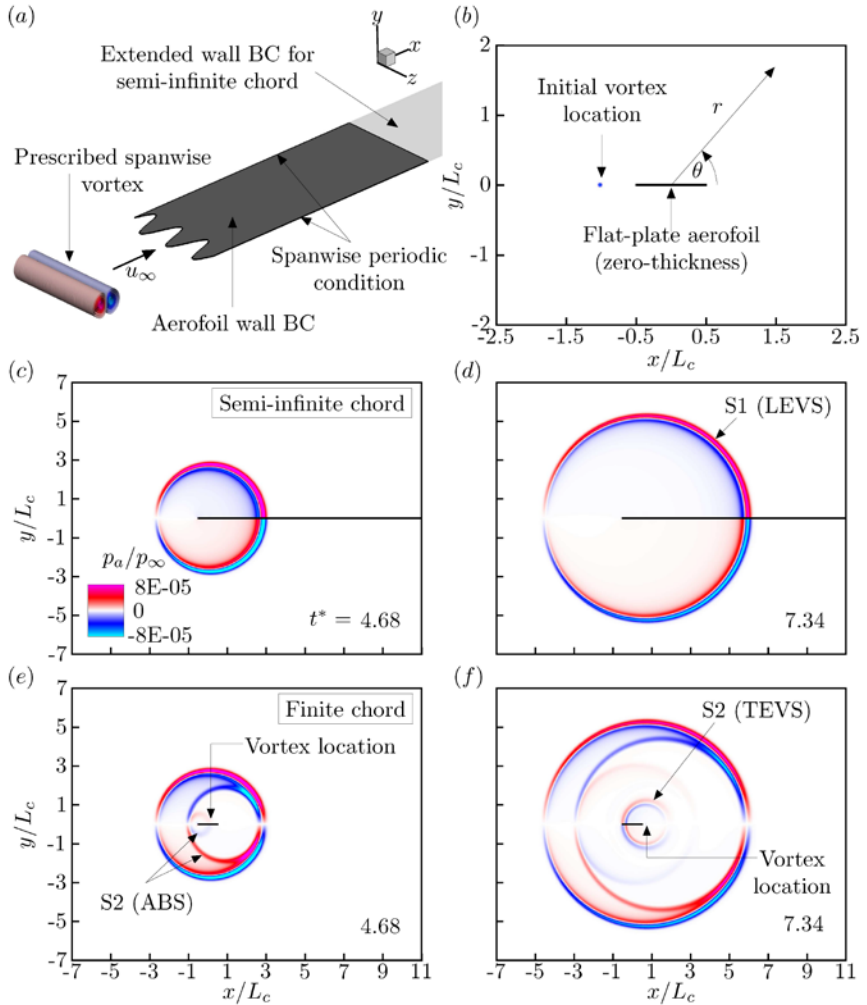

Fig. 1. (*a*) Schematic diagram of the aerofoil-vortex interaction simulations; (*b*) the initial condition viewed from mid-span (*z*=0); (*c* & *d*) acoustic pressure contours obtained by the semi-infinite chord WLE aerofoil at t^*=4.68 and t^*=7.34 respectively; (*e* & *f*) finite chord aerofoil
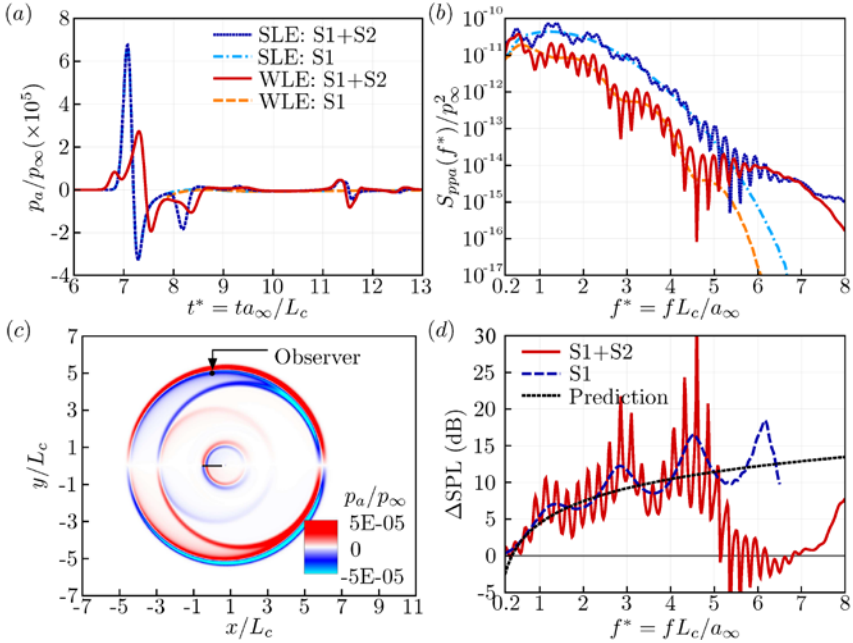
Fig. 2. Far-field acoustic pressure data obtained from the current simulations with two LE geometries (straight and wavy) and two chord lengths (finite and semi-infinite) at an observer $x = (0, 5L_c, 0)$: (a) time signals; (b) power spectra; (c) mid-span instantaneous contour plot of acoustic pressure; and, (d) the noise reduction spectra in comparison with a semi-empirical prediction [2]

The first thing that can be observed in Fig. 2 (b) is that the acoustic power spectra become substantially oscillatory when the secondary sources are included (i.e. the finite-chord cases). In this work it is demonstrated that the spectral oscillations are due to phase relationships between the noise sources (LEVS, TEVS and ABS). Secondly there is a drastic change in the slope of the spectra at high frequencies when the secondary sources are included, in both the SLE and WLE cases. It is also observed that the SLE and WLE cases produce a similar level of acoustic power at the high frequencies after the drastic change takes place. This results in a sudden loss of noise reduction in the high-frequency range shown in Fig. 2 (d) which is a big contrast to the primary-source-only case where the noise reduction keeps increasing with frequency. This work also demonstrates that the loss of noise reduction in the high-frequency range is related with the dominance of TEVS over the other sources. This is shown to be true for the majority of observer angles. In addition to the inviscid case presented here the dominance of TEVS is also shown for moderate Reynolds number flow cases if the vortex has sufficient strength.

96
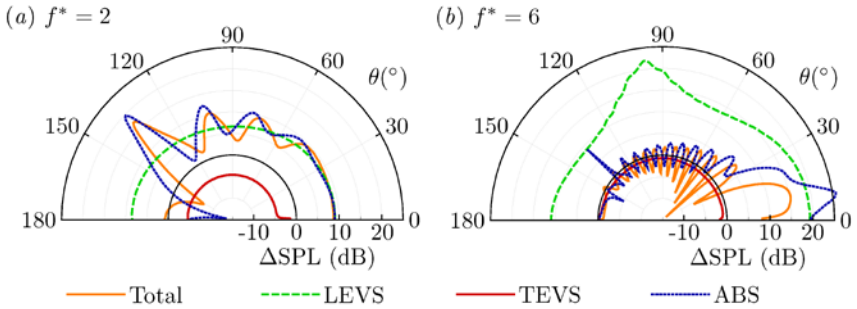
Fig. 3. Directivity profiles of the noise reduction made by WLE compared to SLE, i.e. ΔSPL, at two different frequencies: (a) f^*=2 and (b) f^*=6; the inner semicircle area outlined indicates noise increase

The directivity profiles of the noise reduction made by the WLE at two different frequencies are plotted in Fig. 3. The figure shows that the overall noise reduction (S1+S2) changes tremendously with the observer angle and the frequency by up to multiple tens of decibels. There is a sudden loss of noise reduction in the upstream direction at f^*=2 and an unexpected large gain of noise reduction in the downstream direction at f^*=6. These rather surprising events involved with the secondary sources have not been addressed or encountered in the earlier studies based on either semi-infinite-chord aerofoils [1] or limited observer angles [2].

Acknowledgements

References

1. J.M. Turner, J.W. Kim. Aeroacoustic source mechanisms of a wavy leading edge undergoing vortical disturbances. J. Fluid Mech., v.811, 2017, pp.582-611
2. C. Paruchuri, P. Joseph, S. Narayanan, C. Vanderwel, J. Turner, J.W. Kim, B. Ganapathisubramani. Performance and mechanisms of sinusoidal leading edge serrations for the reduction of turbulence-aerofoil interaction noise. J. Fluid Mech., v.818, pp.435-464

ON THE POSSIBILITY OF ACTIVE CONTROL OF INSTABILITY WAVES IN UNEXCITED TURBULENT JETS

V.F. Kopiev, G.A. Faranosov, S.A. Chernyshev, O.P. Bychkov

TsAGI, Moscow Research Complex, Moscow, vkopiev@mktsagi.ru

A strategy of active control of natural instability waves in subsonic turbulent jets is developed. The strategy is based on the approach tested earlier on tone excited jets. This approach allowed to demonstrate the possibility to control artificially excited instability waves by means of linear adjustment of the excitation and the control action. Analysis of the results for the excited jet control has shown that the approach based on the instability waves generation near the nozzle edge is the most effective in terms of the required amplitude of the control action and, hence, realization of the linear interaction of the waves in the jet.

Peculiarities of such an approach are investigated for the case of the control in broad frequency band. A way to get the reduction of the integral signal level is proposed. The proposed strategy of natural instability waves control is tested on really measured stochastic signals and is shown to be generally realizable. Typical restrictions that should be taken into account during experimental implementation of the strategy are determined.

ON THE DOMINATING INFLUENCE OF THE LARGE-SCALE MOTION IN A JET ON ITS PRESSURE NEAR FIELD AND THE ACOUSTIC FAR FIELD

Felix Kramer, **Ulf Michel**, Charles Mockett

CFD Software E+F GmbH, Berlin, Germany, ulf.michel@cfd-berlin.com

The large-scale motion in a jet is the primary cause for its noise emission in all directions and for all frequencies [1–3]. It is true that the turbulent motion inside the jet appears to be dominated by small-scale velocity fluctuations, but their acoustic radiation efficiency is very small. A computational experiment was performed to study the influence of the large-scale motion on the unsteady pressure field inside and outside a dual stream jet. It is demonstrated with the aid of cross-spectral densities of the pressure fluctuations that the motion is dominated by the influence of instability waves in the jet shear layer, motions that are naturally of large scale. It was already shown in the CEAA 2016 workshop [4] that the pressure field for the peak frequency in each axial position is dominated by a few low-order azimuthal components. It is now shown in addition that the coherence of the pressure fluctuations decays very slowly for axially separated probe positions for this frequency. This explains the rear arc amplification of jet noise due to source interference [3].

The unsteady flow field of a dual-stream jet with a short-cowl nozzle is analysed. The simulation is performed with Detached Eddy Simulation (DES), a hybrid RANS-LES method, using recent improvements to accelerate the RANS to LES transition [5]. The time step corresponds to a sampling Strouhal number $f_s D_e/U_e = 1035$ and every 32nd time step was stored for the later analysis. $D_e = 0.183$ m is the diameter of a circle that has the same area as the sum of the exit areas of the two nozzles. $U_e = [A_p(U_p - U_0) + A_s(U_s - U_0)]/(A_p + A_s) + U_0 = 236$ m/s is calculated with the nominal speeds U_p and U_s in the primary and secondary nozzles and the speed $U_0 = 90$ m/s of the flight stream. The simulation was run over 186 convective time units D_e/U_e. This is very short, but the analysis took advantage of the independence of the azimuthal position of the reference probe for azimuthally or axially displaced probe positions.

All flow data that are possibly relevant for the noise sources were stored on disk but only the pressure fluctuations are analysed here. The one-third octave spectra of the pressure fluctuations in various positions x/D_e downstream of the secondary nozzle are shown in Fig. 1. The radial positions with the largest peak levels of the spectra are chosen. These positions are close to the largest radial gradient of the mean axial velocity in the jet. The pressures are normalized with the ambient pressure p_0. It can be seen how the peak frequencies get smaller with increasing axial distance from the nozzle. This is a well-known result for jet turbulence.
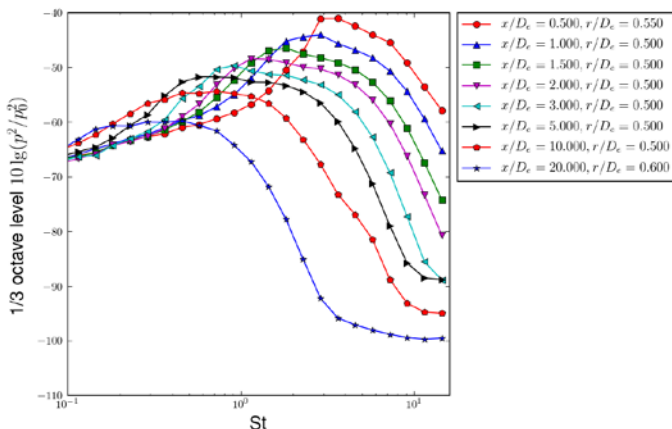
Fig. 1. One-third octave pressure spectra inside jet for various distances x/D_e from the nozzle for the radial position with highest one-third octave level (p_0 is ambient pressure)
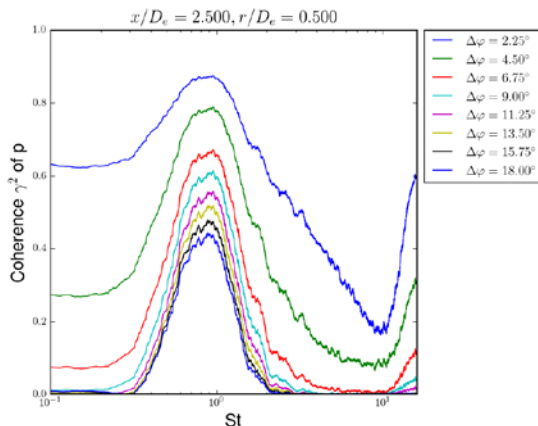

Fig. 2. Coherence spectra for x/D_e=2.5 for circumferentially displaced probe positions

The computational experiment made it possible to evaluate the cross spectra and coherence spectra for the pressures for azimuthally displaced "probe" positions. Results for the coherence spectra at x/D_e=2.5 for azimuthally displaced probe positions are shown in Fig. 2. The range around the peak Strouhal number St=0.9 decays only slowly with increasing azimuthal probe separation $\Delta\varphi$, while the rest of the spectra at higher and lower Strouhal numbers decays rapidly. The coherence is seen to increase again for very high Strouhal numbers,

but one must consider that the pressure levels are more than 50 dB lower in this range. This range is likely dominated by the radiated sound field from more upstream positions in the jet, an assumption to be checked by analysing the radial and axial components of the phase speeds.

The high azimuthal coherence of the pressure fluctuations in a relatively narrow frequency band is likely caused by the growth of instability waves in the jet's shear layer. These instability waves were studied by Michalke and Hermann [6] for a jet in a flight stream. They are dominated by low order azimuthal modes and their most unstable frequencies depend for given jet and flight speeds primarily on the shear layer thickness. The thin shear layers close to the nozzles are most unstable for high frequencies and the thick shear layers further downstream for low frequencies. It was shown by Michalke [1] that the mode numbers m of the instability waves are directly related to the order m of the Fourier decomposition of the cross spectra. We conclude that the dominance of low-order azimuthal components of the pressure fluctuations in a relatively narrow frequency band is caused by instability waves in the jet and that the wave-like motion in the jet shear layer dominates the jet noise emission.

A similar behaviour as in Fig. 2 can be observed in Fig. 3 for axially separated probe positions. The coherence for two positions separated by one jet diameter is astonishingly high at γ^2=0.65. This can also be explained by the dominance of instability waves.

The results for other axial positions are very similar to Figs. 2 and 3 and differ only in the peak frequency.
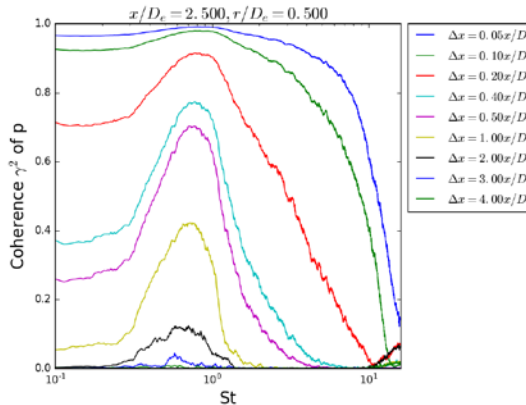
Fig. 3. Coherence spectra for x/D_e=2.5 for axially displaced positions, Δx=0.05 D_e to 4 D_e

The assumption that the instability waves are the cause of the pressure fluctuations is supported by an evaluation of the axial phase speeds of the fluctuations. This is shown in Fig. 4 for the Strouhal number 0.7. The phase speed

of the pressure fluctuations is seen to be almost independent of the radial position and is identical to the flow speed only in the middle of the shear layer for r/D_e=0.5.
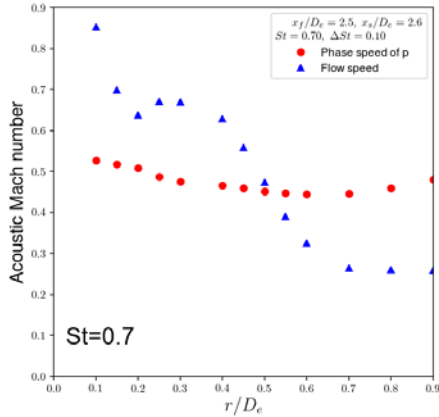
Fig. 4. Axial component of phase speed and mean-flow speed as function of radial position r/D_e for St=0.7

References

1. A. Michalke (1972): An expansion scheme for the noise from circular jets. Z.Flugwiss. 6, 229-237
2. A. Michalke (1977): On the effects of spatial source coherence on the radiation of jet noise. J. Sound Vib 55, 377-394
3. U. Michel (2009) The role of source interference in jet noise. AIAA-2009-3377
4. C. Mockett, U. Michel, F. Kramer (2016): Large Scale Motion in a Dual Stream Jet. CEAA 2016.
5. Mockett, C., Fuchs, M., Garbaruk, A., Shur, M., Spalart, P., Strelets, M., Thiele, F. and Travin, A. "Two Non-Zonal Approaches to Accelerate RANS to LES Transition of Free Shear Layers in DES," Progress in Hybrid RANS-LES Modelling, edited by S. Girimaji et al., Vol. 130 of Notes on Numerical Fluid Mechanics and Multidisciplinary Design, Springer Verlag, 2015, pp. 187-201
6. A. Michalke, G. Hermann (1982): On the inviscid instability of a circular jet with external flow. J. Fluid Mech., Vol. 114, 1982, pp. 343–359.

INVESTIGATION OF THE ACOUSTIC ACTUATORS CREATION POSSIBILITY FOR CONTROLLING FLOW IN SWIRLING JET

S.Yu. Krasheninnikov, **A.K. Mironov**, P.D. Toktaliev
Central Institute of Aviation Motors, Moscow, pavel_d_m@mail.ru

Swirled flows are widely used for intensification of mixing processes and for flame front stabilization in different technical devices (e.g. swirlers in combustion chamber of aviation engine). It was shown in [1-2] that the swirled jets can be susceptible to small external impact, both gas-dynamic and acoustic types, under certain conditions. It is known that flow regimes characterized by global instability of a swirled jet are corresponded to the swirled number $S \sim 1$, and they are not used at operation conditions in combustion chambers. However, the presence of regular periodic motion of the medium (precession in the particular case), which has a set of own frequencies, for $S > 1$, leads to the possibility of manage of resonance and interference phenomena in the jet.

In the present work, a calculation and experimental investigation of resonant and interference phenomena in a swirled jet with $S>1$ under external acoustic influence is carried out, as well as an analysis of the possibility of designing acoustical actuators using these phenomena to active control of the characteristics of a swirled jet, primarily the length of the recirculation zone and the velocity profiles in the mixing layers.

References

1. S.Yu. Krasheninnikov, A.K. Mironov, D.E. Pudovikov, P.D. Toktaliev. Investigation of the generation of sound waves produced by turbulent jets // Fluid Dynamics, 2016, V.50(3), pp.371-386
2. S.Yu. Krasheninnikov, V.P. Maslov, A.K. Mironov, P.D. Toktaliev. Investigation of the flow structure and acoustic field of a turbulent jet with a high swirling intensity // TsAGI Science Journal. 2016, V. 47 (2), pp.111-137

BACKGROUND ACOUSTIC DISTURBANCES IN HIGH SPEED WIND TUNNELS

V.A. Lebiga[1,2], V.N. Zinovyev[1], A.Yu. Pak[1]

[1]Khristianovich Institute of Theoretical and Applied Mechanics SB RAS

Novosibirsk, lebiga@itam.nsc.ru

[2]Novosibirsk State University, Novosibirsk

The basic relations between the output hot-wire signal and characteristics of the acoustic field are considered in terms of the fluctuation diagram, i.e. dependence of the normalized hot-wire output on the probe overheating parameter. This approach allows determining both intensity of acoustics and the direction of propagation of acoustic waves in the flow as the angle χ between the normal to the front of the acoustic wave and the mean flow velocity vector. This angle χ depends (and can be calculated) on the location of the intersection point of the fluctuation diagram with the abscissa axis. It is shown also that the hot-wire approach allows not only obtaining information on the intensity of acoustic fluctuations propagating in the flow, but also to identify sources of disturbances and their localization.

The results of measurements of background fluctuations in wind tunnels of several research centers are presented, namely TsAGI, ITAM SB RAS (Russia), ETW (Cologne, Germany), ASTRC NCKU (Tainan, Taiwan). It is shown that the prevailing contribution to the flow fluctuations in test sections of the blow-down wind tunnels is provided by acoustic fluctuations radiated from the boundary layer on the walls of the nozzle and test section, from the wall perforation, from slots and gaps in the test sections. Contrariwise, in the closed circuit wind tunnels the most important can be temperature inhomogeneities in the absence or ineffectiveness of heat exchangers, as well as in cryogenic wind tunnels. In this case, the contribution of acoustic disturbances in total fluctuations decreases, however it can be not correct for some ranges of the frequency spectrum.

ADJOINT-BASED SOUND SOURCE IDENTIFICATION

Mathias Lemke, **Jörn Sesterhenn**

Technische Universität Berlin, Berlin, Germany, office@tnt.tu-berlin.de

The identification of sound sources is usually realized by means of microphone array methods, such as beamforming. A variety of implementations is known. The methods are usually based on simplifying models, e.g. the assumption of a constant speed of sound in combination with a simple base flow. Usually input parameters are needed that are a priori unknown, such as the type of the sources, e.g. mono- or dipoles.

The identification of sound sources (in terms of location, phase, amplitude and type) in complex flows is currently only possible to a limited extent.

The basic idea of the adjoint-based sound source identification is to reformulate the problem into an optimization task. For this purpose, a numerical simulation of the Euler or Navier-Stokes equations is supplemented by initially unknown momentum and energy sources. These source terms are adjusted in terms of location, phase and amplitude such that the resulting numerical model or the resulting numerical simulation of the sound field optimally matches existing measurement data. If this is the case, the source terms match possible sources in the experiment (there is no unambiguousness in principle). The large number of free parameters is determined numerically efficiently by the adjoint approach. Preliminary work in the fields of acoustics [1] and fluid mechanics [2, 3] are available. In particular, complex flows can be taken into account. By simultaneous adaptation of momentum and energy terms, source types can be identified. Under certain circumstances it is also possible to determine fluid-dynamic properties from acoustic measurements.

The application of the method and initial results are described in [4, 5]. The aim of the work was the validation of the approach. By means of a simple acoustic setup, consisting of one speaker and eight microphones, see Fig. 1 (left), it was shown that sound sources can be correctly identified. However, the adjoint-based solution was not unique, according to the experimental setup, but shows the possibility to determine the directivity of the source. The reference signal of 5 kHz was correctly identified, see Fig. 1 (right).

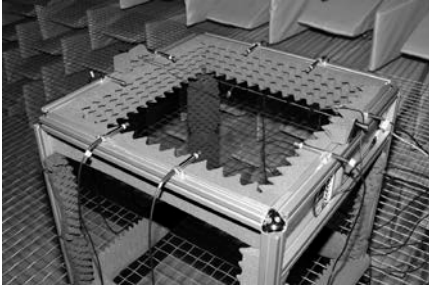Pending is the application of the method to a specific application in the field of flow acoustics.
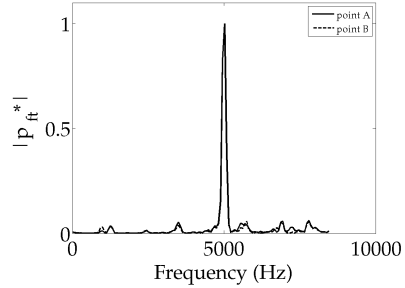
Fig. 1.

References

1. M. Lemke, F. Straube, F. Schultz, J. Sesterhenn, and S. Weinzierl, "Adjoint-based time domain sound reinforcement," in Audio Engineering Society Conference: 2017 AES International Conference on Sound Reinforcement – Open Air Venues, Aug 2017.

2. M. Lemke, J. Reiss, and J. Sesterhenn, "Adjoint based optimisation of reactive compressible flows," Combustion and Flame, vol. 161, no. 10, pp. 2552– 2564, 2014.

3. M. Lemke and J. Sesterhenn, "Adjoint-based pressure determination from PIV data in compressible flows — validation and assessment based on synthetic data," European Journal of Mechanics - B/Fluids, vol. 58, pp. 29 – 38, 2016.

4. M. Lemke, C. Westphal, J. Reiss, and J. Sesterhenn, "Adjoint based data assimilation of sound sources," in Fortschritte der Akustik - DAGA 2015 (S. Becker, ed.), pp. 635–638, DEGA, March 2015.

5. M. Lemke, Adjoint based data assimilation in compressible flows with application to pressure determination from PIV data. PhD thesis, Technische Universität Berlin, 2015.

OVERVIEW, STRATEGIES AND CHALLENGES IN POST-PROCESSING: EXPLORING LARGE DATASETS, WORKFLOW AUTOMATION AND ANALYZING COLLECTIONS OF FILES
Antoine Ligier

Genias Graphics GmbH & Co KG, Regenstauf, Germany, antoine.ligier@genias-graphics.de

In its CFD Vision 2030 study [1], NASA forecasts 100B point transient simulations and thousands of unsteady parametric simulations to be performed in production by 2025. Transient CFD simulations will reach a trillion points per time-step in 2030. New technologies need to be developed in order to cope with large datasets and collections of result files.

With the ever increasing size of simulation data, new visualization techniques are to be applied, in order to cut down on the associated hardware requirement, as well as to minimize the time-to-picture. The disk read data transfer rate is evolving more slowly than the size of the simulation data [2]. The time to load and visualize a dataset is hence constantly increasing.
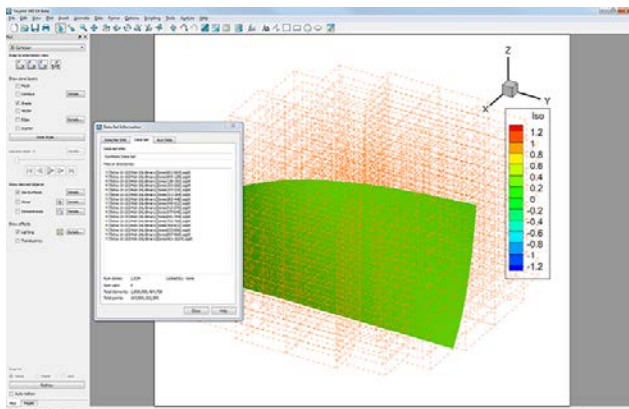
Fig. 1. Iso-surface on a trillion-cells simulation using 120Gb of RAM, Tecplot Inc., 2015

Tecplot 360EX leverages the Sub-Zone Load-on-demand (SZL) technology, a lazy-loading implementation which allows to significantly cut down on the amount of data to be read from disk. The memory requirements and time-to-picture are cut by orders of magnitude: it is now possible to load a billion-points simulation on a laptop with 8Gb of RAM.

Current architectures for the analysis of collections of files, such as in optimization studies, design of experiment or experimental campaigns, solely rely

on the analysis of integrated values and exported images. While these are a convenient way of representing their associated dataset, discrepancies in the underlying field data may be overlooked, e.g. when using a handful of integrating values to represent multi-million points simulations.
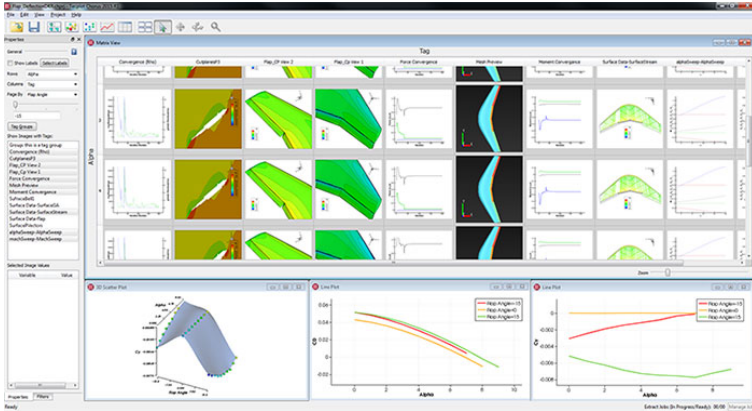
Fig. 2. Parametric study of an airplane: integrated values and images
Tecplot Inc., 2015

The innovating framework Tecplot Chorus gives an overview of a collection of result files, while enabling the visualization of the actual physics of each dataset. This permits to quickly identify the root cause in anomalies in the metadata, as well as being able to seamlessly explore the various datasets in details.

Post-processing thousands of large datasets is time consuming. Workflows hence need to be automated.

The new Python API PyTecplot leverages all of Tecplot 360EX capabilities while opening usage of third-party libraries. The state of the art interface permits to seamlessly access the data loaded in Tecplot 360EX within your Python environment, and to manage your Chorus cases.

The presentation will describe the strategies to be used to plot and animate your CFD results in the exact way you want, analyze complex solutions, arrange multiple layouts and communicate your results with professional images and animations.

References

1. CFD Vision 2030 Study, A Path to Revolutionary Computational Aerosciences. NASA/CR–2014-218178, 2014.
2. Scott T. Imlay, Craig Mackey: Improved Performance of Large Data Visualization using Sub-Zone Load On Demand, Tecplot Inc., 2013.

GPU CABARET SOLUTIONS FOR THE COJEN JET NOISE EXPERIMENT

A.P. Markesteijn[1], S.A. Karabasov[1,2]

[1]*GPU-prime Ltd, Cambridge, UK, a.p.markesteijn@gmail.com*
[2]*School of Engineering and Material Science, Queen Mary University of London, Mile End Road, London, UK, s.karabasov@qmul.ac.uk*

Development of high-fidelity jet noise prediction models for dual stream flows to complement and potentially replace the existing scaling law models such as those developed in [1–3] is of great interest to turbofan engine designers. Up to present, a few experimental campaigns have been launched to systematically study the dual stream jet noise and provide databases of flow and noise data for validation of theoretical and computational models. One of such databases was generated as the result of CoJen: the EU-funded Computation of Coaxial Jet Noise project, which data are now in the public domain. The flow field and acoustic data from CoJen were used in [4] for validation of several Reynolds Averaged Navier Stokes (RANS) and Large Eddy Simulation (LES) based methods. For example, the work of [5] presented a detailed account of Particle Image Velocimetry (PIV) techniques used in the CoJen experiment. An experimental near-field acoustic array technique was used in [6] to study the axial, temporal and azimuthal structure of the pressure field of jet flows at various operating conditions from the CoJen experiment. CoJen data were also considered in [7] who applied an LES method combined with the Ffowcs Williams – Hawkings (FW-H) approach for far-field noise predictions. In the context of co-axial jet noise modeling, a combination of the Lattice-Boltzman method and the FW-H approach was used in [8] who used the measurements of [6] for validation. In [9], a combination of the RANS solutions and a ray-tracing method based on the Lighthill acoustic analogy was used to investigate the co-axial jet noise production mechanisms in application to the CoJen experiment. Hydrodynamic stability and noise generation mechanisms for CoJen jets were investigated in [10]. More recently, in [11] the flow data from the CoJen experiment were analysed using PIV and Laser Doppler Anemometry (LDA) techniques.

In this paper, we will apply an LES method combined with the FW-H technique for flow and noise calculation of several benchmark co-axial jet cases from the CoJen experiment. The method we use is based on the GPU CABARET solver. A detailed description of the CABARET solver can be found in [12-16]. This current solver is a GPU implementation of the low-dissipative, low-dispersive CABARET scheme [17–19], with asynchronous time stepping [20] for the acoustics sensitive solution of Navier-Stokes equations in the framework of Monotonically Integrated LES [21]. The flow solver
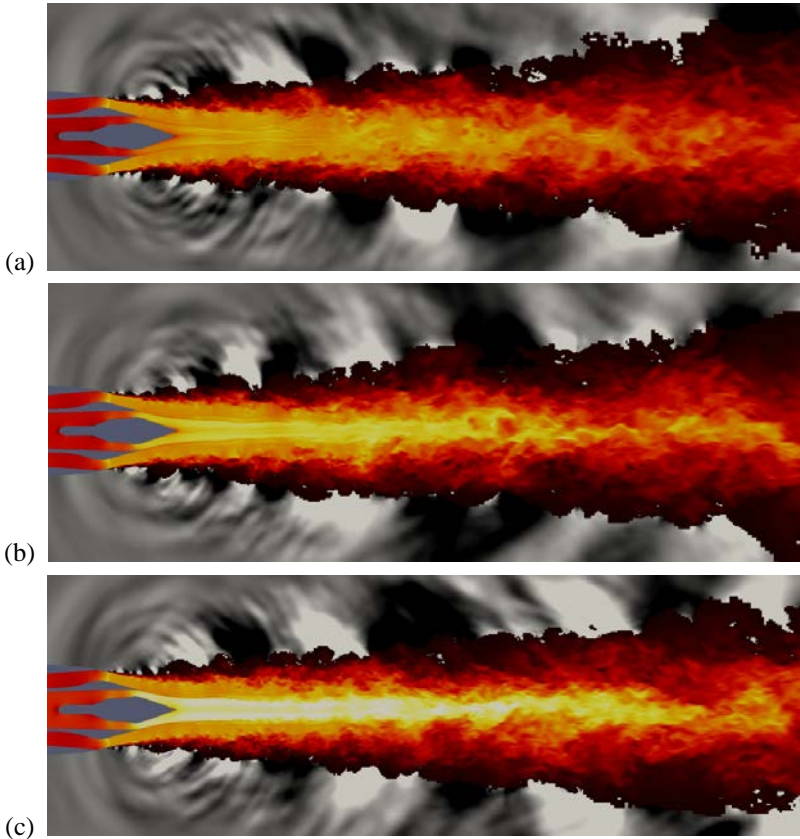
Fig. 1. Instantaneous velocity and pressure fields for three different operation points for the axi-symmetric short-cowl CoJeN nozzle. (a) OP 1.1 (b) OP 1.2 (c) OP 1.3.

is coupled with the penetrable FW-H integral surface method for jet flow and noise prediction. The implementation of this makes industrially relevant LES studies of jet noise modeling possible in reasonable time (several days) using just a single workstation computer to handle computational grids circa 20 and 80 million grid cells. In [16], the GPU CABARET solver has also been extended to include split-hexa (hanging node type) meshes, allowing one to accomplish the mesh generation using the OpenFOAM utility "snappyHexMesh" (sHM). This mesh utility enables automatic hexa-dominant mesh generation from triangulated surface geometries (e.g. CAD geometry), an essential need for complex LES-based optimization techniques. Furthermore, sHM also has the possibility to "snap" the mesh to the geometry as well as the ability to gen-

erate "layers" of body-fitted grid near the boundaries if need be. By using sHM and extending CABARET to include hanging nodes, it is possible to generate meshes and solve flow and acoustics for complicated geometries while retaining the hexa-dominancy for accuracy, which is enhanced thanks to a very compact stencil of the governing CABARET advection scheme that takes one cell in space and time.

In the current work, the GPU CABARET solver on sHM meshes in combination with the penetrable integral surface formulation FW-H method following [22–24] is applied for flow and noise calculations for one of the short-cowl nozzle geometries considered in [5].

References

1. Fisher, M.J., and Preston, G.A., and Bryce, W.D., "A Modeling of the Noise from Simple Co-axial Jets," AIAA–1993–4413, October 1993.
2. Stone, J.R., Krejsa, E.A. and Clark, B.J., "Semi-Empirical Model for Coannular Nozzle Component Noise Extraction and Correlation Including the Effects of Noise Reduction Devices," AIAA–2003–1060, 2003.
3. Khavaran, A. and Bridges, J. Jet Noise Scaling in Dual Stream Nozzles, NASA/TM-2010-216887
4. Vuillemin, A., Loheac, P., Rahier, G., Vuillot, F. & Lu-poglazoff, N. 2005 Aeroacoustic numerical method assessment for a double stream nozzle. In 11th AIAA/CEAS Aeroacoustics Conference. DOI: 10.2514/6.2005-3043.
5. Skeen, A. 2006 The development of high-speed PIV techniques and their application to jet noise measurement. PhD thesis, University of Warwick
6. Tinney, C. E. and Jordan, P. 2008 The near pressure field of co-axial subsonic jets. J. Fluid Mech. 611, 175–204, DOI: 10.1017/S0022112008001833.
7. Vuillot, F., Lupoglazoff, N., Rahier, G. Double-stream nozzles flow and noise computations and comparisons to experiments, 46th AIAA Aerospace Sciences Meeting and Exhibit 7 - 10 January 2008, Reno, Nevada.
8. Casalino, D. and Lele, S.K. Lattice-Boltzmann simulation of coaxial jet noise generation, Center for Turbulence Research, Proceedings of the Summer Program 2014.
9. Almeida, O., Barbosa, J.R.,Moro, J.B., Self, R.H. Noise Source Distribution of Coaxial Subsonic Jet-Short-Cowl Nozzle, J. Aerosp. Technol. Manag. Sao Jose dos Campos, vol 6, no1, pp 43-52, Jan-Mar, 2014
10. Gloor, M.R. Numerical investigation on hydrodynamic stability and noise radiation of coaxial jet flows, PhD Thesis ETH Zurich, 2014
11. Mead, C.J., Wrighton, C., Britchford, K. An Experimental Study of Co-Axial Jets Using Acoustic, PIV&LDA Methods (CoJen), AIAA 2015-3122.

12. Markesteijn, A.P., Semiletov, V.A., Karabasov, S.A. "CABARET GPU Solver for Fast-Turn-Around Flow and Noise Calculations", AIAA-2015-2223

13. Markesteijn, A.P., Semiletov, V.A., Karabasov, S.A. "GPU CABARET solutions for the SILOET jet noise experiment: Flow and noise modelling", AIAA-2016-2967

14. Markesteijn, A.P. and Karabasov, S.A. "GPU CABARET Solutions for the NASA SHJAR Jet Noise Experiment: Flow and Noise Modeling", AIAA 2017-3852.

15. Markesteijn, A.P. and Karabasov, S.A. "GPU CABARET Solver Extension to Handle Complex Geometries Utilizing snappyHexMesh with Asynchronous Time Stepping", AIAA 2017-4184

16. Markesteijn, A.P. and Karabasov, S.A. "CABARET solutions on Graphics Processing Units for NASA jets: grid sensitivity and unsteady inflow condition effect", CR Mecanique (Proc. French Academy of Sciences), in press.

17. Goloviznin, V. M., Samarskii, A. A., "Finite difference approximation of convective transport equation with space splitting time derivative", Jour Matem. Mod., 1998 , 10(1), 86–100.

18. Karabasov, S. A., and Goloviznin, V. M., "Compact Accurately Boundary Adjusting high-REsolution Technique for Fluid Dynamics", J. Comput. Phys., 2009, 228, 7426-7451.

19. Chintagunta, A., Naghibi, S.E., and Karabasov, S.A. "Flux-corrected dispersion-improved CABARET schemes for linear and nonlinear wave propagation problems", Computers & Fluids, August 2017.

20. Semiletov, V. A., and Karabasov, S. A., "CABARET scheme with conservation-flux asynchronous time-stepping for nonlinear aeroacoustics problems", Journal of Computational Physics, 2013, 253(15), 157165.

21. Fureby, C. and Grinstein, F.F. "Large eddy simulation of high-Reynolds-number free and wall-bounded flows". J. Comput. Phys., 181:68-97, 2002.

22. Shur, M. L., Spalart, P. R., Strelets, M. Kh. 2005 "Noise Prediction for increasingly complex jets. Part I: Methods and tests. Part II: Applications Int. J. Aeroacoustics.", 4(34), 21366.

23. Faranosov, G.A., Goloviznin, V.M., Karabasov, S. A., Kondakov, V. G., Kopiev,V. F., Zaitsev, M. A. 2013 "CABARET method on unstructured hexahedral grids for jet noise computation Computers and Fluids", 88, 165-179.

24. Welch, P. D. 1967 The Use of Fast Fourier Transform for the Estimation of Power Spectra: A Method Based on Time Averaging Over Short, Modified Periodograms, IEEE Transactions on Audio Electroacoustics , AU-15, 70-73.

AEROACOUSTIC LOW-SPEED WIND TUNNEL FACILITY FOR CFD VALIDATION

V.V. Pakhov, S.A. Mikhailov

KNRTU-KAI,Kazan,VVPakhov@kai.ru

This paper outlines experience obtained during the modification of a conventional low-speed wind tunnel for aeroacoustic purposes. Modification includes building an anechoic chamber, developing of an acquisition system, performing noise reflection investigation tests and obtaining preliminary CFD validation cases. The schematic of the wind tunnel facility with the measurement systems is shown on Fig. 1. The measurement facility consists of the wind tunnel T-1K of KNRTU-KAI, equipped with anechoic chamber, the rotor rig and measurement system based on conventional measurement microphones and National Instruments equipment.
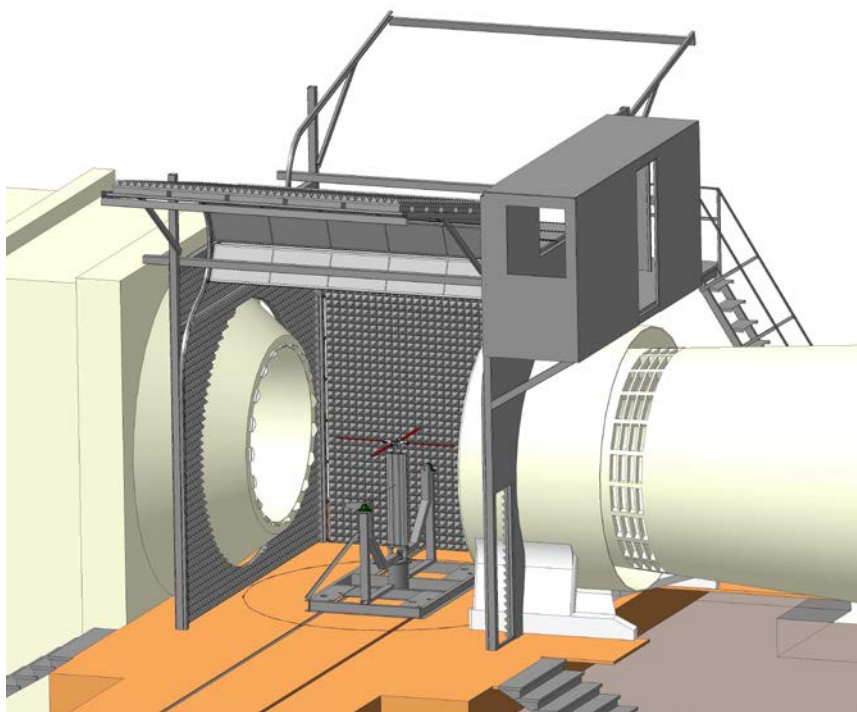
Fig. 1. Schematic of the modified wind tunnel

Nowadays the most common method for rotorcraft and aircraft design is CFD research. Experimental facilities are used more for validation purposes of CFD computation results. But CFD validation still requires the use of extensive experimental data. Quality of experimental data is especially important for interdisciplinary problems, and this is especially true for aeroacoustics. So, creation of the aerodynamic experimental facility, which can mainly provide data for CFD validation, is a reasonable idea, especially if its costs can stay within certain limits. This can be achieved with a conventional low-speed wind tunnel instead of specialized one. Thus, the motivation of this paper is to show that the experimental aeroacoustic facility of KNRTU-KAI, which was created in a conventional wind tunnel, can provide usable data for CFD validation.

Recognition and reduction of noise sources is a well known practice in aircraft industry. Noise standards for aircraft become tougher with each new edition of FAR-36 regulatory document. Typical noise level of an aircraft is significantly lower than self-noise of T-1K, and for higher speed the difference is even more noticeable. Performing aeroacoustic measurements in specific experimental conditions is a challenging idea. But the rotorcraft noise is higher than the aircraft and theoretically can be higher than the self-noise of T-1K. Then, rotorcraft can operate in hover mode, which requires no flow in wind tunnel. Thus, for several rotorcraft tests, the wind tunnel self-noise is not a lethal factor. Noise standards for rotorcraft are also very low and tend to become even lower. But rotorcraft noise is usually more complex than the noise from other types of aircraft and significantly less experimental data is available, making even a small experimental dataset useful. The T-1K acoustic facility was created with this in mind.

The key part of this facility is a low-speed (up to 50 m/s) closed-circuit T-1K wind tunnel of KNRTU-KAI. It is a conventional multi-purpose wind tunnel, with the nozzle diameter of 2,25m and test section length of 3m. Second part is an anechoic chamber with retractable walls with twin-layer construction. This construction paradigm has been chosen because conventional anechoic elements are too big and fragile. Also retractable walls allow mounting works for equipment in test section. First layer is low-frequency anechoic layer made of Helmholtz resonators calculated for dominant frequency of wind tunnels self-noise. The dominant frequency is the bpf (blade passing frequency) for the wind tunnel fan, which is close to 100Hz. Most tests aimed at measuring helicopter main rotor models are also performed with bpf near 100 Hz. Schematic of Helmholtz resonator is shown on Fig. 2a)

A conventional melamin-based anechoic pyramid plates, which geometry is shown in Fig. 2b), was used as a second layer to deal with higher frequencies. Twin-layer construction showed good performance in first noise reflection tests, the reflection intensity was about 6,5 times lower than the initial signal.
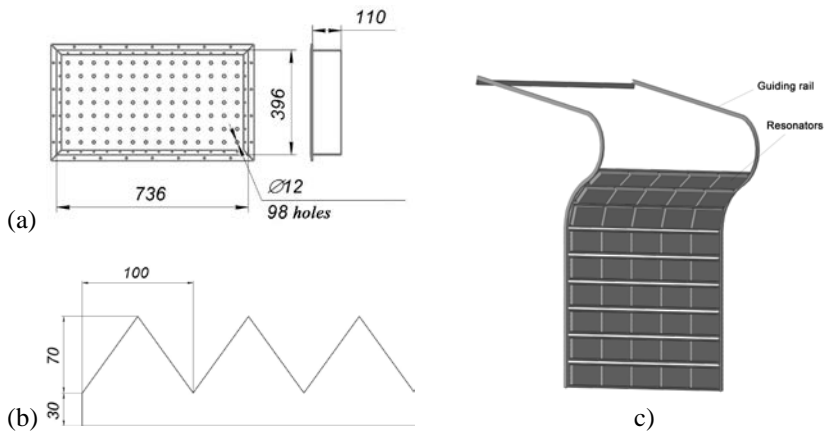
Fig. 2. Anechoic chamber of T-1K: a) Helmholtz resonator schematic;
b) Melamin pyramids dimensions; c) T-1K anechoic chamber wall structure
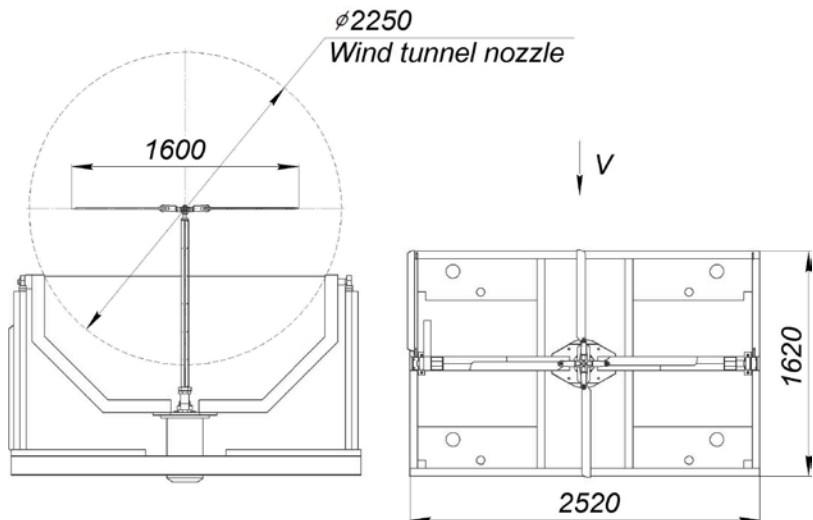

Fig. 3. Rotor rig used in the T-1K wind tunnel; dimensions are in millimeters

      Third part of the facility is a rotor rig for helicopter main rotor model tests. This rotor rig has the following specifications: it can reach up to 2500 rpm, collective pitch can vary from -15° to +15°, cyclic pitch can be applied, rotor`s angle of attack can vary from -30° to +30°. Schematic of the rotor rig is shown on Fig. 3. The rotor rig was used for various experiments, such as visualization of tip vortices and acoustics investigations.

The final part of the facility is the measurement system. A proprietary measurement system has been used for this facility. The measurement system consisted of DBX RTA-M microphones, based on Panasonic WM-61A cartridges. Acquired signal was amplified by an in-house device and read by NI-PXI 4496 ADC card. This design allowed performing measurements with up to 204 kS/s sampling rate with 24-bit analog-to-digital conversion. It can support up to 64 channels.

An example of validation case of experimental data with CFD results can be seen in Fig. 4 [1]. This result was obtained in the above described facility. On this figure one can see a signal from a microphone, positioned in plane of rotation of the helicopter`s main rotor model and installed at 1.2 of rotor`s radius distance away from its axis of rotation. Angular speed was set to 900 rpm and collective pitch to 8°, hover mode. Paper [1] contains data for other positions of the microphone relative to the rotor.

The results of the study [1] indicated that, the experimental results were in a good agreement with CFD computations and could be used for validation purposes of CFD computations. Further modifications of the facility could bring better results.
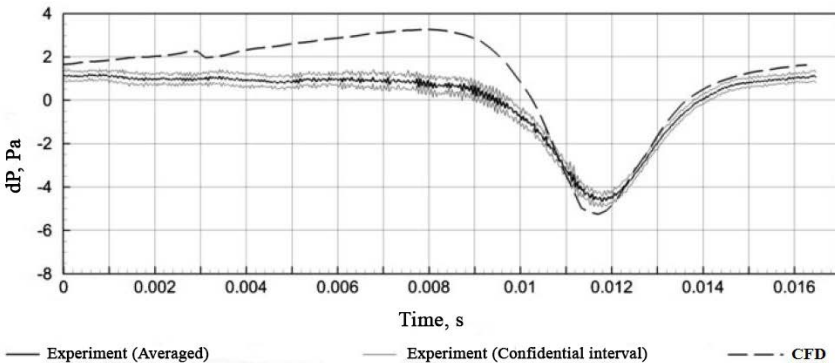
Fig. 4. Acoustic CFD validation example [1]

References

1. Stepanov R., Pakhov V., Bozhenko A., Batrakov A., Garipova L., Kusyumov A., Mikhailov S., Barakos G.N, "Experimental and numerical study of rotor aeroacoustics." *International Journal of Aeroacoustics*, Vol. 16, Issue 6, 2017.

MISMATCHING EIGEN-MODE BASES IN INDUCT SOUND FIELD ANALYSIS WITH INHOMOGENEOUS MEAN FLOW

Mirko Spitalny, Ulf Tapken

German Aerospace Center, Berlin, Germany, mirko.spitalny@dlr.de

The radial mode analysis (RMA) is the standard tool for the calculation of the tonal sound power in flow ducts of turbomachinery applications. In this method CAA or experimental data is fitted to a sound field model. This model is composed of harmonic functions according to Equation 1, which is a solution of the convective wave equation in cylindrical coordinates [1]. From a pressure distribution $p(x,r,\varphi)$ at a single frequency component the modal amplitudes a_{mn} can be calculated with a least squares fit procedure [2]. In a subsequent step these mode amplitudes can be used to calculate the sound power [3].

The mentioned sound field model includes the so called modal basis which consists of the axial wavenumbers k_{mn} und the radial mode shape functions f_{mn} for all propagating, individual azimuthal (m) and radial (n) mode orders and represents an Eigen-solution of the system. For a constant mean flow profile (plug flow) the modal basis can be calculated analytically. If an inhomogeneous mean flow profile is considered a numerical modal basis has to be utilized which can come from the solution of an extended eigenvalue problem [4]. Further assumptions in both cases are that the mean flow field is homogeneous in axial and circumferential direction:

$$p(x, r, \varphi) = \sum_{m=-\infty}^{\infty} \sum_{n=0}^{\infty} a_{mn}^{\pm} \cdot e^{i(k_{mn}^{\pm} x + m\varphi)} \cdot f_{mn}(r) \qquad (1)$$

In CAA or experimental setups the assumptions regarding the flow field will not necessarily be perfectly met or the flow field can only be determined with a given uncertainty. This can lead to a mismatching of the modal basis of the model sound field with the real sound field. Also in some cases the analytical solution is preferred due to its robustness and low computational costs, for example if a lot of frequencies have to be analyzed, even though it has some drawbacks regarding the representation of the mean flow. Figure 1 depicts the differences in axial pressure distribution for a synthetic sound field of azimuthal mode m=0 between two different mean flow field assumptions (plug flow and 1/5-power-law boundary layer with a thickness of 10%). Both flow profiles feature an equivalent mass flow. The Mach number of the plug flow is 0.4. It is visible that an offset exists for the amplitude as well as for the frequency. In the RMA this leads to differences in the calculated sound power.

The differences in the sound power are also depending on the sampling positions of the sound field, which is of higher relevance for experimental data than in CAA applications.
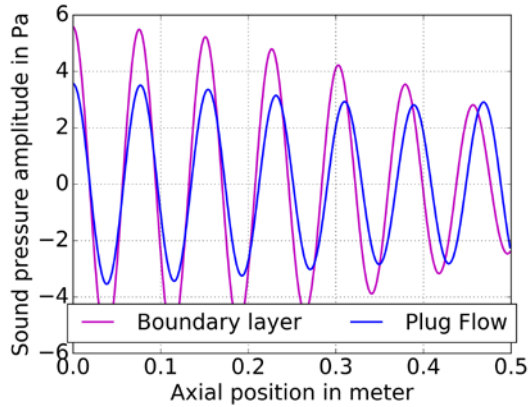
Fig. 1. Axial pressure distribution for a superposition of modes (0,0), (0,1) and (0,2) for a boundary layer profile and the equivalent plug flow
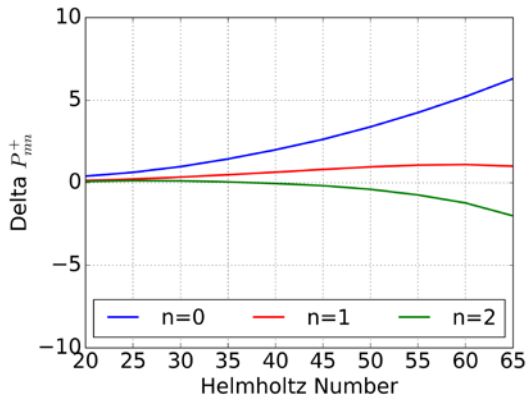

Fig. 2. Difference in calculated sound power between a modal basis for plug flow and for a flow profile with a 1/5 power law boundary layer (10% thickness) of mode $m = 0$ and the first tree radial orders versus Helmholtz number

In a previous study [5] the author has shown for an exemplary, experimental data set that there can be significant differences of up to 5dB in the calculated total sound power and up to 10 dB in the sound power of individual modes, depending on the consideration of the mean flow field and the sensor positions.

For a synthetic test case the sound power calculated with a mismatching modal basis shows an offset, which also varies with the analyzed frequency. This is shown in Fig. 2 for the first three radial mode orders of the azimuthal

mode order m=0. It will be shown, that the deviation in sound power also depends on the number of dominant radial modes.

The present study aims at a more general understanding of the influence of mismatching modal bases on the sound power calculation. Therefor synthetic sound fields are generated and assessed for a wide range of parameters, of which the most prominent are the Helmholtz number, the hub to tip ratio, the boundary layer thickness and the sampling positions of the sound field.

The deviation from the different modal bases can be especially relevant when comparing CAA results with experimental data for validation purposes, as the experimental data is usually sampled at fewer positions.

In his talk the author will give an overview of the problem and present possible mitigations in order to increase the accuracy of the calculated sound power.

References

1. Tyler J. M. and Sofrin T. G.: Axial flow compressor noise studies, 1962
2. Moore, C.: Measurement of Radial and Circumferential Modes in Annular and Circular Ducts. Journal of Sound and Vibration, 62(2):235–256, 1979
3. Morfey C. L.: Acoustic Energy in Non-Uniform Flows, Journal of Sound and Vibration 14(2) , 1971
4. Kousen, K. A.: Pressure modes in ducted flows with swirl, 2nd AIAA/CEAS Aeroacoustic Conference, 1996
5. Spitalny M., Tapken U.: Radial Mode Analysis of Ducted Sound Fields with Sensor Rakes and Wall Flush Sensor Arrays under Consideration of a Radial Flow Profile, 22nd AIAA/CEAS Aeroacoustic Conference, 2016

ACOUSTIC MODEL OF A HELMHOLTZ RESONATOR UNDER GRAZING TURBULENT FLOW

Lewin Stein, **Jörn Sesterhenn**

Technische Universität Berlin, Berlin, Germany, office@tnt.tu-berlin.de

To date, acoustic models of duct systems with turbulent flow depend on fitted constants/expansive test series. We present a more universal model; its constants are replaced by physically significant parameters with a clear definition. For the user, this allows an intuitive sense how a modification of design parameters affects acoustic properties.

In most practical cases, when gases (compressible fluids) stream along a hollow space, acoustic and turbulent flow are strongly coupled. Many examples can be listed in which this coupling is of greatest importance. Noise silencers consisting of cavity arrays are installed in most duct systems, in which tonal noise (due to a constant operating frequency) needs to be reduced: Air conditioning systems, ventilation plants, combustion engines. Beside silencing properties, cavities may give rise to desirable tones of wind instruments like transverse flutes and organs or undesired 'window buffeting' of moving vehicles. Acoustic cavity resonances may even cause severe material damage for instance in pipeline intersections.

More specifically, by proceeding with previous works by Goody [1], Howe [2] and, Golliard [3] we derive a new acoustic model of a resonant cavity in grazing flow (Fig. 1).
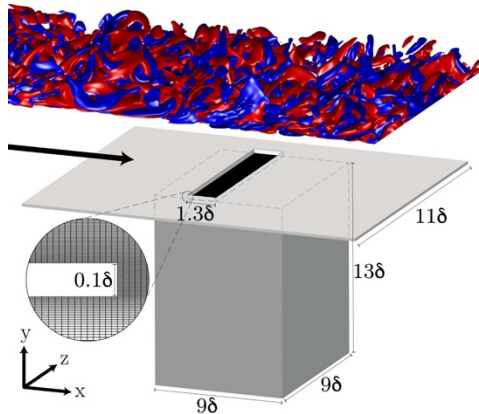
Fig. 1. Setup of the Direct Numerical Simulation [4]: In streamwise x-direction, a turbulent boundary layer streams over a rectangular cavity, which is flush-mounted inside the bottom wall. The cavity is connected via a rectangular neck/opening with the flat plate.
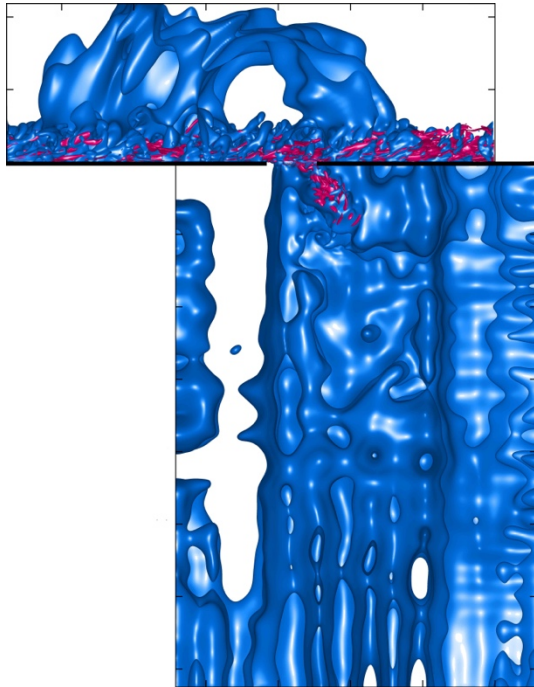
Fig. 2. An isosurface snapshot of the Direct Numerical Simulation is shown [4]: the vorticity is red; the pressure is blue. 1 Billion grid points and 8 Million CPU-hours are used to simulate 30 ms of physical time.

First, to establish a reference database we conducted a detailed three-dimensional Direct Numerical Simulation at the Mach number M=0.1 [4] of the setup depicted in Fig. 1. The setup is comparable to the experiments of [3]. A snapshot of the simulation is shown in Fig 2.

Second, utilizing the lumped element method, we set up a model, consisting of exchangeable/adaptable elements. Fig. 3 shows a sketch. In the present case, the boundary layer thickness is smaller than the streamwise neck length. This implies a complex coupling of Kelvin-Helmholtz waves at the neck zone and the acoustic waves resonating inside the cavity. The acoustic element describing this coupling is based on Howe's Rayleigh conductivity of an aperture in two-sided flow [2]. Thereby we make extra efforts to redefine occurring constants, to make them universally accessible and to give them a physical meaning. Especially, the focus lies on the eddy convection velocity.
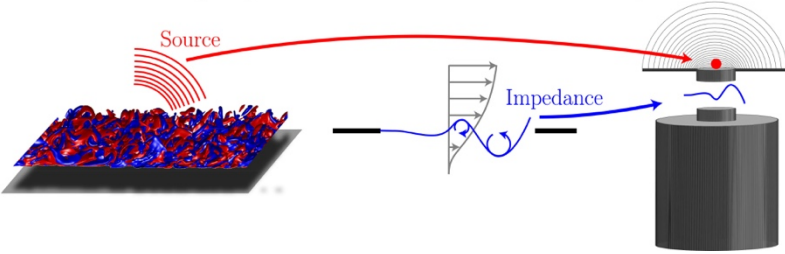
Fig. 3. Governing elements of the newly derived Goody-Howe-Golliard Model from left to right: The driving source term of pressure fluctuations, the impedance of an aperture in grazing flow and the lumped element method for the description of linear acoustics in duct systems (cross-sectional jumps etc.).
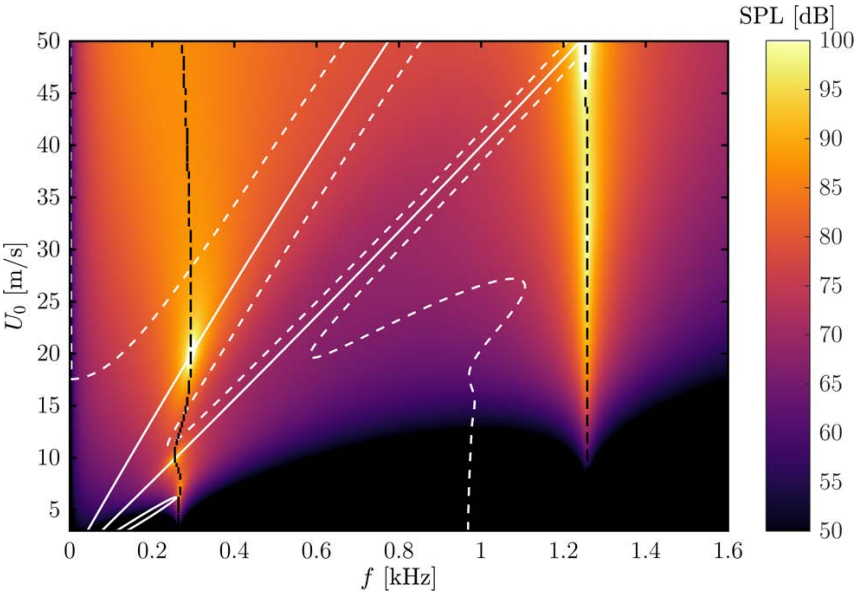
Fig. 4. SPL spectra prediction of the new Goody-Howe-Golliard Model: the black lines belong to reactivity terms; the white lines are linked to the resistance.

Finally, we will validate the model. On one hand, we carry out a comparison with the Direct Numerical Simulation [4]. On the other hand, we demonstrate the model applicability over a whole Mach number range from 0.01 to 0.14 (cf. Fig. 4) corresponding to the experimental study [3]. Even so, the mod-

el is linear, resonance conditions between acoustic cavity modes (black dashed lines) and fluid dynamic unstable modes (white line) are correctly predicted.

References

1. M. Goody. Empirical Spectral Model of Surface Pressure Fluctuations. AIAA J., v.42(9), 2004.
2. M.S. Howe, Acoustics of Fluid-Structure Interactions. Cambridge monographs on mechanics, 1998.
3. J. Golliard. Noise of Helmholtz-resonator like cavities excited by a low Mach-number turbulent flow. Ph.D. thesis, University of Poitiers, 2002.
4. L. Stein, J. Reiss, J. Sesterhenn. Numerical Simulation of a Resonant Cavity: Acoustical Response Under Grazing Turbulent Flow, New Results in Numerical and Experimental Fluid Mechanics XI 136. Springer, 2018.

ON COMPUTATIONAL AERODYNAMICS AND AEROACOUSTICS OF MOVING AIRFOILS

Y. Sun[1], **S. Zhong**[1], X. Zhang[1], X. Huang[2], I.V. Abalakin[3],
T. Kozubskaya[3], N. Zhdanova[3]

[1]*Hong Kong University of Science and Technology, Hong Kong SAR, China*
[2]*Peking University, China*
[3]*Keldysh Institute of Applied Mathematics RAS, Moscow, Russia*

A detailed study of flow around moving airfoils including the influence of movement on their aerodynamic and aeroacoustic properties is of crucial importance in many applications. In particular, wing motion contributes significantly to the thrust generation mechanisms of natural flyers and to the corresponding acoustic radiation. The broadband noise generated by a moving airfoil is essential in solving the problems of the fan-outlet guide vane interaction, rotor-rotor interaction for a contra-rotating open rotors or wind turbines. Within a scope of possible set-ups relating to aerodynamics and aeroacoustics of moving airfoils, the paper considers two problems.

The first problem is the simulation of flow over a flapping foil. A peculiarity here is that the airfoil motion is simulated using Immersed Boundary Condition (IBC) method, namely the Brinkman penalization method, to mimic the no-slip boundary conditions on the interface between a moving body and compressible viscous fluid. The method is developed for unstructured meshes [1]. The results are analysed in terms of time-averaged and time-dependent aerodynamic loads.

A NACA0012 foil with the chord length $c = 1$ moves in homogeneous flow with Mach number M=0.2 and oscillates with plunging and pitching motions as shown in Fig. 1.
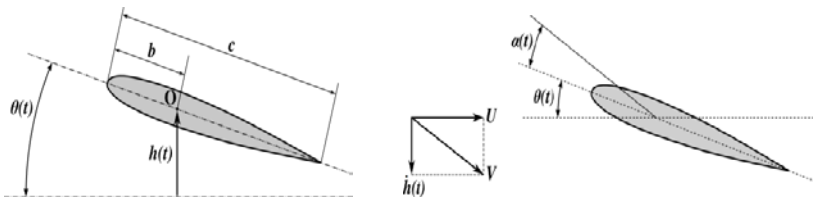
Fig. 1. Scheme of the foil pitching and plunging oscillations

Here the replacement $h(t) = h_0 \sin(\omega t)$ corresponds to the vertical plunging motion with amplitude h_0 and linear frequency $f = \omega/2\pi$. The foil pitches around one-third chord with a pitch angle given as $\theta(t) = \theta_0 \sin(\omega t + \psi)$, where θ_0 denotes the pitch amplitude and ψ is the phase angle between the pitching and plunging motion.

Following an experimental case by Anderson et al. [2] the plunging amplitude h_0 is set to 0.75, phase angle ψ is set to $\pi/2$ and the Reynolds number is set to $\mathrm{Re} = \rho u_\infty c / \mu = 40\,000$. The computations were carried out for different Strouhal numbers $St = f\,h_0/u_\infty$: 0.25, 0.35, 0.45. For $\psi = \pi/2$ the pitching amplitude is expressed as $\theta_0 = \mathrm{arctg}\left(\pi St\right) - \alpha_0$ where α_0 is a nominal angle of attack which is set to $15°$.

(a)   (b)
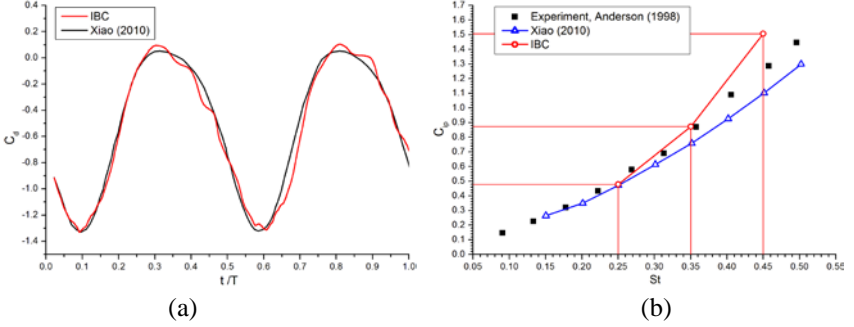
Fig. 2. (a) Instant drag coefficient; (b) mean power coefficient

The obtained instant drag coefficient for one period of oscillations with the Strouhal number $St = 0.35$ well correlates with the results of [3] where moving reference frame method is used (Fig. 2a). The discrepancy is caused by using the non-boundary conforming approach.

An acceptable agreement between numerical and Anderson experimental results is corroborated by Fig. 2b where the measured and predicted mean thrust and power coefficients are shown. The mean power coefficient is expressed as

$$ C_{ip} = \frac{2}{T}\left[\int_0^T F_y\left(t\right)\frac{dh\left(t\right)}{dt}\,dt + \int_0^T M\left(t\right)\frac{d\theta\left(t\right)}{dt}\,dt \right]. $$

The second problem is the simulation of the leading edge noise of a heaving airfoil being subjected to harmonic gust. An innovated hybrid method is used to incorporate to heaving motion to the background flow in the linearised Euler equations. The acoustic properties are compared with those of the stationary.

A simulation of leading edge noise for a heaving NACA 0012 airfoil is divided to two stages. In the first stage, the periodic background flow is computed using an Unsteady Reynolds-Averaged Navier-Stokes (URANS) solver. The $k - \omega$ SST turbulence model is used, and fine grids are used near to wall $(y^+ < 1)$ to resolve the boundary layer. The heaving motion of the airfoil is achieved by using a deforming mesh that is two chord-lengths away from the airfoil. In the second stage, the linearised Euler equation (LEE) with the periodic background flow is solved by a high-order finite difference CAA code [4, 5].

In the CAA simulations, the reference frame was changed to the airfoil, such that the airfoil stayed stationary as the mean flow varied with time. To study the acoustic response, the single velocity-component gust is introduced to the computational domain to mimic the oncoming turbulence [6]. A series of simulations are conducted at a freestream speed $u_\infty = 60$ m/s. The amplitude of the gust is $A_g = 0.4$ m/s, and the gust wavelength is $\lambda_g = 0.03$ m. Fig. 3 is the schematic of the problem.
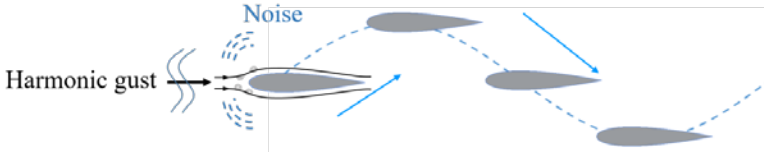

Fig 3. Illustration of the leading edge noise of a heaving airfoil

In this work, the effects of heaving amplitude and frequency on the leading edge noise are investigated, and the cases are listed in Table 1. The heaving frequency doubled from Case 1 to 3, leading to the increase of $St_c = 2\pi f_h c / u_\infty$, while the Strouhal number based on the heaving amplitude $St_A = 2\pi f_h A_h / u_\infty$ is fixed, where f_h is the heaving frequency, c refers to the airfoil chord length, and A_h is the heaving amplitude. For Case 3 to 6, simulations were conducted under the same heaving frequency while the heaving amplitude increased.

No.	u_∞ [m/s]	f_h [Hz]	A_h [m]	St_A	St_c
1	60	10	0.02	0.021	0.157
2	60	20	0.01	0.021	0.314
3	60	40	0.05	0.021	0.628
4	60	40	0.10	0.042	0.628
5	60	40	0.20	0.084	0.628
6	60	40	0.30	0.126	0.628

Table 1. List of the investigated cases with single frequency gust

Fig. 4 shows that far-field directivities p_{rms} of the heaving airfoils, and the results of a stationary airfoil are also plotted (in black solid line). In general, the heaving airfoil can lead to a reduction of sound. However, the dependence with the two parameters St_A and St_c is different. In Fig. 4(a) where $St_A = 0.021$ is fixed, the p_{rms} predictions from different St_c cases are close, suggesting that sound reduction is insensitive to the parameter St_c. In contrast, with the increase of St_A there is less sound radiate (Fig. 4(b), the black arrow). Also, the sound radiation lobe is not alternated due to the heaving motion.
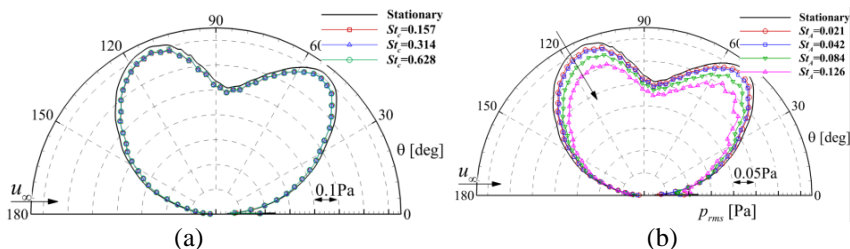
Fig. 4. Comparison of p_{rms} directivities from the heaving airfoil and the stationary airfoil

Acknowledgment

References

1. Abalakin, I.V., Zhdanova, N.S. and Kozubskaya, T.K. Immersed Boundary Method Implemented for the Simulation of an External Flow on Unstructured Meshes. Math. Models Comput. Simul., 2016, v. 8, No. 3, p. 219-230.
2. Anderson, J.M., Streitlien, K., Barrett, D.S. and Triantafyllou, M. S. Oscillating foils of high propulsive efficiency. J. Fluid Mech., 1998, v. 360, p. 41-72.
3. Xiao, Q and Liao, W. Numerical investigation of angle of attack profile on propulsion performance of an oscillating foil. Comput. Fluids, 2010, v. 39, No. 8, p. 1366-1380.
4. Zhang, X. and Chen X. Broadband wave propagation from an aeroengine fuct. 2013, AIAA Journal, v. 52, No. 1, p. 43-51.
5. Gea-Aguilera, F., Zhang, X., Chen, X., Gill J.R. and Nodé-Langlois, T. Synthetic turbulence methods for leading edge noise predictions. AIAA Paper 2015-2670, 2015.
6. Gill J.R., Zhang X. and Joseph P. Symmetric airfoil geometry effects on leading edge noise. The Journal of the Acoustical Society of America, 2013, v. 134, No. 4, p. 2669-2680.

A COMPARISON OF ACOUSTIC FAR-FIELD PREDICTION METHODS FOR TURBULENT FLOWS

Siyang Zhong, **Xin Zhang**

The Hong Kong University of Science and Technology, Hong Kong, China,
aexzhang@ust.hk

Introduction

In aeroacoustic problems, especially in computational aeroacoustics (CAA) studies, it is often of interest to compute acoustic far-field directivities from the well resolved, unsteady nearfield flow. The integral solution of Ffowcs Williams and Hawkings (FW-H) equation [1] or the Kirchhoff method [2] is often used for this purpose. The Kirchhoff method is applied in the linear region where sound propagates and the fluctuation variables should be acoustically related. The FW-H equation is derived precisely from the flow governing equations, and the complete solution of it that contains both surface and volume integrals could yield accurate results as the Navier-Stokes equations. However, the computation of the volume integral term in the FW-H solution has practical difficulties: 1) it is extremely expensive despite the increasing computation power, and 2) it suffers from the so-called *cause and effect* issue since unknown variables are involved in the source terms. Therefore, many efforts have been made to extract far-field directivities by only performing surface integrals under the assumption that the acoustic contribution by the unsteady flow exterior to the integration surface is negligible.
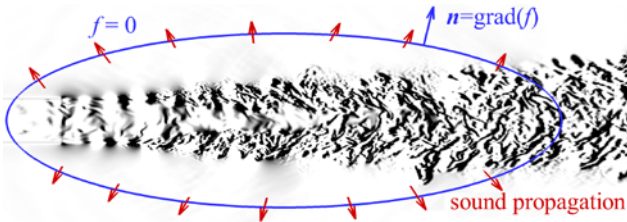
Fig. 1. Schematic of the sound extrapolation that using near field flow data to compute acoustic far-field directivities

Figure 1 shows the schematic of the sound extrapolation method and the integration surface is placed in the region where sound propagates. The Farassat formula 1A [3] that only contains the surface integral part of the FW-H solution is widely used for aeroacoustics problems. However, the predicted sound field might be contaminated by the passage of the non-acoustic fluctuations across the integration surface in turbulent flows.

Some strategies might be useful to avoid the spurious wave contamination such as to use on-body or open section integration surfaces. However, these methods suffer from limitations of narrow range of the application since they are inconsistent with mathematical formulations. Several methods have been proposed to compute the acoustic far-field directivity with only surface integrations. One category of methods is to introduce correction terms to the FW-H equation to account for the omitted volume integral parts [4, 5], often with convoluted formulations. For the flows where the turbulent fluctuations are vortical wave dominant, an effective method is to use an alternative acoustic variable such that the vortical component is effectively filtered because of the divergence-free property [6]. However, the sound prediction might be contaminated in general turbulent flows with convecting pressure fluctuations. To avoid the spectral leakage caused by an integration surface, Wright and Morfey [7] developed a method of using transition profile. It turns out to be the mathematical description of the averaging approach of using different integration surfaces in case the transition zone is stair-like. The method of averaging of FW-H prediction results by multiple closely placed surfaces was developed by Sparlart and Shur *et al.* [8, 9] under the assumption that the error induced by each surface is cancelled due to the random phase shift. The method was widely used for varies aeroacoustic problems owing to its simplicity. Recently, a generalised sound extrapolation method was developed based on a new acoustic analogy using an indirect acoustic variable [10]. The non-acoustic components are filtered out during the filtering process under Taylor's approximation [11]. A conventional Green's function method is used to solve the resulting third order equation, and the acoustic pressure at far field is obtained from the asymptotic property. The method was applied to several aeroacoustic problems including airfoil-gust interaction, and vortex shedding noise from a cylinder and co-flowing jet noise. Good results were obtained.

Problem statement

Each of the methods listed above has its advantage and disadvantages regarding the accuracy and the cost of time and storage. In this work, studying of the performance of several of the representative methods mentioned above is conducted, including **M1**: the classical FW-H method, **M2:** the technique of performing averaging of different FW-H results, **M3:** the method filtering out the vortical wave and **M4:** the newly developed generalised sound extrapolation method.

Two typical aeroacoustic problems are studied. The first case is the noise generated by a NACA0002 airfoil interacting with oncoming Gaussian spectrum turbulence, which is a significant source of broadband noise in turbofan engines or contra-rotating open rotors. The second case is the sound production

by a co-flowing jet, in which case the identification of source and prediction of far-field directivity are challenging.

Airfoil-turbulence interaction noise prediction

For the case of airfoil gust interaction noise, the Mach number is 0.5, and the integral length scale of the Gaussian spectrum turbulence is given as 0.1 chord length of the NACA0002 airfoil. The angle of attack is 0 degree. Figure 1 shows the instantaneous pressure distributions. The results by the methods **M3** and **M4** that filter out the non-acoustic fluctuations are plotted in Fig. 1 (right) and the results match fairly well with the flat plate solution by Amiet [12]. The results using **M1** and **M2** will be presented and discussed in the final version of the abstract.
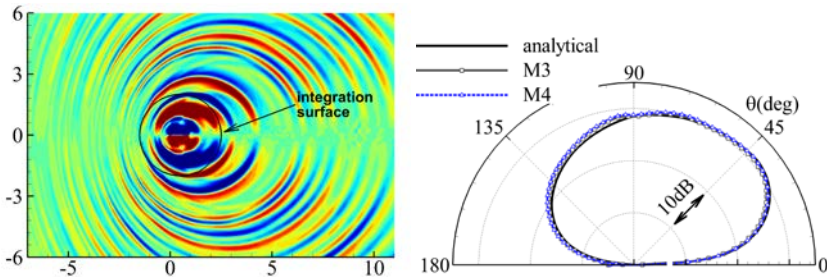
Fig. 2. The near field sound pressure distribution (left) and the predicted acoustic far-field directivities by **M3** and **M4** (right)

Co-flowing jet noise prediction

The second case in this study is the sound generated from a co-flowing jet, using an established DNS database [13]. The jet Mach number is 0.8, and the co-flow Mach number is 0.2, and the Reynolds number is Re=8000. Figure 3 shows the distribution of density gradient and the locations of the integration surfaces are shown in Fig. 2, and the radiation pattern using the dilatation rate. The distance from the observer to the jet nozzle exit is r=500, which is sufficiently large to satisfy the far-field condition.

Figure 4(a) shows the predicted results by method **M1** (the original FW-H method without performing averaging). The predicted spectra by different integration surfaces are inconsistent, and significant differences are observed in the predicted far-field directivities. Predictions using **M3** with the data collected on surfaces S3 (z ranges from 0-40) and S4 (z ranges from 0-45) are shown in Fig. 4(b). There is also a noticeable difference in the results by the two surfaces because convection component is also included in the pressure fluctuations. The results suggest that both the original FW-H method **M1** and the method (**M3**)

which filters the vortical wave are not suitable for the aeroacoustics problem with convecting pressure fluctuations.
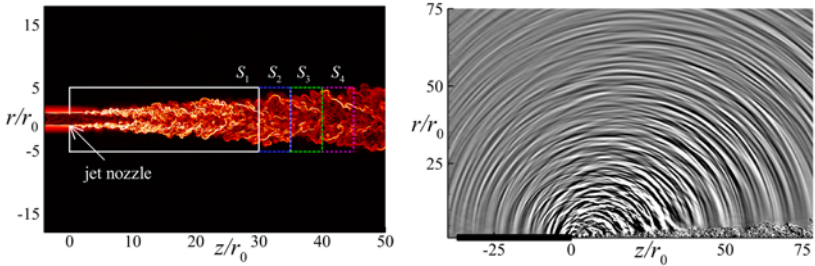

Fig. 3. The near field distributions of the density gradient ρ_z (left) and the radiation pattern indicated by the dilatation rate
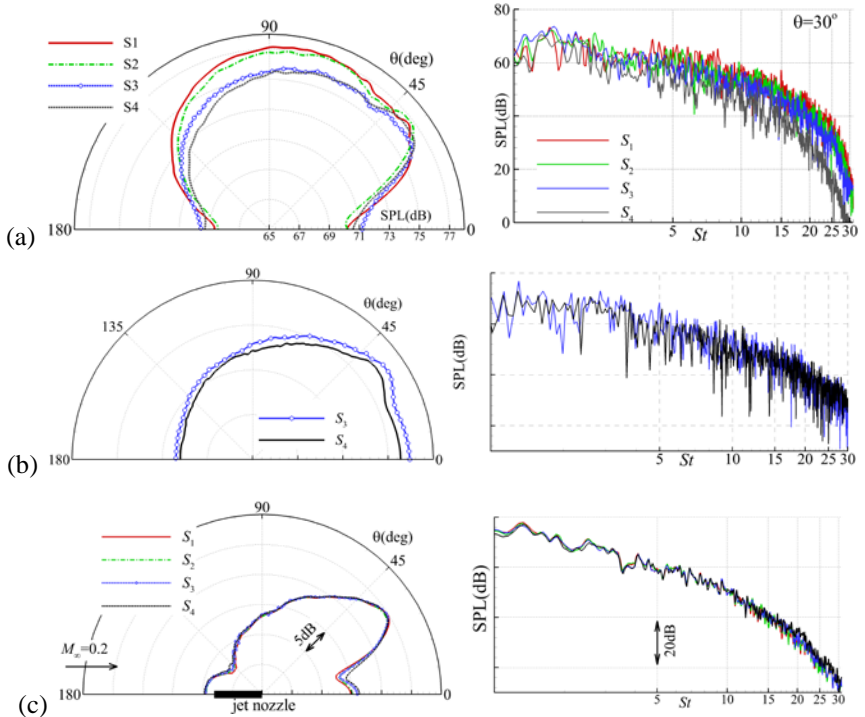

Fig. 4. The predicted results by (a) the FW-H method M1, (b) the vortical-wave filtering method M3, and (c) the generalised sound extrapolation method M4: the far-field directivities (left) and the predicted spectra at 30deg (right)

By contrast, the results by the generalised sound extrapolation method **M4** are shown in Fig. 4(c), and consistent results in both spectra and far-field directivities are obtained for different integration surfaces. As for the far-field directivity, there is a silent zone at low observer angles and a radiation peak at observer angle around 30 degrees. The consistent results in acoustic suggest that the potential non-acoustical contamination induced by turbulence that might be different across different surfaces is well suppressed owing to the filtering procedure adopted in the proposed method. In the final version of the abstract, the results by method **M2** that performs averaging over the FW-H results of different integration surface will be presented in the final version of the abstract. As for the computation cost, the number of the surface source panels is 96431, the number of the time step is 6251 and the resultant time and storage are shown in Table 1. In the current configuration, **M1** has the smallest storage and time cost since only the primitive variables are required, and it costs the least computation time. **M4** yield a more accurate result at the cost of more extensive storage requirement of 26 variables to extract the indirect acoustic variable and the longer time since FFT calculations are also needed. However, the storage could be greatly reduced if the indirect acoustic variables are output from the CFD/CAA solvers, which is easy and only five variables are needed. Also, as shown in the recent work by the authors, the computation time using the generalised sound extrapolation method can be reduced to 1.5 hour for this case, if the frequency domain solution is used [14]. As for the multi-surface FW-H method **M2**, it can be expected that the cost depends on the number of surfaces to use. For each surface, it may require similar storage or computation time as **M1**, while the total computation cost might be the same order as the generalised sound extrapolation method, which will be provided in the final version of the abstract.

Table 1. Time and storage costs of different sound extrapolation methods, N is the number of surfaces used for averaging by FW-H method

Method	M1	M2	M3	M4
Time(s)	23299	**23299×N**	25400	34466
Storage(GB)	9.2	**9.2×N**	35.0	45.6

References

1. J.E. Ffowcs Williams and D.L. Hawkings, "Sound generation by turbulence and surfaces in arbitrary motion," *Phil. Trans. R. Soc. A*, vol. 264, no. 1152, pp. 321-342, 1969.
2. F. Farassat, "Acoustic radiation from rotating bladesthe Kirchhoff method in aeroacosutics," *J. Sound Vib.*, vol. 239, no. 4, pp. 785-800, 2001.
3. K.S. Brentner and F. Farassat, "Analytical comparison of the acoustic analogy and Kirchhoff formulation for moving surfaces," *AIAA J.,* vol. 36, no. 8, pp. 1379-1386, 1998.
4. G. Rahier, M. Huet and J. Prieur, "Additional terms for the use of Ffowcs Williams and Hawkings surface integrals in turbulet flows," *Comput Fluids,* vol. 2007, pp. 158-172, 2015.
5. D.P. Lockard and J.H. Casper, "Permeable surface corrections for Ffowcs Williams and Hawkings integrals," *AIAA Paper 2005-2995,* 2005.
6. S.Y. Zhong and X. Zhang, "A sound extrapolation method for aeroacoustics far-field prediction in presence of vortical waves," *J. Fluid Mech.,* vol. 820, pp. 424-450, 2017.
7. M.C. Wright and C.L. Morfey, "On the extrapolation of acoustic waves from flow simulations with vortical out flows," *Int. J. Aeroacoustics,* vol. 14, pp. 217-227, 2015.
8. P.R. Spalart and M.L. Shur, "Variants of the Ffowcs Williams-Hawkings equation and their coupling with simulations of hot jets," *Int. J. Aeroacoustics,* vol. 53, pp. 477-492, 2009.
9. P.R. Spalart , M.L. Shur, M.K. Strelets and A.K. Travin, "Initial noise predictions for rudimentaey landing gear," *J. Sound Vib.,* vol. 330, pp. 4180-4195, 2011.
10. S.Y. Zhong and X. Zhang, "A generalised sound extrapolation method for turbulent flows," *Proc. R. Soc. A* 474: 20170614.
11. G.I. Taylor, "The spectrum of turbulence," *Proc. R. Soc. A,* vol. 164, no. 919, pp. 476-490, 1938.
12. R.K. Amiet, "Acoustic radiation from an airfoil in a turbulent stream," *J. Sound Vib.,* vol. 41, no. 4, pp. 407-420, 1975.
13. R.D. Sandberg, B.J. Tester, "Mach-number scaling of individual azimuthal modes of subsonic co-flowing jets," *J. Fluid Mech*. Vol. 793, pp. 209–228, 2016.
14. S.Y. Zhong and X. Zhang, "On the frequency domain formulation of the generalised sound extrapolation method," *J. Acou. Soc. Am.*, under review, 2018.

Author Index

Scientific publication

Fifth International Workshop

COMPUTATIONAL EXPERIMENT
IN AEROACOUSTICS

Books of abstracts

September 17-22, 2018
Svetlogorsk
Kaliningrad region
Russia

Makeup: *L.V. Dorodnitsyn*
Cover: *M. Dolinina*